Ore Geology Reviews 81 (2017) 641–671

Contents lists available at ScienceDirect

Ore Geology Reviews

journal homepage: www.elsevier.com/locate/oregeorev

Mo deposits in Northwest China: Geology, geochemistry, geochronology and tectonic setting

Yan-Shuang Wu [a], Yan-Jing Chen [b,c,*], Ke-Fa Zhou [a]

[a] Xinjiang Research Center for Mineral Resources, Xinjiang Institute of Ecology and Geography, Chinese Academy of Sciences, Xinjiang 830011, China
[b] Key Laboratory of Orogen and Crust Evolution, Peking University, Beijing 100871, China
[c] State Key Laboratory of Geological Processes and Mineral Resources, China University of Geosciences, Wuhan 430074, China

ARTICLE INFO

Article history:
Received 10 December 2015
Received in revised form 11 July 2016
Accepted 15 July 2016
Available online 18 July 2016

Keywords:
Northwest China
Central Asia Orogenic Belt
Mo deposit
Ore geology
Continental collision
Subduction-related accretion

ABSTRACT

Northwest China, covering northern Xinjiang, northern Gansu and westernmost Inner Mongolia, mainly includes Junggar Basin and its surrounding mountains such as Chinese Altay, Junggar, Chinese Tianshan and Beishan. It lies at the junction of Siberia, Tarim and Kazakhstan plates, and is a key sector of the Central Asian Orogenic Belt (CAOB), characterized by multistage Phanerozoic continental growth. Herein at least nine Mo-only or Mo-dominated, fourteen Cu-Mo, two W-Mo and one Be-Mo deposits have been discovered. These 27 deposits occur in Altay, West Jungar, West Tianshan, East Tianshan and Beishan areas, and have been formed during accretionary or collisional orogenies. The majority of the deposits are porphyry type, followed by the skarn and quartz vein types. The orebodies occur mainly as veins, lens, pods in the positions from inner intrusions through contact zones to the hostrocks distal to causative intrusions. The host-rocks are variable in lithologies, including granites, porphyries, volcanic breccias and tuffs, and sedimentary rocks. Outward from orebodies to hostrocks, the wallrock alteration is zoning from potassic (K-feldspar-quartz-mica), through phyllic (quartz-sericite-chlorite-epidote), to propylitic or argillic alterations, with skarn specifically occurring in skarn-type systems. Hydrothermal mineralization generally includes four stages, from early to late, represented by (1) potassic feldspar-quartz veins or veinlets, (2) quartz-molybdenite stockworks, (3) quartz-polymetallic sulfide stockworks, and (4) quartz ± carbonate ± fluorite veins or veinlets. The ore-forming fluids were initially magmatic in origin and shew high-temperature and high-salinity, containing daughter mineral- and/or CO_2-bearing fluid inclusions; and eventually evolved to low-temperature, low-pressure, low-salinity and CO_2-poor meteoric water. The porphyry Mo deposits can be further subdivided into two subtypes, i.e., Dabie- and Endako-types. The Endako-type Mo deposits, e.g., Suyunhe and Hongyuan, together with all the Cu-Mo systems, were formed in the Palaeozoic subduction-related magmatic arcs. The Dabie-type porphyry Mo deposits, represented by giant Donggebi and Baishan, together with the Mo-only, Mo-dominated and W-Mo or Be-Mo deposits were formed in syn- to post-collisional tectonic setting, with isotope ages ranging 260–213.2 Ma, with the Kumutage skarn-type Mo system being an exception aged 319 Ma. The Dabie-type porphyry Mo deposits are characterized by the CO_2-bearing fluid inclusions that cannot be observed in the Endako-type porphyry Mo systems. The Re contents in molybdenites from porphyry and porphyry-skarn Cu-Mo systems are mainly >100 ppm, suggesting a source significantly contributed by the mantle; whereas the Re contents in molybdenites from the Mo-only or W-Mo deposits are mainly <100 ppm, indicating a genetic relation to the crust-sourced granitic magmatism. Therefore, the types of porphyry Mo deposits and their contrasting geological and geochemical characteristics are a powerful indicator of the tectonic settings; and the available data from the Mo deposits in NW China indicate a Late Carboniferous-Permian transformation from subduction-related accretionary orogeny to continental collision orogeny.

1. Introduction

Porphyry Mo deposits are the most important molybdenum source in the world, and mainly occur in subduction-related continental arcs, (back-arc) rifts and continental collision orogens (Chen and Wang, 2011; Chen et al., 2014; Li et al., 2012b; Yang et al., 2012c, 2013b, 2015b), also termed Endako-, Climax- and Dabie-types, respectively (Chen et al., 2014, 2017a,b; Mi et al., 2015; Zhong et al., 2017; Yang et al., 2017b). The Mo deposits formed in subduction-related continental arcs are generally fluorine-poor and CO_2-poor systems associated with calc-alkaline intrusions exemplified by Endako (Selby et al., 2000) and

* Corresponding author.
E-mail addresses: yjchen@pku.edu.cn, gigyjchen@126.com (Y.-J. Chen).

http://dx.doi.org/10.1016/j.oregeorev.2016.07.010
0169-1368/

MAX (Lawley et al., 2010) deposits in British Columbia, Canada, and Diyanqinamu (Wang et al., 2017a) and Chalukou (Zhang and Li, 2016) deposits in Great Hingan Range and Zhaiwa deposit (Deng et al., 2013a, 2013b) in Qinling Orogen, China. The Mo deposits formed in rifts are associated with alkaline magmas developed in back-arc or intracontinental rifts, formed by fluids with high F/Cl but variable CO_2/H_2O and K/Na ratios, as exemplified by the Climax (Wallace, 1995), Urad-Henderson (Seedorff and Einaudi, 2004a, 2004b) and Questa (Klemm et al., 2008) deposits in Rocky Mountains, USA, and the Caosiyao (Wu et al., 2016a) and Zhangmajing deposits in Northeastern China (Chen et al., 2017b). The porphyry Mo systems in syn- to post-collisional tectonic settings are formed by fluids with high CO_2/H_2O, F/Cl and K/Na ratios, associated with high-K calc-alkaline to shoshonitic magmas, as represented by the deposits at Qian'echong (Yang et al., 2013b; Mi et al., 2015) and Yaochong (Wang et al., 2014a) in Dabie Shan, at Yuchiling (Li et al., 2012b, 2013a), Nanihu (Yang et al., 2012c) and Donggou (Yang et al., 2015b) in Qinling Orogen, China.

The Northwest (NW) China, including northern Xinjiang, northern Gansu and westernmost Inner Mongolia, lies at the junction of Siberia, Tarim and Kazakhstan plates, and is the central sector of the Central Asian orogenic belt (CAOB). This region is characterized by multistage Phanerozoic continental growth, followed by continental collision and post-collisional intraplate tectonism, comprising Junggar Basin and its surrounding mountains such as Chinese Altay, Junggar, Chinese Tianshan and Beishan. The Northwest (NW) China underwent multistage tectono-magmatic events and was well known as an important metalliferous province hosting numerous mineral systems (e.g., Cu, Au, Mo, Fe, Pb, and Zn). To date at least 27 Mo deposits, including Mo-only, Mo-dominated and Mo-bearing systems, have been discovered and reported in NW China (Table 1; Fig. 1). These Mo deposits are predominantly presented as porphyries (n = 22), skarns (n = 4) and quartz veins (n = 1), formed in a long time span from the Paleozoic to Early Mesozoic. The geology, geochemistry and geochronology of individual deposits have been studied, and a large amount of data was accumulated, but not well summarized and unknown by international geologists, except for the three giant porphyry Mo systems at Baishan and Donggebi in East Tianshan (Xiang et al., 2013; Wu et al., 2014, 2017b), and Suyunhe in West Junggar (Shen et al., 2017; Yan et al., 2015).

In this paper, we summarize the geological, geochemical and geochronological characteristics of the Mo deposits, outline their spatial and temporal distribution, and discuss their geneses and tectonic settings. We also invoke a Permian tectonic transformation from subduction-related accretionary orogeny to continental collision orogeny.

2. Regional geology

Northwest China refers to the area north of Tarim basin and including Altay Shan, Junggar, Tianshan and Beishan orogens (Fig. 1; Chen et al., 2012b). These orogens are part of the CAOB (Chen, 2000; Xiao et al., 2008a; Windley et al., 2007) or the Altaids (Sengor and Natalìn, 1996). Northwest China is in the center of the CAOB, that is an accretionary orogenic area comprising ophiolite suites, magmatic arcs, Precambrian microcontinental massifs and accretionary terranes, which resulted from the collision between the Siberia and Tarim-North China plates along the Kumishi Suture (also called Solonker Suture in NE China) that mainly occurred in the Permian (Sengor and Natalìn, 1996; Chen, 1997, 2000; Xiao et al., 2009a). It has a complex tectonic framework (Fig. 1). The Chinese Altay Shan is an accretionary complex onto the southern margin of the Siberia continental plate, with the Erqis tectonic suture as its southern boundary. The area from the Erqis suture southward to the Kumishi Suture, including Junggar basin and orogens, Turpan basin, Tianshan Mountains, Ili block and other units, constitutes a wide Tianshan–Junggar accretionary belt that can be regarded as part of the Kazakhstan plate. The South Tianshan accretionary complex, containing ophiolite segments representing the South Tianshan Ocean, has been interpreted as the zone suturing Tarim and Kazakhstan plates (Ma et al., 1997; Shu et al., 2001; Li et al., 2006c; Xiao et al., 2008a; Xiao and Kusky, 2009). In the Beishan area, the tectonic unis between the Kumishi Suture and the Duanghuang Block are mainly subduction-related basin-arc systems, and are included into the NW China in this paper. Thus, the NW China is characterized by Paleozoic magmatic arcs, accretionary wedges, slices of ophiolitic rocks, and microcontinents forming a collage that may be compared to the present-day western Pacific aarchipelago (Hsu et al., 1995).

A Precambrian tectonic reconstruction is difficult due to poor exposures of Precambrian terranes and paucity of published research data, whereas details of Paleozoic tectonics are still hotly debated because of the complexity of the NW China lithotectonic units. Nevertheless, geologists are gradually reaching consensus on the following issues: (1) NW China is one of the most remarkable area of Phanerozoic continental/crustal growth in the world (e.g., Chen and Jahn, 2004; Chen and Arakawa, 2005; Gu et al., 2006); (2) the continental growth mainly resulted from Paleozoic oceanic subduction and closure (e.g., Sengor and Natalìn, 1996; Xiao et al., 2008a; Tang et al., 2006a); (3) Phanerozoic geodynamic evolution includes three main tectonic regimes (e.g., Chen, 1997, 2000; Li and Xiao, 1999; Li and Xu, 2004), i.e., Paleozoic subduction-related accretionary orogenesis, Permian or Late Carboniferous–Triassic intercontinental collision (Tu and Ding, 1986), and Mesozoic–Cenozoic intracontinental deformation related to far-field impact of Tethyan orogenesis; (4) the paleo-oceans within the Tianshan–Junggar belt (domain of Kazakhstan plate) mainly closed in the mid-Carboniferous (ca. 320 Ma) (e.g., Chiaradia et al., 2006; Chen and Chen, 2007), followed by the closure of the Erqis Ocean during the Late Carboniferous–Permian (Xiao et al., 2009a) and then the South Tianshan Ocean (Kumishi suture) during the Permian (Tu and Ding, 1986; Zhang et al., 2007; Xiao et al., 2008a, 2009a); (5) granitoids and related volcanic rocks were mainly developed in the period of Devonian–Triassic, and dominated by I-types in Devonian–Early Carboniferous and by S- or A-types in Late Carboniferous–Triassic, respectively (e.g., Gu et al., 2006; Zhang et al., 2003; Chen and Arakawa, 2005; Pirajno et al., 2008, 2009); (6) magmatic hiydrothermal, epithermal, seafloor hyodrothermal Cu, Pb-Zn, Au and Fe mineralization mineralization mainly occurred in the period from the Devonian to Permian, and magmatic hydrothermal Mo, W and Sn and orogenic-type Au mineralization in the period of Permian to Triassic (Chen et al., 2000a, 2001, 2007a,b; Qin et al., 2002; Rui et al., 2002a; Mao et al., 2005; Wu et al., 2006a); and (7) marine sedimentation ended diachronologically in the period from Early Carboniferous in Altay-Tianshan area (Chen, 1997) to Late Permian or Triassic in southern Tianshan (Tu and Ding, 1986; Chen and Chen, 2007; Xiao et al., 2008b).

The Beishan Orogen developed from a Neoproterozoic to Paleozoic archipelago characterized by multiple accretionary and collisional processes, and can be roughly taken as an eastern counterpart of the Eastern Tianshan, with the Hongshishan mélange (Xiao et al., 2010) corresponding to the Kanggur ophiolite slice zone. However, some of the tectonic units in the southern Beishan Orogen may be compared with the Southern Tianshan orogenic belt, and alternately, the three mélange zones south of the Hanshan Massif, i.e., the Mingshui–Xiaohuangshan mélange the Hongliuhe–Xichangjing mélange and the Liuyuan–Yinaoxia mélange (Mao et al., 2012b), may be incorporated into the Kumishi Sutue, and the volcanic-sedimenary rocks between the Hanshan Massif and the Liuyuan-Yinaoxia Fault can be regarded as a wide, complicated accretionary complex, termed the Mazongshan-Liuyuan accretionary complex. In this huge accretionary complex, thethe eclogite lenses can be observed at Gubaoquan area, yielding a zircon U–Pb age of 465 Ma (Liu et al., 2011; Qu et al., 2011); granitoids were emplaced over a long period, from mid-Palaeozoic (Silurian–Devonian: 440–374 Ma), through Permian–Triassic (290–220 Ma), to Late Triassic (200 Ma) (Li et al., 2009b, 2012a, 2013a, 2013b; Mao et al., 2012b; Zhang et al., 2012a, 2012e). The Liuyuan mélange was also intruded by a gabbro that yielded a weighted zircon $^{206}Pb/^{238}U$ age of

286 ± 2 Ma, indicating that the Liuyuan mélange formed prior to this time (Mao et al., 2012a).

3. Timing and spatial distribution of the Mo deposits

3.1. Preamble

The molybdenite Re–Os and zircon U–Pb geochronology are the most powerful tools to elucidate the age of mineralization and magma emplacement (Stein et al., 2001), and their application makes the timing of Mo mineralization and associated magmatism to be well constrained. Table 2 summarizes the available isotopic age data for the Mo deposits in NW China, including molybdenite Re–Os ages, zircon U–Pb ages, and Rb–Sr isochron ages of fluid inclusions in hydrothermal quartz (e.g. Lailisigaoer deposit). The ages fall into two groups (Fig. 2), i.e., Hercynian or Late Paleozoic (411.6–270 Ma) and Indosinian or Late Permian-Triassic (260–213.2 Ma), and show a southeastward younging trend.

The Hercynian deposits are mainly Cu-Mo association, as represented by Tuwu-Yandong and Baogutu porphyry systems, with minor Mo-only or Mo-dominated, as exemplified by the Sunyunhe porphyry system. By contrast, the Indosinian deposits are lacking of Cu-dominated association, but predomintant of the Mo-only or Mo-dominated systems (e.g. Donggebi and Baishan), with the Xiaobaishitou W-Mo and Asikaerte Be-Mo deposits being the exceptions.

The 27 Mo-only, Mo-dominated and Mo-bearing deposits occur in the mountains surrounding the Junggar Basin, including Altay, W Junggar, E Junggar, West Tianhsan, E Tianshan and Beishan, roughly showing a southeastward increase in Mo-mineralization, compared to the Cu-mineralization. These Mo-containing orogenic regions exhibit different geological characteristics, mineralization styles, metallogenic ages and tectonic controls, and thus, will be separately introduced below.

3.2. Altay Shan

The Altay Shan has potential for the exploration of precious (Au, Ag), base (Cu, Mo, Pb, Zn, Fe) and rare metals (Li, Be, Nb, Ta), and non-metallic mineral deposits such as gems and muscovite (Zheng et al., 2012a). It extends for more than 2500 km from Kazakhstan, parts of Russia, across northwest China (Xinjiang) to western Mongolia, and has been formed through a complex series of events that include oceanic spreading, subduction and accretion (Goldfarb et al., 2003; Pirajno, 2013; Xiao et al., 2009b; Chen et al., 2012b; Yang et al., 2009a). The area includes four tectonic units from north to south (Chen et al., 2012b. To the north, the Late Devonian–Early Carboniferous Nurt volcanic basin developed on a pre-Devonian crystalline basement. The Koktokay Paleozoic magmatic arc or the Central Altay terrane, south of the basin, constitutes the central part of the Altay Shan and contains high-grade metamorphic rocks and granites ranging in age from Neoproterozoic to earliest Triassic. In the Koktokay area, there develops the well-known largest pegmatite field in the world. The Kelan Devonian–Carboniferous fore-arc basin developed on the southern margin of the pre-Devonian metamorphic basement represented by the Central Altay terrane, hosting both the Ashele VMS-type Cu-Zn and Keketale SEDEX-type Pb-Zn deposits. The Armantay–Erqis accretionary terrane, furthest to the south, consists of high-grade metamorphic rocks (gneiss and schist) and Devonian–Carboniferous fossiliferous sedimentary rocks, intruded by post orogenic Mesozoic granites.

In the Altay Shan, four Mo-bearing deposits have been discovered already. The Asikaerte Be-Mo deposit (No. 4) occurs in Koktokay pegmatite field, yielding molybdenite Re–Os isochron ages of 218.6 ± 1.3 Ma (Wang et al., 2015a), which accords well with the zircon U–Pb ages of 219.2 ± 2.9 Ma and 222.6 ± 4.6 Ma for nuscovite albite granite, and 218.2 ± 3.9 Ma for pegmatite (Table 2). Three other Cu-Mo deposits were formed in the Palezoic (Fig. 1 and Table 2). The Xilekuduke deposit is a typical porphyry Cu-Mo system developed in a subduction-related arc setting. Its molybdenite Re–Os isochron age is 327.1 ± 2.9 Ma, in agreement with the zircon U–Pb age of 329.6 ± 4.1 Ma obtained from the causautive porphyry (Long et al., 2009, 2011). This suggests that the Altay Shan was a magmatic arc around the mid-Carboniferous time. As indicated by the molybdenite Re–Os and zircon U–Pb ages (Table 2), the Yulekenhalasu porphyry Cu-Mo system was formed in Late Devonian (371 to 382 Ma), structurally modified in Early Carboniferous (Re–Os ages: 331 to 357 Ma), and intruded by a postore granodiorite porphyry dike with zircon U–Pb age of 265.6 ± 3.7 Ma. The Suoerkuduke skarn-type Cu-Mo mineralization was contrained to have occurred during 317 to 305 Ma, but the trachydacitic porphyries yielded zircon U–Pb ages of 387.6 ± 1.8 and 383.8 ± 1.7 Ma (Zhao et al., 2015), suggesting that a further detailed geochronological study is still in need.

3.3. Western Junggar

The Western Junggar orogenic belt is bounded by the Altay Shan to the north and by the Western Tianshan to the south, extending westward to the Balkhash orogenic region in Kazakhstan and eastward to the Junggar Basin (Fig. 1). This region is characterized by Palaeozoic volcanic rocks (Zhu and Xu, 2006; Zhou et al., 2008). The Late Palaeozoic volcanic rocks exclusively outcrop in the Saur and Barluke mountains and Karamay region (Wang et al., 2004; Geng et al., 2011; Tang et al., 2010b; Zhang et al., 2011), and the Early Palaeozoic volcanic rocks can be observed in the Xiemisitai and Sharburt areas. Main structures in the Western Junggar are a series of NE-trending faults, including the Dalabute fault/suture, and the Mayile and Barluke faults. The Dalabute fault/suture is the most important because it controlled the location of intense magmatism and associated mineralization.

The economically important mineralization includes Au, Cr, Cu and Mo, typically represented by the Hatu orogenic-type Au deposit (Rui et al., 2002b; Shen et al., 2015) and the Sartuhai podiform chromite deposit (Zhou et al., 2001). Mo mineralization is exemplified by the Baogutu porphyry Cu-Mo deposit (Song et al., 2007; Shen et al., 2010), and the Suyunhe and Hongyuan porphyry Mo deposit (Zhong et al., 2015a,b; Shen et al., 2017). All these deposits were formed in the transition from Carboniferou to Permian, under a subduction-related magmatic arc (Shen et al., 2015).

3.4. Eastern Junggar

The East Junggar orogenic belt is bound by the Altay Shan and the Tianshan, and extends eastwards into Mongolia. The East Junggar is widespread of Palaeozoic volcanic-sedimentary rocks, with the Devonian being the most extensive. The Devonian-Carboniferous units comprise mafic to intermediate lavas and tuffs, and minor interclations of sandstones, limestones, cherts and conglomerates. They are locally overlain by the Permian volcanic-sedimentary rocks, and underlain by the metamorphosed Ordovician-Silurian (e.g. Huangcaopo Gp.) siltstone, silty mudstone, tuff and andesite, (BGMRX, 1993). The Devonian-Carboniferous volcanic rocks are characterized by their calc-alkaline geochemistry (Xiao et al., 2011; Zhang et al., 2010c), including some adakitic, Nb-rich basalts and high-temperature high-Mg andesites (Long et al., 2009; Niu et al., 2006). The oldest rock is an andesite with a concordant U–Pb zircon age of 441 ± 2 Ma (Zhang et al., 2008b), indicative of Ordovician calc-alkaline volcanism in East Junggar (Long et al., 2012). Limited Permian igneous rocks have alkaline geochemical affinities (Chen and Jahn, 2004; Han et al., 2006a).

Granitic rocks in Eastern Junggar yielded isotope ages of mainly Late Devonian, Carboniferous and Early Permian (Chen and Jahn, 2004; Zhang et al., 2006c), with positive εNd and εHf data which are an indicator of a juvenile origin (Chen and Jahn, 2004; Jahn et al., 2000; Zhang et al., 2009c) related to an island arc (Chen, 1997, 2000; Xiao et al., 2009b). The Armantay-Erqis and Kelamaili ophiolite belts yield

Table 1
Geological characteristics of the Mo deposits in Northwest China.

No.	Deposit, County, Province	Type	Metal	Reserve @ ore grade	Size	Host- or wall-rocks and other rocks in the deposit	Structure	Intrusion	Orebody occurrence	Major alteration	Ore mineral	Gangue mineral	Reference
1	Suoerkuduke, Fuyun, Xinjiang	SK	Cu, Mo		M	Middle Devonian andesite, andesite porphyry and andesite tuff, Beitashan Fm.	NNW- and SSE-trending faults	Diorite to granodiorite porphyry	Stratiform and lens in skarn	Grt, Epi, Act, Di, Bio, Chl, K, Ca, Si, Kao, Ab	Mo, Cpy, Py, Pyr, Po, Sp, Bn, Mt	Grt, Di, Epi, Act, Chl, Bio, Qz, Tr, Kfs	Zhao et al. (2015), Wan et al. (2014)
2	Xilekuduke, Fuyun, Xinjiang	P	Cu, Mo	Cu: 0.1–3.76%; Mo: 0.06–0.12%	M	Early Carboniferous tuffaceous siltstone, sandstone, silty limestone, tuff and chert, Nanmingshui Fm.	NNW-trending faults	Granite porphyry, quartz diorite	Stratiform, lens and veins in intrusion and contact zone	Hom, Si, K, Chl, Epi, Ser, Kao, Ca, Py, Sk	Mo, Cpy, Py, Mt, Ga, Sp, Mrc	Qz, Ser, Chl, Epi, Pl, Kfs, Bio, Ca, Fl, Hb, Gyp	Long et al. (2015), Wang et al. (2010b)
3	Yulekenhalasu, Qinghe, Xinjiang	P	Cu, Mo	Cu: 171 Kt @ 0.25–0.79%; Mo: 0.06%	M	Middle Devonian volcanics, volcaniclastic rock, Beitashan Fm.; Early Carboniferous terrigenous clastic rock, pyroclastic rock, Jiangbasitao Fm.	NW-trending faults	Diorite porphyry	Stratiform, veins and lens in intrusion	Chl, Epi, Ser, Py, Ca, Bio, Tr, Ab, Fl, K	Cpy, Py, Mo, Bn, Mt, Ga, Po, Apy,	Qz, Pl, Kfs, Bio, Epi, Chl, Hb, Ca, Gyp	Yang et al. (2012b)
4	Asikaerte, Fuyun, Xinjiang	P	Be, Mo		L	Late Ordovician quartz-mica schist, biotite gneiss and migmatite, Habahe Gp.	NW- and NS-trending faults	Muscovite-albite granite	Stratiform and veins in contact zones	Si, Bio, Ab	Mo, Cpy, Py, Mt, Bs, Sp	Qz, Brl, Ms, Mc, Ab	Wang et al. (2015a)
5	Suyunhe, Yumin, Xinjiang	P	Mo	Mo: 570 Kt @ 0.05– 0.09%	G	Middle Devonian volcanic-sedimentary rocks, Barluk Gp.	NE-, EW- and ENE-trending faults	Monzogranite porphyry, granite	Lens in wall rocks	Si, K, Ser, Chl, Epi, Ca, Kao, Bio	Mo, Py, Sch, Cpy, Mt, Hem	Qz, Kfs, Bio, Hb, Ser,	Zhong et al. (2015a, 2015b), Shen et al. (2016)
6	Baogutu, Tuoli, Xinjiang	P	Cu, Mo	Cu: 630 Kt @ 0.28%; Mo: 180 Kt @ 0.011%	L	Early Carboniferous volcanic rocks, Baogutu Gp.; sedimentary rocks, Xibeikulasi Gp.	ENE-trending faults	Diorite porphyry, quartz diorite	Veins in intrusion or contact zones	K, Si, Ms, Chl, Ca, Epi, Bio, Ser, Ab, Lmt	Py, Cpy, Apy, Po, Mo, Sp, Cc	Qz, Kfs, Chl, Ser, Bio	Shen et al. (2010, 2013), Zhang et al. (2010d)
7	Hongyuan, Kelamayi, Xinjiang	P	Mo	Mo: 0.036–0.177%		Early Carboniferous tuffaceous siltstone and siliceous siltstone, Baogutu Fm	ENE-trending faults	Granite porphyry	Bedded veins and lens in intrusion	Ser, Si, Ms, Chl, Ca	Mo, Cpy, Py, Po, Apy	Qz, Cal, Chl, Ser, Ms	Yan et al. (2015)
8	Mengxi, Yiwu, Xinjiang	P	Cu, Mo	Cu: 0.21–0.43%, Mo: 0.01–0.034%		Ordovician metamorphosed crystal tuff, siltstone, silty mudstone, andesite, and quartz schist and felsic hornfels, Huangcaopo Gp.	NE- trending faults	Granite porphyry	Veins in intrusion and contact zones	K, Grn, Phy, Chl, Si, Epi, Ca	Cpy, Py, Mo, Mt, Ml, Lm, Cv	Fsp, Qz, Ca, Ser, Chl	Wang et al. (2010a)
9	Dabate, Wenquan, Xinjiang	P	Cu, Mo	Cu: 52 Kt @ 0.33–0.69%; Mo: 5.6 Kt @ 0.065%	S	Late Devonian tuff, tuffaceous breccia, lava, Tuosikuertawu Fm.	WNW-trending faults	Rhyolitic porphyry	Veins and lens in intrusion and contact zones	Si, Ca, Chl, Agl, Ser, Kao, Fl	Mo, Cpy, Py, Cc	Qz, Cal, Chl, Epi, Fl, Anh	Li (2012)
10	Kekesai, Bole, Xinjiang	P	Cu, Mo	Mo: 0.033–0.085%		Late Devonian tuff, andesite, dacite, tuffaceous siltstone, Tuosikuertawu Fm.	EW-trending faults	Granodiorite and granite porphyries	Veins and lens in intrusion and contact zones	Si, K, Ser, Kao Ca, Chl	Py, Po, Cpy, Mo, Gl, Sp, Mt	Qz, Chl	Yang et al. (2016a)
11	Dongtujin, Jinghe, Xinjiang	P	Cu, Mo	Cu: up to 4%	S	Late Devonian tuffaceous siltstone, silty mudstone	ENE– and WNW–trending faults	Biotite granodiorite	Veins and lens in intrusion	Si, Ca, Epi, Sk	Mo, Cpy, Py, Sp, Gl	Qz, Cal, Epi	Wang et al. (2006)
12	Lailisigaoer, Jinghe, Xinjiang	P	Cu, Mo	Mo: >4.6 Kt @ 0.062–0.32%	S	Late Silurian calcareous or muddy siltstone, calcareous quartz-feldspathic sandstone, silty limestone, Boluohuoluoshan Fm.	NE-trending faults	Granodiorite and quartz diorite porphyries	Veins and lens in intrusion or contact zones	Si, K, Ser, Chl, Ca	Mo, Cpy, Py, Sp, Sch, Pyr	Qz, Kfs, Bio, Chl, Cal, Hb	Zhu et al. (2012)
13	Kendenggaoer, Jinghe, Xinjiang	SK	Cu, Mo	Cu: 19 Kt @ 0.56–1.2%; Mo: 1 Kt @ 0.036–0.31%	S	Carboniferous limestone, sandstone and siltstone, Dongtujinhe Fm.	NW-trending faults	Granodiorite, limestone	Veins and lens in contact zones	Sk. Si, Chl, Epi	Cpy, Mo, Bn, Py, Mt, Po, Sp, Ga, Apy	Di, Alm, Act, Epi, Qz, Wo, Tr, Chl, Ves	Jia et al. (2011)

14	Tuwu-Yandong, Hami, Xinjiang	P	Cu, Mo	Cu: 200 Kt @ 0.43%; Mo: 37 Kt @ 0.08%	L	Carboniferous volcanic lava and pyroclastic rock, Qi'eshan Gp.	ENE- trending faults	Plagiogranite and tonalite porphyries	Veins and lens in porphyry	Si, Bio, Phy, Chl, Gyp, Ab, Epi, Ca	Cpy, Bn, Py, Sp, Mt, Mo, Cc	Qz, Ser, Epi, Chl, Bio, Ca, Kao, Gyp	Xiao et al. (2015)
15	Kumutage, Hami, Xinjiang	SK?	Mo	Mo: 0.061–0.11%		Late Paleozoic gabbro intruding Precambrian basement	EW- and ENE-trending faults	Granite	Lens in the gabbro or skarn	Si, Ca, Chl, Epi, Ml, Grt	Mo, Cpy, Py, Mag, Ml	Qz, Ca, Chl, Epi	Zhang et al. (2010a)
16	Chihu, Hami, Xinjiang	P	Cu, Mo	Mo: 0.02–0.04%; Cu: 0.2–0.3%		Early Carboniferous andesitic-basaltic lava, breccia and tuff, Kushui Fm.	Nearly E-trending faults	Plagiogranite porphyry, altered diorite porphyry	Lens in intrusion and contact zones	Si, Chl, Epi, Grn	Mo, Cpy, Py, Bn, Cc	Qz, Ser, Chl, Pl, Kao	Wu et al. (2006b)
17	Donggebi, Hami, Xinjiang	P	Mo	Mo: >500 Kt @ 0.114%	G	Early Carboniferous metamorphosed sandstones of various kinds, Gandun Fm.	NE-, ENE- and N–S-trending faults	Porphyritic granite	Lens and pods distal to porphyry	Si, Ca, Chl, Epi, Ser, K, Fl	Mo, Cpy, Py, Mag, Sp, Gl, Sch	Qz, Kfs, Bio, Ser, Chl, Epi, Cal, Tur, Brl, Fl	Wu et al. (2014)
18	Yuhai, Hami, Xinjiang	P	Cu, Mo	Cu: 0.22–0.76%; Mo: 0.02–0.031%	S	Late Carboniferous spilite- keratophyre association, Wutongwozi Fm.	NE-trending faults	Quartz diorite porphyry	Veins and lens in porphyry	Epi, Chl, Si, K	Mo, Cpy, Py, Mt	Qz, Chl, Epi, Kfs	Wang et al. (2016b)
19	Sankakou, Hami, Xinjiang	P	Cu, Mo	Cu: 6.394%; Mo: 0.013%		Early Carboniferous metamorphosed quartz sandstone, siltstone, and slate, phyllite	EW-trending faults	Plagiogranite porphyry	Lens and veins in intrusion	Si, Ser, Chl, Epi, Bio, Kao	Cpy, Py, Mo, Cc, Ml, Bn	Qz, Ser, Chl, Epi, Bio,	Li et al. (2004a), Qin et al. (2009)
20	Xiaobaishitou, Xingxingxia, Xinjiang	SK	W, Mo	W: 0.23–3.06%; Mo: 0.082%		Mesoproterozoic schist, gneiss, marble, wollastonite-bearing schists, Jianshanzi Fm., Kawabulag Gp.	NE-trending faults	Coarse-grained biotite granite	Veins, lens, pods and crescents in contact zones	Grt, Epi, Chl, Si, Fl, Ca	Sch, Mo, Bs, Py, Sp, Ga, Cpy	Grt, Di, Wo, Epi, Tr, Act, Chl, Qz, Cal, Fl	Deng et al. (2016)
21	Baishan, Hami, Xinjiang	P	Mo, Re	Mo: >500 Kt @ 0.06%	G	Early Carboniferous felsic hornsfels, biotite schist, Gandun Fm.	EW-trending faults	Granite porphyry	Bedded veins and lens distal to porphyry	Si, Ca, Chl, Epi, Ser, Kao, K, Bio	Mo, Cpy, Py, Sp, Gl, Mt	Qz, Kfs, Bio, Ser, Chl, Epi, Cal	Xiang et al. (2013), Zhang et al. (2015a)
22	Huanangou, Guazhou, Gansu	P	Mo, W	Mo: 0.03–0.038%		Middle Ordovician rhyolite, andesite and sericite-quartz schist, Huaniushan Gp.	NE- and NW-trending faults	Monzogranite	Veins in intrusion and contact zones	Ser, Kao, Chl, Ca, Si, K, Zo	Mo, Cpy, Mt, Lm, Sch, Py, Sp	Qz, Kfs, Pl, Ca, Epi	He and Dong (2012)
23	Huaheitan, Liuyuan, Gansu	QV	W, Mo	Mo: 25 Kt @ 0.08%	M	Mesoproterozoic biotite-bearing felsic hornfels, Pingtoushan Gp.	EW- and WNW-trending faults	Huaniushan alkali-feldspar granite	lens in metamorphic rocks and intrusion	Si, Py	Mo, Py, Po, Cpy, Ga, Mt, Apy	Qz, Kfs, Bio, Ms, Ca, Fl, Crd	Zhu et al. (2014)
24	Hongshanjing, Subei, Gansu	P	Mo	Mo: 0.036–0.073%		Middle Carboniferous tuffaceous slate and phyllite and andesite, Yinaoxia Fm.	WNW-trending faults	Moyite, monzogranite	Veins and lens in intrusion	Si, Py, Ser	Mo, Py, Sp, Ga, Mt, Lm, Bn, Mrc	Pl, Qz, Mc, Epi, Chl, Bio, Ser, Ca, Fl, Ap	Zhang et al. (2012c)
25	Liushashan Ejin Banner, Inner Mongolia	P	Mo, Au	Mo: 0.224%	L	Carboniferous rhyolite, dacite, tuff, Baishan Fm.	NW-trending faults	Granodiorite	Veins and lens in intrusion	Si, K, Ser, Chl, Epi	Mo, Sch, Py, Cp	Qz, Kf, Bio, Chl, Cc	Nie et al. (2002)
26	Elegen, Ejin Banner, Inner Mongolia	P	Cu, Mo	Mo: 0.04–0.08%; Cu: 0.05–0.31%	M	Ordovician andesite, andesitic basalt and tuff, Xianshuihu Fm.	WNW- and EW-trending faults	Granodiorite porphyry, porphyritic granodiorite	Veins and dense dissemination in intrusion	Si, K, Chl, Epi, Ser	Mo, Cpy, Py, Ml, Mt, Ilm	Qz, Kfs, Pl, Ms, Ser, Hb	Nie et al. (2005)
27	Xiaohulishan, Ejin Banner, Inner Mongolia	P	Mo, Au	Mo: 33.5 Kt @ 0.09%	M	Ordovician andesitic breccia, crystal tuff and altered andesite, Xianshuihu Fm	NE-trending faults	Porphyritic granite, greisen	Veins and lens in intrusion	Si, K, Ab, Grn, Epi, Ser, Py, Ca	Mo, Py, Sp, Ga, Mt, Bs	Qz, Ab, Kfs, Pl, Ms, Fl, Toz	Peng et al. (2010)

Abbreviations: For genetic type: P = porphyry; SK = skarn; QV = quartz vein. For tonnage and size: Kt = 1000 t; G = giant (>500 Kt Mo); L = large (100–500 Kt Mo); M = medium (10–100 Kt Mo); S = small (<10 Kt Mo). For alteration and minerals: Ab, albite; Act, actinolite; Agl, argillization; Alm, Almandine; Anh, anhydrite; Ap, apatite; Apy, arsenopyrite; Bio, biotite; Bn, bornite; Brl, beryl; Bs, bismuthinite; Ca, carbonate; Cal, calcite; Cc–chalcocite; Chl, chlorite; Cpy, chalcopyrite; Cv, covellite; Di, diopside; Epi, epidote; Fl, fluorite; Fsp, Feldspar; Gl, galena; Grn, greisen; Grt, garnet; Gyp, gypsum; Hb, hornblende; Hem, hematite; Ilm, ilmenite; K, potassic alteration; Kao, kaolinite; Kfs, K-feldspar; Lm, Limonite; Lmt, laumontite; Mag, magnetite; Ml, malachite; Mo, molybdenite; Mrc, marcasite; Ms, muscovite; Mt, magnetite; Phy, phyllic alteration; Pl, plagioclase; Po, pyrrhotite; Pro, propylitization; Py, pyrite; Pyr, pyrrhotite; Qz, quartz; Sch, scheelite; Ser, sericite; Si, silicification; Sk, skarn; Sp, sphalerite; Toz, topaz; Tr, tremolite; Tur, tourmaline; Ves, vesuvianite; Wo, Wollastonite.

zircon U–Pb ages of 503 ± 7 Ma (Xiao et al., 2009b) and 342 ± 3 Ma, respectively, where the Early Carboniferous radiolaria can be observed (Shu and Wang, 2003) and taken as indicator of oceanic subduction zone (Wang et al., 2003). Moreover, all the Late Palaeozoic lithostratigraphic rocks were subjected to SW-vergent folding and NE-directed thrusting, which is taken as an indicator of a southwardly-retreated subduction in the Late Paleozoic (Xiao et al., 2009a).

The East Junggar orogen contains many types of ore deposits, including porphyry (-skarn) Cu-Mo-Au, orogenic-type Au, magmatic Cu-Ni, epithermal Au, magmatic hydrothermal Sn. Geochronological studies of the ore deposits indicate that they formed from the middle Devonian to the late Permian. The porphyry ore deposits formed in two epochs: the mid-Devonian and the Late Carboniferous (Long et al., 2009; Xue et al., 2010; Wan et al., 2011). The magmatic Cu-Ni deposits formed in the Early Permian (Zhang et al., 2008c). The orogenic gold lodes mainly occur in the north side of the Kalameili Fault, represented by the Qingshui and Laoyaquan deposits (Chen et al., 1995; Chen, 1997), and are considered to have been formed in the period of Permian to Triassic (Li and Chen, 2004). Five epithermal gold deposits were documented and suggested to have formed in Late Palaeozoic by Chen et al. (2012b), taking Jinshangou as an example. Hitherto at least 14 magmatic hydrothermal tin deposits or occurrences have been discovered in the Hongtujing-Laoyaquan granite batholith north of the Kalameili Fault (Chen et al., 1995), thereof, the Be'erkuduke deposit was proven to have formed in Permian (Tang et al., 2006).

The Mengxi porphyry Cu-Mo system has been proven to be of enconomic significance, which yielded zircon U–Pb age of 413.2 ± 3.9 Ma (Qu, 2011) and molybdenite Re–Os isochron age of 411.6 ± 3.2 Ma (Qu et al., 2009), was definitely formed in the Early Devonian. This is the oldest porphyry-type deposits known in the Northwest China.

3.5. Western Tianshan

The western Tianshan formed by multiple interactions between the Junggar Terrane and the Tarim Block, which are located north and south of it, respectively. The overall geological structure of the belt is broken by numerous faults, of which the North Tianshan (also called Kangur), Bingdaban-Shaquanzi and Nikolaev Line (Kumishi), faults are most conspicuous (Fig. 1; Gao et al., 2009b). These major faults divide the Western Tianshan into several tectonic units (K2a, K2b, K2c, K2e, K2f and K2g in Fig. 1). The Western Tianshan is characteristic of Carboniferous volcanic sequences, hosting numerous Fe, Au and Cu-Au-Mo deposits (Duan et al., 2014; Jiang et al., 2014; Li et al., 2013a; Zhai et al., 2009; Zhang et al., 2010b, 2012b, 2014a).

The basement of the western Tianshan consists of sillimanite–biotite–quartz schists, garnet–plagioclase–granulites, gneisses, amphibolites, migmatites and marbles, with zircon U–Pb ages ranging from 1910 to 882 Ma (Chen et al., 2000b; Gao et al., 2009a; Li et al., 2009a and references therein). The Precambrian basement is unconformably overlain by a thick cover of Silurian neritic sedimentary and volcanic rocks, Devonian-Carboniferous volcanic-sedimentary sequence composed of limestone, sandstone, shale, lava, tuff and pyroclastic rocks, and Permian post-collisional clastic sediments and volcanic rocks (Gao et al., 1998; Zhu et al., 2009). The intrusive rocks in the Western Tianshan are dominated by Palaeozoic diorites, granodiorites and granites (Gao et al., 2009a; Han et al., 2010; Huang et al., 2013; Wang and Wang, 2010; Yang et al., 2012b).

In the Western Tianshan, the porphyry(–skarn) Cu-Mo deposits are mainly associated with the Late Devonian to Carboniferous igneous rocks in the northern margins of the Ili block, e.g., Kendenggaoer skarn Cu-Mo deposit, Dongtujin porphyry Cu-Mo deposit, Kekesai porphyry Cu-Mo deposit, and Dabate porphyry Cu-Mo deposit (Fig. 1 and Table 2). The Paleozoic granitic belts occur along the south and north margins of the Yili block and have been interpreted as related to southward subduction of the northern Tianshan ocean (Tang et al., 2010a, 2014; Li et al., 2015) and northward subduction of the southern Tianshan ocean (Gao et al., 2009a; Zhu et al., 2009; Dong et al., 2011), respectively. Then tectonic setting of these Cu-Mo deposits was related to the subduction of oeanic plates.

Zhu et al. (2010) obtained a molybdenite Re–Os isochron age of 379.9 ± 8.3 Ma from the the Lailisigaoer porphyry Cu-Mo deposit, and suggested the mineralization occurred in post-collisional setting, considering that the subduction-related volcanism in this area was not

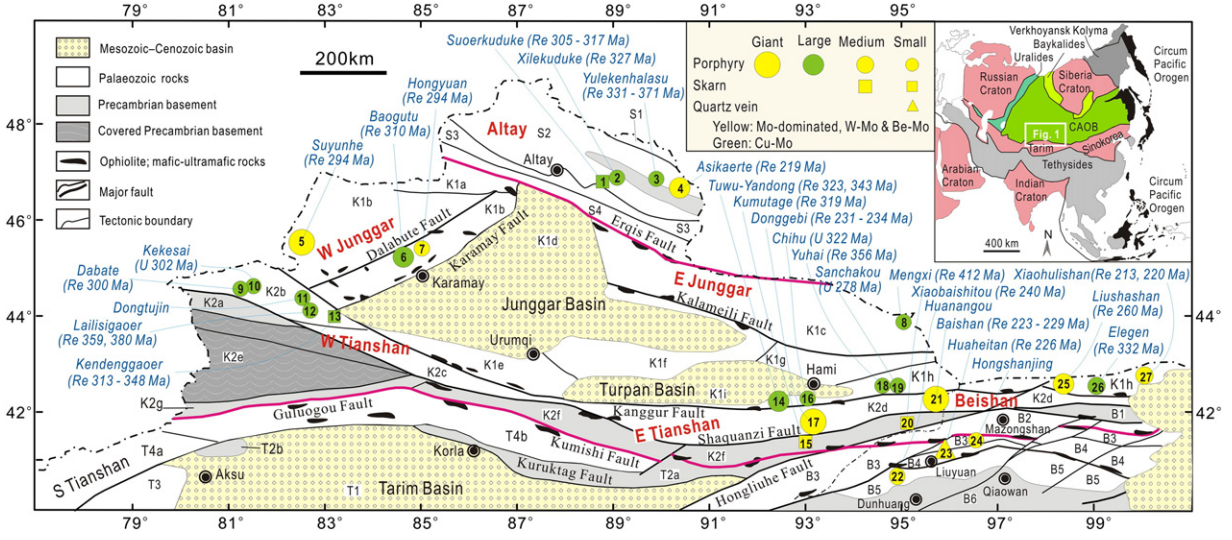

Fig. 1. Tectonic framework of Northwest China, showing the locations of Mo deposits (modified after Chen et al., 2012b and Zhang et al., 2015b). CAOB, Central Asian Orogenic Belt. Siberia Plate: S1, Nurt Late Devonian-Early Carboniferous volcanic basin; S2, Koktokay Palaeozoic magmatic arc; S3, Kelan Devonian-Carboniferous fore-arc basin; S4, Armantay-Erqis accretionary wedge. Kazakhstan Plate: K1a, Zharma-Sawur island arc; K1b, Western Junggar accretionary complex; K1c, Eastern Junggar accretionary complex; K1d, Junggar Mesozoic-Cenozoic basin; K1e, Yelianhabirga Late Palaeozoic back-arc basin; K1f, Bogada Late Palaeozoic aulacogen; K1g, Harlike Palaeozoic island arc; K1h, Dananhu-Queershan island arc; K1i, Turpan Mesozoic-Cenozoic basin; K2a, Sayram massif; K2b, Wenquan terrane; K2c, Boloholo Palaeozoic arc-basin system; K2d, Yamansu-Heiyingshan Palaeozoic arc-basin system; K2e, Ili Carboniferous-Permian rift; K2f, central Tianshan pre-Devonian massif; K2g, Nalati pre-Devonian massif. Tarim Plate: T1, Tarim Mesozoic-Cenozoic basin; T2a, Kuruktag Precambrian massif; T2b, Muzart massif; T3, Kalatierek Late Palaeozoic passive marginal sediments; T4a, Southwest Tianshan Late Palaeozoic fold-and-thrust belt; T4b, Southern Tianshan (or Kumishi) Palaeozoic accretionary complex. B1, Hanshan arc with Precambrian basement; B2, Mazongshan arc; B3, Shuangyingshan Carboniferous-Permian basin-arc system; B4, Huaniushan arc; B5, Shibanshan arc; B6, Duanhuang Precambrian massif.

earlier than 365 Ma. This intperetation is supported by a SHRIMP zircon U–Pb age of 374 ± 4 Ma obtained from the granodiorite stock which was considered as ore-causative intrusion (Xie et al., 2013). However, the granodiorite porphyry yields a group of zircon U–Pb ages ranging from 346 ± 1.2 Ma to 362 ± 12 Ma (Table 2). These ages accord well with a molybdenite Re–Os isochron age of 359 ± Ma, and thus many reseachers (Li et al., 2006b; Zhang et al., 2009a; Xue et al., 2011) believed that the Lailisigaoer porphyry Cu-Mo deposit was formed in a subduction-related magmatic arc.

3.6. Eastern Tianshan

The Eastern Tianshan is topographically between the Junggar Basin in the north and Tarim Basin in the south. It is an important component of the CAOB constructed through a prolonged Paleozoic accretionary orogeny and the Permian-Triassic continental collision (Chen, 2000; Xiao et al., 2009b). Four epochs of granitoids have recongnised (Zhou et al., 2010), namely, the Devonian (386.5–369.5 Ma) in Jingerquan area, Early Carboniferous (349–330 Ma) in Tuwu-Yandong and Changtiaoshan-Bailingshan areas, Late Carboniferous–Permian (320–252 Ma) and Triassic (246–230 Ma) in the Kanggur-Yamansu basin-arc system. The main structures in the area are characterized by a series of approximately EW-trending faults including the Dacaotan, Kanggur, Yamansu and Shaquanzi-Aqikuduke faults (Ma et al., 1993). The Eastern Tianshan is subdivided into three tectonic units: from north to south, (1) the Bogeda–Harlik volcanic arc system (K1f, K1g and K1h in Fig. 1) which is partly covered by the Turpan Basin (K1i in Fig. 1), (2) the Kanggur-Yamansu-Heiyingshan arc-basin system (K2d in Fig. 1), and (3) the Central Tianshan Massif (K2f in Fig. 1). These tectonic units have different rock associations and host distinct mineralizations (Pirajno et al., 2011; Qin et al., 2011; Chen et al., 2012b).

The Bogeda–Haerlike volcanic arc system comprises well-developed Ordovician–Carboniferous volcanic rocks, granites and mafic–ultramafic intrusions and contains a lot of Cu and Au deposits or prospects. The Dananhu–Tousuquan area is widespread of Devonian to Carboniferous basaltic to andesitic volcanic rocks and intrusive rocks, which is locally overlain by the Lower Carboniferous carbonates and calcareous mudstones (Mao et al., 2005). In this area, the Tuwu, Yandong, Chihu, Yuhai and Sanchakou porphyry Cu-Mo deposits have been discovered. All these deposits were foemed in the Late Paleozoic.

The Yamansu–Heiyingshan arc-basin system is characterized by Palaeozoic volcanic and sedimentary rocks that are intruded by voluminous Carboniferous–Triassic felsic and mafic–ultramafic complexes (Zhou et al., 2010). This unit was strongly deformed and known as Kanggur shear zones, consisting mainly of greenschists, mylonites and tectonites, hosting a number of orogenic-type Au deposits (e.g., Kanggur) and magmatic Cu-Ni sulfide deposits (e.g., Huangshan and Huangshandong). In last decade, two giant porphyry Mo deposits (Donggebi and Baishan) were reported (Wu et al., 2017b).

The Central Tianshan Massif comprises pre-Dovonian or Precambrian basement that is overlain by Late Palaeozoic volcanic rocks and intruded by Palaeozoic to Triassic granitoids, and hosts some hydrothermal magnetite (e.g. Tianhu iron deposit) and Mo-W deposits such as Kumutage Mo and Xiaobaishitou W-Mo skarn systems (BGMRX, 1993; Qin et al., 2011; Shen et al., 2014a). The Kumutage skarn Mo deposit was formed in the Late Carboniferous, but the Xiaobaishitou skarn W-Mo deposit formed in Triassic (Deng et al., 2016).

The Mo deposits in Eastern Tianshan are dominantly porphyry-type, followed by skarn type. Three of four Mo-only or Mo-W deposits were formed in the Triassic, whilst all the porphyry Cu-Mo deposits were formed the Late Palaeozoic.

3.7. Beishan

The Beishan Orogen is an EW-trending mountain belt with peaks up to 2000 m in easternmost Xinjiang, Gansu and Inner Mongolia in northwestern China. It is separated from the Chinese Tianshan Orogenic Belt by the NE–trending Hongliuhe Fault to the west and from the Inner Mongolian Orogenic Belt by the Cenozoic Badain Jaran Desert to the east. To the south is the Dunhuang Block, which has an Archean basement possibly linked to the Tarim Craton and to the north is the Southern Mongolian Accretionary System, a part of the CAOB (Xiao et al., 2010). It is traditionally divided into the following tectonic units (e.g. Gong et al., 2003; Guo et al., 2012; He et al., 2002; Xiao et al., 2010; Zuo et al., 1990, 1991), from north to south: the Dananhu-Queershan Silurian–Permian island arc (K1h, a part of the Bogeda–Harlik arc system), the Kanggur-Yamansu-Heiyingshan arc-basin system (K2d), the Hanshan arc with Precambrian basement (B1), the Carboniferous Mazhongshan arc (B2), the Shuangyingshan Carboniferous-Permian basin-arc system (B3), the Huaniushan Ordovician–Permian arc (B4), Shibanshan Carboniferous–Permian volcanic arc (B5), and the Duanhuang Precambrian massif (B6).

The structure of the Beishan belt is complicated due to the effects of multiple subduction, accretion and collision from the Cambrian to Permian (Xiao et al., 2010), when superposed folds, magmatic intrusions and faults formed. The long history of magmatism during the evolution of the Paleo-Asian Ocean produced many igneous rocks in the Beishan Orogen. The granitic magmatism mainly occurred in two major periods of the Silurian to Early Devonian (mid-Palaeozoic) and the Late Permian to Triassic (Mu et al., 1992; Zhang et al., 2012c,d; Zheng et al., 2012b, 2013; Li et al., 2012a). A majority of the Paleozoic intrusions have the mineralogical and geochemical features of post-collisional granites. This similarity has been used to constrain the collision time of the Beishan belt, leading to inconsistent interpretations of the tectonic settings. As a result, the time of continental collision in the Beishan Orogen varies from pre-Devonian (Zheng et al., 2012b) to Late Carboniferous (Zhang et al., 2012a) or later (Xiao et al., 2010).

The Mo deposits in Beishan Orogen are dominantly porphyry-type (Peng et al., 2010; Nie et al., 2002, 2005; Yang et al., 2013c), with the Huaheitan quartz vein W-Mo deposit being the only one exception (Zhu et al., 2014). Available isotope age data show that the Mo-dominated and Moly-only deposits were formed in the Indosian Orogeny (200–260 Ma), and possibly related to continental collision; the only one Cu-Mo system, i.e. Elegen, formed at ca. 332 Ma (Table 2), was likely generated by the subduction-related arc magmatism.

4. Ore geology and geochemistry

4.1. Host rocks

In the Altay Shan, three Cu-Mo deposits are hosted in the volcanic lava, tuff and pyroclastic rocks interclated with tuffaceous siltstone, shale, sandstone and carbonate of Middle Devonian Beitashan Fm. and Early Carboniferous Nanmingshui or Jiangbasitao Formations. The only one Be-Mo deposit is hosted in the quartz-mica schist, biotite gneiss and migmatite within the Late Ordovician Habahe Group.

In the Western Juggar orogenic belt, the giant Suyunhe porphyry Mo system is hosted in the Middle Devonian Barluk Group that consists of tuff, andesitic tuff, and breccia-bearing tuff. The Hongyuan porphyry Mo deposit and Baogutu porphyry Cu-Mo deposit are hosted the Early Carboniferous Baogutu Formation, which composed of volcaniclastic, tuffaceous siltstone and siliceous siltstone. In the Eastern Juggar, the Mengxi deposit is hosted in the Ordovician Huangcaipo Group metamorphosed crystal tuff, andesite, siltite and quartz schist and felsic hornfels.

In the Western Tianshan, three Cu-Mo deposits are hosted in Late Devonian Late Devonian lava, tuff, tuffaceous breccia and pyroclastic rocks intercalated with siltstone, silty mudstone. The Lailisigaoer deposit, which is the oldest one in Western Tianshan, is hosted in a Late Silurian fine-grained clastic-carbonate sequence; whilst the Kendenggaoer skarn Cu-Mo deposit occurs in a Carboniferous clastic-carbonate sequence.

Table 2
Isotopic ages of Mo deposits in NW China.

No	Deposits	Porphyry/ore	Num	Method	Age (Ma)	Reference
1	Suoerkuduke	Trachydacitic porphyry	1	SHRIMP zircon U-Pb	387.6 ± 1.8	Zhao et al. (2015)
		Trachydacitic porphyry	1	SHRIMP zircon U-Pb	383.8 ± 1.7	Zhao et al. (2015)
		Molybdenite	7	Re-Os isochron	317.1 ± 7.6	Liu et al. 2013
		Molybdenite	8	Re-Os isochron	305 ± 7	Wan et al. (2014)
2	Xilekuduke	Granite porphyry	1	SHRIMP U-Pb	329.6 ± 4.1	Long et al. (2009)
		Molybdenite	8	Re-Os isochron	327.1 ± 2.9	Long et al. (2011)
3	Yulekenhalasu	Granodiorite porphyry	1	SIMS zircon U-Pb	265.6 ± 3.7	Zhao et al. (2009)
		Monzonitic granite porphyry	1	SIMS zircon U-Pb	381.6 ± 2.5	Zhao et al. (2009)
		Mylonite	1	SIMS zircon U-Pb	362.5 ± 4	Xiang et al. (2012)
		Molybdenite	3	Re-Os isochron	331.5 ± 4.8	Xiang et al. (2012)
		Molybdenite	3	Re-Os isochron	357.3 ± 5.2	Xiang et al. (2012)
		Molybdenite	3	Re-Os isochron	371.3 ± 1.7	Xiang et al. (2012)
4	Asikaerte	Nuscovite albite granite	1	LAICPMS zircon U-Pb	219.2 ± 2.9	Wang et al. (2015a)
		Muscovite albite granite	1	LAICPMS zircon U-Pb	222.6 ± 4.6	Wang et al. (2015a)
		Pegmatite	1	LAICPMS zircon U-Pb	218.2 ± 3.9	Wang et al. (2015a)
		Molybdenite	6	Re-Os isochron	218.6 ± 1.3	Wang et al. (2015a)
		Molybdenite	7	Re-Os isochron	228.7 ± 7.1	Liu et al. (2015)
5	Suyunhe	Granite	3	LAICPMS zircon U-Pb	309.3 ± 3.3, 310.2 ± 1.3, 309.5 ± 1.5	Zhong et al. (2015b)
		Granite	1	LAICPMS zircon U-Pb	308.8 ± 4.1	Yang et al. (2015a)
		Molybdenite	5	Re-Os isochron	294.4 ± 1.7	Zhong et al. (2015a)
6	Baogutu	Diorite	1	LAICPMS zircon U-Pb	320.1 ± 2.2	Li et al. (2014)
		Granodiorite porphyry	1	LAICPMS zircon U-Pb	309.8 ± 2.2	Li et al. (2014)
		Quartz diorite porphyry	2	LAICPMS zircon U-Pb	314.9 ± 1.7, 309 ± 1.9	Tang et al. (2009)
		Diorite porphyry	1	LAICPMS zircon U-Pb	313.9 ± 2.6	Tang et al. (2009)
		Intrusive body	2	SHRIMP zircon U-Pb	312.8 ± 2.9, 319 ± 3	Wei and Zhu (2015)
		Molybdenite	2	Re-Os isochron	310 ± 3.6	Song et al. (2007)
7	Hongyuan	Porphyraceous granodiorite	2	LAICPMS zircon U-Pb	300.8 ± 3.6, 302.2 ± 3.1	Li (2013)
		Molybdenite	5	Re-Os isochron	294.6 ± 4.6	Li (2013)
		Molybdenite	9	Re-Os isochron	314.3 ± 1.9	Yan et al. (2014)
8	Mengxi	Granite porphyry	1	LAICPMS zircon U-Pb	410 ± 11	Wang et al. (2013)
		Granite porphyry	1	LAICPMS zircon U-Pb	413.2 ± 3.9	Qu (2011)
		Molybdenite	6	Re-Os isochron	411.6 ± 3.2	Qu et al. (2009)
9	Dabate	Rhyolite	1	SHRIMP zircon U-Pb	315.9 ± 5.9	Zhang et al. (2008d)
		Granite porphyry	1	SHRIMP zircon U-Pb	278.7 ± 5.7	Zhang et al. (2008d)
		Granite porphyry	1	SHRIMP zircon U-Pb	288.9 ± 2.3	Tang et al. (2008)
		molybdenite	7	Re-Os isochron	301 ± 20	Zhang et al. (2006d)
		Molybdenite	6	Re-Os isochron	300.3 ± 2.1	Li (2012)
10	Kekesai	Granodiorite	1	SHRIMP zircon U-Pb	317± 6	Zhang et al. (2008e)
		Monzonitic granite	1	LAICPMS zircon U-Pb	301.9 ± 1.8	Zhu et al. (2011)
		Monzonitic granite	1	LAICPMS zircon U-Pb	305.5± 1.1	Zhang (2011)
		Granodiorite	1	LAICPMS zircon U-Pb	288.7 ± 1.5	Zhang (2011)
12	Lailisigaoer	Granodiorite	1	SHRIMP zircon U-Pb	374 ± 4	Xie et al. (2013)
		granodioritic porphyry	1	LAICPMS zircon U-Pb	346 ± 1.2	Xue et al. (2011)
		Granodioritic porphyry	1	LAICPMS zircon U-Pb	350 ± 0.65	Xue et al. (2011)
		Monzodioritic porphyry	1	LAICPMS zircon U-Pb	354 ± 0.65	Zhang et al. (2009a)
		Granodioritic porphyry	1	LAICPMS zircon U-Pb	346 ± 1.2	Zhang et al. (2009a)
		Granodioritic porphyry	1	SHRIMP zircon U-Pb	362 ± 12	Li et al. (2006b)
		Granodioritic porphyry	1	Rb-Sr isochron	350 ± 15	Li et al. (2006b)
		Quartz	1	Rb-Sr isochron	341 ± 9	Li et al. (2006b)
		Molybdenite	5	Re-Os isochron	359 ± 8	Li et al. (2006b)
		Molybdenite	5	Re-Os isochron	379.9 ± 8.3	Zhu et al. (2010)
13	Kendenggaoer	Molybdenite	7	Re-Os isochron	313.9 ± 2.5	Jia et al. (2011)
14	Tuwu-Yandong	Porphyry	4	LAICPMS zircon U-Pb	348.3 ± 6.0, 339.3 ± 2.2, 323.6 ± 2.5, 324.1 ± 2.3	Xiao et al. (2015)
		Tonalite	1	SIMS zircon U-Pb	334.7 ± 3	Wang et al. (2014b)
		diorite Porphyry		SIMS zircon U-Pb	340.0 ± 3.0	Shen et al. (2014a, 2014b)
		Plagiogranite porphyry		SIMS zircon U-Pb	332.2 ± 2.3	Shen et al. (2014a, 2014b)
		Plagioclase granite porphyry	1	SIMS zircon U-Pb	338.3 ± 1.4	Guo et al. (2010)
		Andesite	1	SHRIMP zircon U-Pb	336.9 ± 8.3	Hou et al. (2005)
		Plagioclase granite porphyry	1	SHRIMP zircon U-Pb	333 ± 2, 334 ± 2	Liu et al. (2003)
		Granodiorite porphyry	1	Zircon U-Pb	356 ± 8	Qin et al. (2003)
		Plagiogranite porphyry		SHRIMP zircon U-Pb	333 ± 4	Chen et al. (2005)
		Granodiorite porphyry	1	SHRIMP zircon U-Pb	361 ± 8	Rui et al. (2002b)
		Molybdenite	6	Re-Os isochron	343 ± 26	Zhang et al. (2008a)
		Molybdenite	7	Re-Os isochron	323 ± 2	Rui et al. (2002b)
15	Kumutage	Molybdenite	5	Re-Os isochron	319.1 ± 4.5	Zhang et al. (2010a)
16	Chihu	Plagiogranite	1	SHRIMP zircon U-Pb	322 ± 10	Wu et al. (2006b)
		Granodiorite porphyry	1	SHRIMP zircon U-Pb	322 ± 3	Liu et al. (2003)
17	Donggebi	Porphyritic granite	1	LAICPMS zircon U-Pb	237 ± 4.7	Wu et al. (2013a)
		Granite porphyry	1	LAICPMS zircon U-Pb	233.2 ± 4.1	Wu et al. (2013a)
		Molybdenite	5	Re-Os isochron	233.2 ± 2.2	Wu et al. (2013a)
		Molybdenite	7	Re-Os isochron	231.1 ± 1.5	Tu et al. (2012)
		Molybdenite	8	Re-Os isochron	231.9 ± 6. 5	Wu et al. (2013b)
		Molybdenite	8	Re-Os isochron	234.3 ± 1.6	Han et al. (2014)
18	Yuhai	Diorite	1	LAICPMS zircon U-Pb	441.6 ± 2.5	Wang et al. (2016b)
		Granodiorite	1	LAICPMS zircon U-Pb	430.4 ± 2.9	Wang et al. (2016b)

Table 2 (*continued*)

No	Deposits	Porphyry/ore	Num	Method	Age (Ma)	Reference
		Granodiorite	1	SHRIMP zircon U-Pb	422.3 ± 4	Zhang et al. (2016)
		Molybdenite	4	Re-Os isochron	355.7 ± 2.4	Wang et al. (2016b)
19	Sankakou	Plagiogranite	1	SHRIMP U-Pb	278 ± 4	Li et al. (2004)
20	Xiaobaishitou	Granite	2	LAICPMS zircon U-Pb	242 ± 1.7, 240.5 ± 2.1	Deng et al. (2016)
		Molybdenite	6	Re-Os isochron	239.7 ± 3.6 to 251.4 ± 3.6	Deng et al. (2016)
21	Baishan	bioTite plagioclase granite	1	SHRIMP zircon U-Pb	239 ± 8	Li et al. (2006a)
		Granite porphyry	1	LAICPMS zircon U-Pb	228.1 ± 8	Zhang et al. (2015a)
		Molybdenite	8	Re-Os isochron	224.8 ± 4.5	Zhang et al. (2005)
		Molybdenite	7	Pyrite Re-Os	225 ± 12	Zhang et al. (2005)
		Molybdenite	6	Re-Os isochron	229 ± 2	Li et al. (2006a)
		Molybdenite	8	Re-Os isochron	227 ± 4.3	Zhang et al. (2009b)
		Molybdenite	7	Re-Os isochron	223.5 ± 3.2 to 227.5 ± 3.1	Tu et al. (2014)
23	Huaheitan	Huaniushan moyite	1	LAICPMS zircon U-Pb	229.5 ± 2.6	Zhu et al. (2013a)
		Molybdenite		Re-Os isochron	225.6 ± 2.2	Zhu et al. (2013a)
25	Liushashan	Molybdenite	6	Re-Os isochron	260 ± 10	Nie et al. (2002)
26	Elegen	Molybdenite	5	Re-Os isochron	332 ± 9	Nie et al. (2005)
27	Xiaohulishan	Granite	1	Zircon U-Pb	246.8 ± 1.7	Yang et al. (2012a)
		Molybdenite	6	Re-Os isochron	220 ± 2.2	Peng et al. (2010)
		Molybdenite	3	Re-Os isochron	213.2 ± 4.6	Zhang et al. (2012d)

In Eastern Tianshan, all the porphyry Cu-Mo or Mo-only deposits are hosted in the Carboniferous volcanic-sedimentary succesions. However, the clastic sediment-dominated unit, e.g., the Gandun Formation, is favorable for the Mo-only deposits (Donggebi and Baishan); by contrast, the volcanic rock-dominated unit is favorable the Cu-Mo systems, as exemplified by the four deposits in the Dananhu arc (Nos. 14, 16, 18, and 19), which are hosted in spilite-keratophyre sequence. The Xiaobaishitou skarn W-Mo deposit is hosted in the Mesoproterozoic metamorphic rocks. The Kumutage skarn-type Mo deposit is mainly hosted by a Late Paleozoic gabbro.

In the Beishan orogen, four of six deposits are hosted in pre-Devonian metamorphosed volcanic-sedimenary rocks, and the other two deposits (Hongshanjing and Liushashan) are hosted in the Carboniferous tuffaceous slate, tuffaceous phyllite, rhyolite, dacite and tuff.

To sum up, (1) the host rocks of the Mo-bearing deposits are variable in lithologies. (2) The majority of Cu-Mo deposits are hosted in Late Palaeozoic volcanic-sedimentary sequences, with the Mengxi, Lailisigaoer and Elegen being the exceptions which are hosted in pre-Devonian rocks; by contrast, as shown by the scenarios in Altay, Eastern Tianshan and Beishan areas, the pre-Devonian rocks are more favorable for Mo mineralization. (3) The sediment-dominated sequences are more favourable for Mo mineralization than the volcanic rock-dominated lithostratigraphic units; moreover, felsic rocks are more favaorable for Mo mineralization than the mafic rocks. These phenomena can be clearly shown by comparing the contexts of giant Baishan and Donggebi Mo systems with those of the porphyry Cu-Mo deposits in the Dananhu arc, or comparing the Sunyunhe and Hongyuan Mo deposits with the Baogutu Cu-Mo deposit.

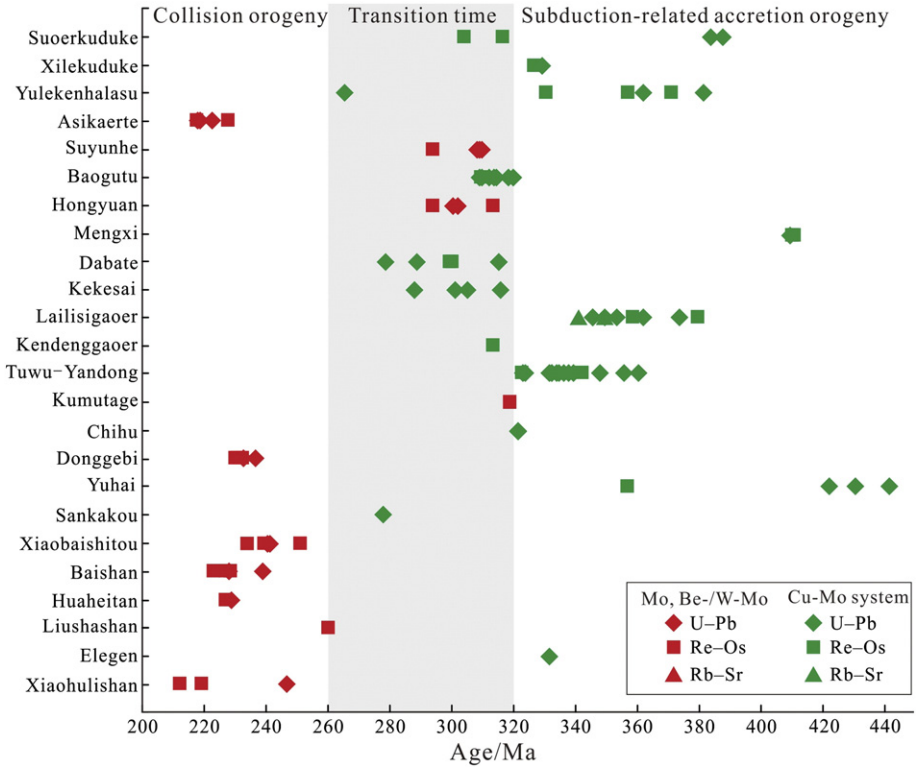

Fig. 2. Isotopic ages of Mo deposits and causative magmatites in the NW China.

4.2. Structures and orebody occurrence

The regional faults control the location of the granitic intrusions, and their subsidieary structures control the occurrences of orebodies. Regional faults and their subsidiary structures are generally NE-, NW- and E-W-trending. The intersections of faults are favorable for hydrothermal mineralization, particularly for location of high-grade orebodies, as exemplified by the combinations of the E-W- and NE-trending faults in the Suyunhe and Kumutage deposits, the NW-trending faults in the Suoerkuduke deposit, the NE-trending faults in the Tuwu-Yandong ore field, and the NE- and NW-trending faults in the Huanangou deposit.

The orebodies are mainly stratiform, veins, and lens in shape, and usually occur in ore-related porphyries and/or in the contact zones between the porphyries and wallrocks. The spatial relationships of orebodies with the causative intrusions include three types: (1) orebodies completely occur within the causative porphyries, as shown in the Hongyuan Mo deposit, Lilisigaoer and Tuwu-Yandong Cu-Mo deposit; and (2) orebodies commonly occur in the contact zones or cover across the porphyry to wall-rocks, e.g., the Baogutu and Mengxi porphyry Cu-Mo deposits; and (3) orebodies completely occur within the hostrocks, some times, distal to the causative porphyries, e.g., the Baishan and Donggebi Mo deposit.

4.3. Wallrock alteration

The porphyry-type deposits show similar wallrock alteration, including potassic, silica, phyllic, propylitic and argillic alteration. The hydrothermal alteration is usually zoned outward from potassic alteration, to a zone of silicification and sericitization, and to the outermost propylitization, from planar infiltration metasomatism to linear injection, and from alkali metasomatism to acidic leaching.

The potassic alteration usually occurred in deep and center part of the porphyry stock, which is characterized by secondary biotite, K-feldspar and quartz. The potassic alteration is closely related to the Mo, W, Be and Cu or Au mineralization. The phyllic alteration (quartz, sericite, chlorite and epidote) is developed in the outer part of the potassic alteration zone, and usually overprints part of the potassic alteration zone. The propylitization is usually developed in the wallrocks, characterized by large amounts of chlorite, epidote and calcite, with weak Mo-Cu mineralization. The argillic alteration is usually structurally-controlled, dominated by kaolinite, occurring as linear injection metasomatism.

The quartz vein-type mineralization usually show similar wallrock alteration and zoning to the porphyry-type. The porphyry-skarn system commonly shows porphyry-style alteration in the causative porphyry, and the skarn assemblages in the contact zones. The skarn-type orebodies, as exemplified by the Xiaobaishitou W-Mo deposit (Deng et al., 2016), show five-stage hydrothermal mineral assemblages: from early to late, (1) prograde skarn mainly composed of garnet and diopside, associated with scheelite; (2) retrograde skarn marked by actinolite and epidote, often associated with oxides that are also grouped into a later stage; (3) quartz-oxide assemblage, represented by magnetite and minor molybdenite; (4) quartz-sulfide veinlets containing molybdenite; and (5) quartz-carbonate-fluorite veinlets.

4.4. Fluid inclusions

Fluid inclusions (FIs) are the "fossils" of ancient fluid systems and can be used as diagnostic markers of different types of hydrothermal deposits (Chen et al., 2007c; Pirajno, 2009, 2013). The fluids are composed mainly of H_2O and CO_2 (or CH_4), with variable salinity (contents of solutes). According to Chen (2010, 2013) and Chen et al. (2014), the epizonogenic fluids originated at depths of <10 km and temperatures of <300 °C (under a geothermal gradient of 30 °C/km) are characterized by low salinity and CO_2-poor. The metamorphic fluids originated from regionally metamorphic devolatilization at depths of >10 km and temperatures of >300 °C are characterized by CO_2-rich and low salinity, commonly form structurally-controlled orogenic-type lode systems, as exemplified by the orogenic-type gold deposits in the world (Goldfarb et al., 2014 and references therein). The magmatic fluids, exsolved from magmas commonly generated at depths of >20 km and temperatures of >600 °C, are characterized by high salinity.

The magmatic hydrothermal systems in volcanic arcs are originally related to subduction of the H_2O-rich oceanic slab, and contain aqueous (W-type) and daughter mineral-bearing aqueous (SW-type) inclusions, but little or no carbonic-aqueous (C-type) inclusions, because the activity of CO_2 is far lower than the H_2O (Chen et al., 2007c). By contrast, the intracontinental magmatic hypothermal systems have been proven to contain carbonic aqueous (C-type), pure carbonic (PC-type) and daughter mineral-bearing carbonic-aqueous (SC-type) inclusions (Chen and Li, 2009; Pirajno and Zhou, 2015), which results from that the continental crust is drier and carbonate-richer than the oceanic crust. It is concluded that the intracontinental magmas and magmatic hydrothermal deposits have higher CO_2/H_2O ratios than those in island and/or continental arcs (Chen et al., 2007c; Chen and Li, 2009). Therefore, fluid inclusions (FIs) can be a key indicator of the classification of porphyry Mo deposits (Chen and Wang, 2011; Li et al., 2012b; Yang et al., 2012c, 2013b, 2015b, 2017b; Wu et al., 2014; Wang et al., 2014a; Chen et al., 2017a; and references therein).

The Endako-type or subduction-related porphyry Mo deposits formed in continental magmatic arcs, exemplified by Endako and MAX in Columbia, Canada (Linnen and Williams-Jones, 1990; Selby et al., 2000; Lawley et al., 2010), contain little or no fluid inclusion of C- or SC-types. The Climax- or rift-type porphyry Mo deposits, developed in continental or back-arc rifts, generally contain C-type FIs, such as the Climax and Urad-Henderson deposits, Colorado, USA (Seedorff and Einaudi, 2004a,b). The Dabie- or collision-type porphyry systems formed in a syn- to post-collisional tectonic setting, represented by the Yanshanian porphyry Mo deposits in the Dabie Shan and Qinling Orogen, always contain abundant C-type FIs, often together with FIs of the C-, SC- and/or multiple mineral-bearing carbonic-aqueous types (Chen et al., 2017a and references therein).

The fluid inclusion study of the Mo deposits in NW China is still poor, which detracts from the understanding of the ore genesis. In spite of the paucity of available data, two types of ore systems can be delineated based on the fluid inclusion characteristics in NW China (Table 3). The majority of Hercynian porphyry-type deposits, such as the Suyunhe (294.4 ± 1.7 Ma; Zhong et al., 2015b) and Hongyuan (294.6 ± 4.6 to 314.3 ± 1.9 Ma; Li, 2013; Yan et al., 2014) Mo deposits in Western Juggar, the Tuwu-Yandong Cu-Mo deposit (322 ± 3 to 323 ± 2 Ma; Rui et al., 2002b; Han et al., 2006b) in Eastern Tianshan, and the Kendenggaoer Cu-Mo deposit (313.9 ± 2.5 Ma; Jia et al., 2011) in Western Tianshan, only contain fluid inclusions of the W- and S-types, and can be assigned to Endako-type porphyry deposits represented by the Diyanqinamu (Wang et al., 2017a) and Chalukou (Zhang and Li, 2016) deposits in Great Hingan Range and Zhaiwa deposit (Deng et al., 2013a,b) in Qinling Orogen, China. The initial ore-forming fluids were high-temperature (up to 590 °C), high-salinity (up to 58.41 wt% NaCl) and CO_2-poor. A small group of the Hercynian porphyry Cu-Mo deposits, such as the Lailishigaoer (359 ± 8 to 372.5 ± 5.0 Ma; Li et al., 2006b; Zhu et al., 2010) in Western Tianshan, the Xilekuduke (327.1 ± 2.9 Ma; Long et al., 2011) and Yulekenhalasu (331.5 ± 4.8 to 371.3 ± 1.7 Ma; Xiang et al., 2012) in Altay Shan, containing only a few C-type FIs, are also compareable with the subduction- or Endako-type porphyry deposits. Alternately, the Lailisigaoer deposit was suggested to have developed in a post-collisional setting (Zhu et al., 2010).

The Indosinian porphyry Mo deposits, e.g. the Baishan (229 ± 2 Ma; Li et al., 2006a) and Donggebi (234.3 ± 1.6 to 231.1 ± 1.5 Ma; Wu et al., 2013a,b) systems, contain the multiple mineral-bearing CO_2- or CH_4-rich FIs, in addition to the FIs of the W-, S- and C-typse (Wu et al., 2014), suggesting that the ore-forming fluids were originally high-temperature, high-salinity, high-pressure and CO_2-rich. The features of the Indosinian Mo deposits are shared by numerous magmatic-

Table 3
Types and microthermometric data of fluid inclusions of several Mo deposits in NW China.

No.	Deposit	Fl type	Th (C°)	Salinity (wt.% NaCl eqv.)	Density (g/cm^3)	pressure (MPa)	Depth (km)	Reference
Indosinian Mo deposits (Dabie-type)								
	Baishan	WL, WV, S, C1, C2	140–420	0.3–6.1	0.47–1.05	15–285	1.5–3.9	Xiang et al. (2013)
	Donggebi	WL, WV, S, C1	152–443	1.8–9.3	0.47–0.99	8–193	5.6–7.9	Wu et al. (2014)
Hercynian Mo deposits in NW China (Endako-type)								
	Suyunhe	WL, WV, S	153–>530	1.2–63.9	0.38–1.26	55.8–143	1.9–4.8	Zhong et al. (2015a)
	Hongyuan	WL, WV, PV, S	145–460	0.2–11.7	0.75–0.92	45.6–78.6	1.5–2.6	Yan et al. (2014)
	Baogutu	WL, WV, PV, S	173–495	0.9–58.4	0.65–1.15	12.6–95.0	0.4–3.2	Shen et al. (2010)
	Lailisigaoer	WL, S, C1, PC	118–395	0.02–52	0.47–1.46	17.0–59.0	1.7–2.2	Zhu et al. (2012)
	Kendenggaoer	WL, PV	100–286	2.7–14.7	0.76–1.04	7.8–26.7	0.8–2.7	Jia (2011)
	Dabate	WL, WV, S	170–390	1.9–18.4	0.58–1.01	14.4–35.7	0.5–1.3	Li (2012)
	Xilekuduke	WL, C1, S	130–590	2.1–63.9				Wang et al. (2009)
	Yulekenhalasu	WL, WV, PV,C1	111–419	3.1–15.0	0.59–1.02			Geng et al. (2013)

Fluid inclusion type: WL: liquid-rich aqueous inclusion; WV: vapor-rich aqueous inclusion; PV: pure vapor inclusion, PC: pure CO_2 inclusion; C1: CO_2-H_2O inclusion; C2: CH_4–H_2O inclusion; S: daughter mineral-bearing inclusion.

hydrothermal deposits formed in intracontinental tectonic settings in China (Chen et al., 2009; Chen and Li, 2009; Pirajno and Zhou, 2015), as exemplified by the Mo deposits at Yuchiling (Li et al., 2012b), Sandaozhuang (Shi et al., 2009), Nannihu (Yang et al., 2012c), Shangfanggou (Yang et al., 2013a), Jinduicheng (Yang et al., 2009b), Tumen (Deng et al., 2013c) and Shimengou (Deng et al., 2011) in East Qinling Mo Belt. This shows that the Indosinian Mo deposits can be assigned to the Dabie- or collision-type.

4.5. Hydrogen-oxygen isotopes

The $\delta^{18}O$ and δD signatures are powerful tracers to constrain the ore-fluid sources. The data for the Mo systems in NW China are summarized in Table 4 and illustrated in Fig. 3. The analyzed $\delta^{18}O_{mineral}$ values range 5.6–16.8‰, yielding calculated $\delta^{18}O_{H2O}$ values between −2.8 and 9.3‰; and the δD_{H2O} values are between −137 and −44 ‰. Most of the data obtained from the hydrothermal minerals are plotted in or adjacent to the box of primary magmatic water, indicating that the fluids were predominantly sourced from magmatism. The other samples are plotted between the magmatic water box and the meteoric water line, suggesting that the fluids possibly mixed with meteoric water. The input of the meteoric water could reduce the $\delta^{18}O$ values. Combined with the data from fluid inclusion studies, it is concluded that the ore-fluids evolved from high-temperature, high-salinity, CO_2-rich magmatic to low-temperature, low-salinity, CO_2-poor meteoric water, through fluid boiling and mixing. Indeed, involvement of meteoric water in late mineralization stage could not be precluded in the hypothermal mineralization, particularly on the margin of a metallogenic system where the advecting magmatic fluids may entrain convecting meteoric water (Sillitoe, 2010), and thus the diagnostic features of a hydrothermal system can only be observed in the early mineralization stages (Chen, 2010).

4.6. Sulfur isotope

The $\delta^{34}S$ ranges and their averages of each Mo deposit in NW China are listed in Table 5 and illustrated in Fig. 4. Available data show that the $\delta^{34}S$ averages of individual deposit fall in the range of −2.5 to 6.3 ‰ (Fig. 4), similar to that of the granitic rocks (Hoefs, 2009) and porphyry Mo deposits worldwide, such as the Climax-type Mo deposits (0.8–6.8‰) (Carten et al., 1993), which are typical of magmatic hydrothermal systems (0 ± 5‰, Ohmoto and Rye, 1979; Hoefs, 2009). Hence the $\delta^{34}S$ isotope compositions indicate that, most Mo deposits in NW China are magmatic hydrothermal in origin.

The $\delta^{34}S$ ranges of somen deposits also show a contribution from the hostrocks. For example, the Mo-bearing quartz veins at the Huaheitan deposit are mainly hosted in the Mesoproterozoic metamorphic rocks, whose sulfide $\delta^{34}S$ values are low to −9.5‰ (Table 5), suggesting a significant contribution from the organic carbon-bearing hostrocks within the Mesoproterozoic Pingtoushan Group. The sulfide $\delta^{34}S$ values of the Xilekuduke deposit are up to 13.9‰, suggesting a contribution from sulfate sulfur possibly in the hostrocks. This deposit is hosted in the Early Carboniferous Nanmingshui Formation which is composed of tuffaceous siltstone, sandstone, silty limestone, chert and tuff. Obviously, the development of chert and silty limestone indicate the possibility of sulfate in the hostrocks.

Table 4
The oxygen and hydrogen isotopic ratios of the Mo deposits in NW China.

Deposit	Host mineral	Sample number	$\delta^{18}O_{mineral}$ (‰)	$\delta^{18}O_{H2O}$ (‰)	δD_{H2O} (‰)	Data source
Suyunhe	Qz	7	6. 6–11. 4	0. 1 – 8. 1	−119 to −95	Zhong et al. (2015a)
Hongyuan	Qz	6	5.6–9.8	0.0 – 7.2	−92 to −84	Yan et al. (2015)
Baogutu	Qz	14	11.3–16.2	4.4 – 9.3	−107 to −86	Zhang et al. (2010d)
Lailisigaoer	Qz	7	10.6–11.8	-1. 3 – 5.5	−101 to −81	Xue et al. (2011)
Kendenggaoer	Qz	5	13.2–16.8	-2.8 – 3.7	−96 to −82	Jia et al. (2011)
Dabate	Qz	13	12.2–15.5	4.2-6.8	−104 to −83	Zhang et al. (2009d)
			13.2–16.3	3-8.4	−95 to −84	Li (2012)
Xilekuduke	Qz	3	9.5–9.7	2.6-2.8	−137 to −122	Guo et al. (2012)
Yulekenhalasu	Qz	11	9.9–13.2	1.4-6.8	−120 to −97	Yang et al. (2012d)
	Cal	1	9.1	2.1	−101	Yang et al. (2012d)
Baishan	Qz	4	9.1–10	3.4-4.3	−105 to −69	Zhang et al. (2009b)
Tuwu-Yandong	Qz	8	7.7–9.7		−69 to −44	Rui et al. (2002a)
	Ser	1	7		−66	Rui et al. (2002a)
	Chl	1	8		−48	Rui et al. (2002a)
	Ep	1	7		−52	Rui et al. (2002a)

Host mineral abbreviations: Cal–calcite; Chl–chlorite; Ep–epidote; Qz–quartz; Ser–sericite.

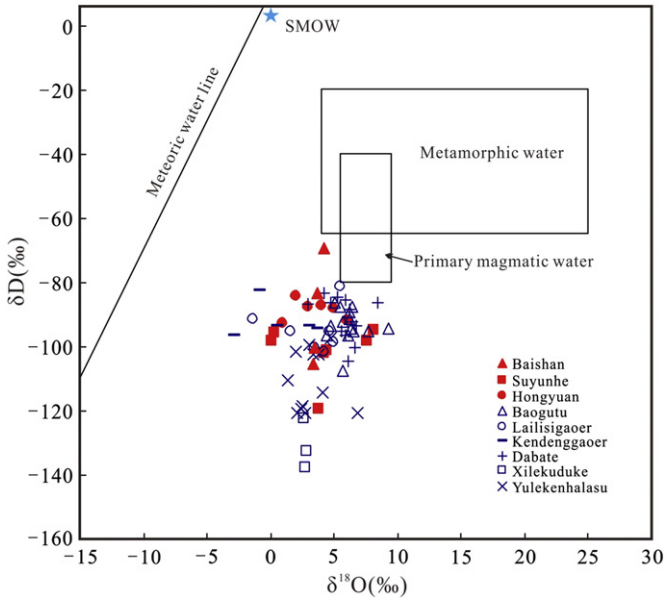

Fig. 3. The δD vs. $\delta^{18}O$ plot for the Mo deposits in the NW China (base map after Taylor, 1974).

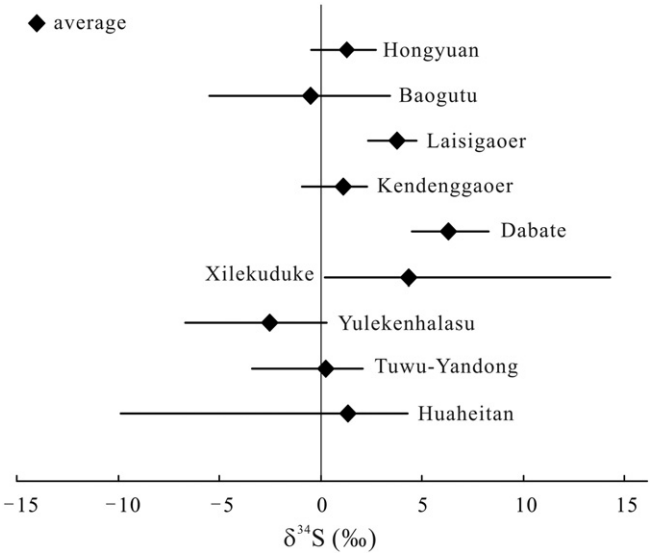

Fig. 4. Sulfur isotope compositions of the Mo deposit in NW China.

4.7. Molybdenite Re contents

The Re contents in molybdenite from different deposits can be used to trace the metal source (Stein et al., 2001; Mao et al., 1999). In general, the Re concentrations in molybdenites from porphyry systems originated from continental crust are lower than 50 ppm, whilst those originated from the mantle are higher than 100 ppm (Chen et al., 2017a,b; Zhong et al., 2017).

In NW China, the majority of Mo-only and Mo-dominated deposits, as well as the Be-Mo and W-Mo deposits, show molybdenite Re contents lower than 100 ppm, or even lower than 50 ppm, except for the Baishan Mo-Re deposit (Fig. 5, Table 6). This case is similar to those observed at the giant Donggou and Yuchiling Mo deposits in Qinling Orogen (Li et al., 2013c; Yang et al., 2015b) and the giant Qian'echong and Shapinggou Mo deposits in Dabie Shan (Mi et al., 2015; Ni et al., 2015), indicating that the Re, Mo and other metals were mainly sourced from the crust or sedimentary rocks. It is notable that most of the Re analyses of molybdenite samples from Baishan Mo-Re deposit are higher than 100 ppm, with an average of 190.4 ppm, which indicates a more contribution from the mantle or juvenile crust to the mineral system.

The Cu-Mo deposits show higher molybdenite Re contents than the Mo-only, Mo-dominated, and the W-Mo and Be-Mo systems (Fig. 5), suggesting a source with more contribution from the mantle. The Suoerkuduke, Xilekuduke, Baogutu, Mengxi, and Elegen Cu-Mo systems yield molybdenite Re concentrations higher than 100 ppm, suggesting a metal source dominated by the mantle. The Re contents in molybdenites from the Dabate and Tuwu-Yandong deposits range from <50 ppm to >100 ppm, with the majority higher than 100 ppm, which may suggest a source dominated by the mantle, but mixed with the continental crust.

The Lailisgaoer, Yuhai and Kendenggaoer Cu-Mo deposits have molybdenite Re contents lower than 100 ppm. The Kendenggaoer is a skarn system occurring in the Western Tianshan. The Re contents in molybdenite range from 11.1 to 59.7 ppm, and such a low value is definitely believed to indicate a contribution from the sedimentary rocks enclosing the Kendenggaoer skarn-type mineral system. The Lailisgaoer porphyry Cu-Mo deposit in Western Tianshan, whose mineralization setting is debated between the post-collisional tectonism (Zhu et al., 2010; Xie et al., 2013) and the subduction-related magmatic arc (Li et al., 2006b; Zhang et al., 2009a; Xue et al., 2011) because it was formed in Late Devonian, yield molybdenite Re contents of <100 ppm, ranging from 18.5 to 73.5 ppm. This deposit possibly originated from a source of crust-mantle mixture, but dominated by the crust. The Yuhai Cu-Mo deposit in Eastern Tianshan was formed in the earliest Carboniferous or earlier (Wang et al., 2016b), shew low Re contents of 21.4 to 83.1 ppm in molybdenites, and might originate from a crust-dominated source with contribution from the mantle.

5. Representative Mo deposits

5.1. Suyunhe porphyry Mo deposit

The Suyunhe Mo deposit (Fig. 6, Table 1), located 80 km southeast of Yuming town, is a recently discovered giant porphyry Mo deposit with proven reserve of 0.56 Mt Mo grading at 0.059–0.084%, in the western

Table 5
The $\delta^{34}S$ values of the Mo deposits in NW China.

Deposit	Number	$\delta^{34}S$ (‰)	Av.	Reference
Hongyuan	11	−0.1 to 2.3	1.3	Yan et al. (2015)
Baogutu	85	−5.1 to 3	−0.5	Cao et al. (2015), Shen et al. (2012), Zhang et al. (2010d), Song et al. (2007)
Laisigaoer	7	2.7 to 4.3	3.8	Xue et al. (2011)
Kendenggaoer	10	−0.6 to 1.9	1.1	Jia et al. (2011)
Dabate	6	4.9 to 7.9	6.3	Li (2012)
Xilekuduke	39	0.4 to 13.9	4.3	Long et al. (2015)
Yulekenhalasu	22	−6.3 to −0.1	−2.5	Yang et al. (2012d)
Tu–Yandong	32	−3 to 1.7	0.3	Wang et al. (2015b), Han et al. (2006b), Rui et al. (2002b)
Huaheitan	6	−9.5 to 3.9	1.3	Zhu et al. (2014)

part of the Barluk Mountain, Western Junggar (Zhong et al., 2015a). The Middle Devonian Baerluke Formation crops out in the mining area, and is composed predominantly of tuff, andesitic tuff and andesitic breccia-bearing tuff. The structures are dominated by the NE-trending fault, although ENE-, and NW-trending faults are also present (Shen et al., 2017).

The ore-associated intrusions comprise three small-sized outcrops and cover area of approximately 0.06 km^2, 0.07 km^2 and 0.03 km^2 respectively (Zhong et al., 2015b). Lithologies of the granites change from fine-grained, porphyritic monzogranite at depth, grading to pink monzogranite porphyry at shallow. The monzogranite porphyry contains phenocrysts of quartz, K-feldspar, plagioclase and biotite, and the matrix comprises fine-grained K-feldspar, plagioclase, quartz, and sericite. Dioritic porphyrite and felsite dikes can be observed in the Suyunhe deposit, trending NE and NW.

The orebodies have lenticular forms and have no distinct boundaries with country rocks, showing gradational contact relationships. Mo mineralization at Suyunhe is dominantly stockworks with minor dissemination. The thickness of the molybdenite-bearing veinlets ranges 0.5–2 cm in general, but a few up to 30 cm. Main ore minerals include molybdenite, scheelite, pyrite, and chalcopyrite, with minor chalcocite, bornite, ilmenite, and pyrrhotite. Gangue minerals are dominated by quartz, K-feldspar, plagioclase, and biotite. The Mo mineralization occurs mainly in quartz veins and veinlets (Shen et al., 2017).

As shown in Table 2, the timing of the Suyunhe Mo mineralization has been determined using different isotopic systems. Secondary ion mass spectrometry (SIMS) zircon U–Pb dating indicates that the deep monzogranite emplaced at 295.3 ± 3 Ma to 298.4 ± 1.9 Ma, and the shallow monzogranite (also called granodiorite by some local geologists) porphyry intruded at 293.7 ± 2.3 Ma to 294.7 ± 2.1 Ma (Shen et al., 2017). The LA-ICPMS zircon U–Pb ages of ore-causative granite porphyry are between 309.3 Ma and 310.2 Ma (Zhong et al., 2015b). The molybdenite samples yielded Re–Os ages of 293.3 ± 4.0 Ma to 296.8 ± 4.3 Ma, with a weighted mean age of 295.0 ± 1.5 Ma, which slightly postdates the magmatic activity (Zhong et al., 2015b).

The mineralization process was divided into three stages, based on vein crosscutting relationships, mineral assemblages and hydrothermal alterations. Stage 1 is characterized by the assemblage of quartz ± K-feldspar ± pyrite ± molybdenite veins. The sulfides occur as disseminations, with pyrite being idiomorphic cubes. Stage 2 is most conducive to Mo mineralization, and is characterized by the stockworks of quartz + molybdenite + other sulfides (including pyrite and chalcopyrite), associating with scheelite. Molybdenite is mainly disseminated in the phyllic (quartz + sericite) alteration zone. Stage 3 is characterized by quartz + calcite ± fluorite veinlets, with little or no pyrite and molybdenite (Zhong et al., 2015a).

5.2. Baishan porphyry Mo deposit

The Baishan porphyry Mo-Re deposit (Fig. 7 and Table 1) is located 140 km southeast of Hami city and 2 km south of the Kanggur Fault. The host rocks are composed of sedimentary rocks of the Lower Carboniferous Gandun Formation, including four members, in ascending sequence, they are: (1) siltstone and carbonaceous shale; (2) tuffaceous graywacke intercalated with tuff and basalt; (3) graywacke, tuff, and shale; and (4) siltstone, carbonaceous shale, and sandstone. The stratigraphic units are WNW-trending, dipping to ENE with an angle of 65–80°. The Gandun Formation was low-grade metamorphosed, and locally overprinted by deep-seated intrusive rocks (Zhang et al., 2005).

The granitic rocks in the Baishan deposit occur as stocks and dikes. The granite porphyry dikes exhibit minor pyrite and molybdenite mineralization. The ore-barren biotite plagioclase granite is 0.5 km southwest of the mining area, and locally cut by the granite porphyry dikes. In the prospecting district, small-sized quartz veins are present and containing molybdenite. The Mo mineralization mainly occurs along an E-W-trending interbedding fracture zone, which dips to north with an

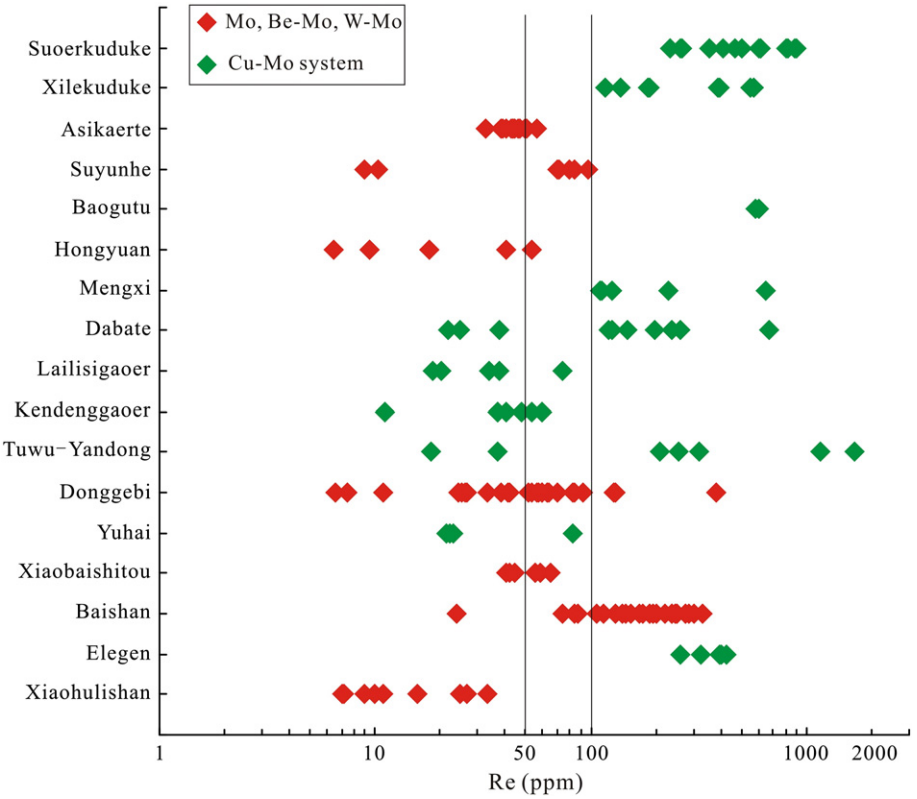

Fig. 5. The Re contents of molybdenites from the Mo deposits in NW China.

Table 6
Molybdenite Re-Os isotope ages and Re contents for the Mo deposits in NW China.

No.	Deposit	Re (ppm)	σ	Age (Ma)	σ	Reference
1	Suoerkuduke	232.7	1.70	316.8	5.0	Wan et al. (2014)
		813.2	8.40	308.6	4.7	Wan et al. (2014)
		261.9	2.70	314.4	5.0	Wan et al. (2014)
		597.4	7.10	302.5	5.1	Wan et al. (2014)
		818.3	7.50	311.0	4.6	Wan et al. (2014)
		265.8	2.20	312.4	4.4	Wan et al. (2014)
		232.2	2.20	306.6	4.5	Wan et al. (2014)
		901.5	11.00	366.1	6.3	Wan et al. (2014)
		892.2	11.00	303.1	5.3	Wan et al. (2014)
		498.3	7.80	320.1	6.4	Liu and Liu (2013)
		355.5	7.40	323.4	7.8	Liu and Liu (2013)
		357.1	3.10	325.7	4.7	Liu and Liu (2013)
		465.0	8.80	325.0	7.4	Liu and Liu (2013)
		409.0	4.10	323.3	5.0	Liu and Liu (2013)
		614.4	4.80	321.7	4.8	Liu and Liu (2013)
		615.6	4.80	322.5	4.5	Liu and Liu (2013)
2	Xilekuduke	572.1	11.00	326.6	7.1	Long et al. (2011)
		551.5	4.50	327.2	4.6	Long et al. (2011)
		138.7	1.20	328.8	4.6	Long et al. (2011)
		184.9	1.40	333.1	4.6	Long et al. (2011)
		390.2	3.20	328.4	4.6	Long et al. (2011)
		186.2	1.40	329.2	4.5	Long et al. (2011)
		393.6	3.00	328.8	4.6	Long et al. (2011)
		117.8	0.90	331.6	4.5	Long et al. (2011)
4	Asikaerte	42.6	0.40	218.8	3.3	Wang et al. (2015a)
		44.8	0.36	219.2	3.1	Wang et al. (2015a)
		40.9	0.32	216.8	3.2	Wang et al. (2015a)
		39.3	0.32	218.4	3.1	Wang et al. (2015a)
		32.4	0.26	221.1	3.1	Wang et al. (2015a)
		43.6	0.37	217.4	3.1	Wang et al. (2015a)
		49.7		226.5	4.5	Liu et al. (2015)
		43.3		230.4	4.8	Liu et al. (2015)
		45.7		229.6	3.9	Liu et al. (2015)
		38.3		235.7	3.4	Liu et al. (2015)
		56.5		231.8	5.5	Liu et al. (2015)
		46.8		224.6	3.1	Liu et al. (2015)
		50.7		227.8	4.2	Liu et al. (2015)
5	Suyunhe	71.5	0.57	294.8	4.2	Zhong et al. (2015a)
		70.0	0.53	295.5	4.1	Zhong et al. (2015a)
		97.4	0.88	294.9	4.3	Zhong et al. (2015a)
		79.8	0.61	293.3	4.0	Zhong et al. (2015a)
		84.7	0.67	294.6	4.1	Zhong et al. (2015a)
		8.9	0.08	295.3	4.3	Zhong et al. (2015a)
		10.3	0.09	296.8	4.3	Zhong et al. (2015a)
6	Baogutu	576.9	4.60	310.1	3.6	Song et al. (2007)
		600.7	4.90	310.4	3.6	Song et al. (2007)
7	Hongyuan	53.3	6.92	298.3	2.3	Li (2013)
		18.0	0.56	288.5	1.6	Li (2013)
		6.4	0.13	298.9	0.9	Li (2013)
		9.4	0.18	289.5	1.1	Li (2013)
		40.5	0.18	293.5	1.5	Li (2013)
8	Mengxi	227.6	2.13	406.7	6.0	Qu et al. (2009)
		126.0	1.18	412.1	6.2	Qu et al. (2009)
		111.3	9.30	411.9	5.9	Qu et al. (2009)
		111.3	8.57	409.7	5.9	Qu et al. (2009)
		113.5	8.48	409.1	5.8	Qu et al. (2009)
		647.1	7.12	395.9	7.4	Qu et al. (2009)
9	Dabate	147.0	1.30	301.6	4.0	Zhang et al. (2006d)
		259.6	3.50	286.5	6.2	Zhang et al. (2006d)
		120.7	1.20	298.7	4.6	Zhang et al. (2006d)
		199.8	1.60	287.5	1.0	Zhang et al. (2006d)
		124.8	1.10	288.9	3.9	Zhang et al. (2006d)
		238.3	1.30	282.1	5.7	Zhang et al. (2006d)
		675.5	5.80	305.0	3.8	Zhang et al. (2006d)
		37.6		298.5	6.9	Li (2012)
		25.0		300.9	5.9	Li (2012)
		21.8		299.3	4.2	Li (2012)
12	Lailisigaoer	33.8		378.0	2.0	Zhu et al. (2012)
		18.5		367.0	3.7	Zhu et al. (2012)
		38.0		376.0	2.4	Zhu et al. (2012)
		20.2		371.0	1.7	Zhu et al. (2012)
		73.5		374.0	2.3	Zhu et al. (2012)
13	Kendenggaoer	36.8	0.32	314.8	4.7	Jia et al. (2011)
		47.7	0.44	317.7	4.7	Jia et al. (2011)
		59.7	0.79	314.5	5.6	Jia et al. (2011)
		53.4	0.54	315.1	5.0	Jia et al. (2011)

Table 6 (*continued*)

No.	Deposit	Re (ppm)	σ	Age (Ma)	σ	Reference
		11.1	0.09	318.0	4.4	Jia et al. (2011)
		36.8	0.33	314.6	4.7	Jia et al. (2011)
		40.2	0.30	312.9	4.5	Jia et al. (2011)
14	Tuwu-Yandong	1167.0		325.0		Rui et al. (2002b)
		1665.0		325.0		Rui et al. (2002b)
		18.3		318.0		Rui et al. (2002b)
		209.0		321.0		Rui et al. (2002b)
		321.1		322.0		Rui et al. (2002b)
		257.8		321.0		Rui et al. (2002b)
		37.1		324.0		Rui et al. (2002b)
17	Donggebi	53.6	0.45	229.9	3.2	Tu et al. (2012)
		51.3	0.39	231.3	3.2	Tu et al. (2012)
		6.5	0.06	234.4	3.3	Tu et al. (2012)
		84.2	1.03	231.5	3.9	Tu et al. (2012)
		56.9	0.52	231.9	3.4	Tu et al. (2012)
		7.4	0.06	233.5	3.3	Tu et al. (2012)
		24.4	0.19	233.5	3.3	Tu et al. (2012)
		59.0	1.14	241.7	0.9	Wu et al. (2013a)
		91.3	1.09	234.1	2.6	Wu et al. (2013a)
		81.9	1.45	241.4	4.7	Wu et al. (2013a)
		62.9	1.17	237.3	2.4	Wu et al. (2013a)
		70.6	2.43	234.4	1.2	Wu et al. (2013a)
		384.8	6.05	228.7	2.6	Wu et al. (2013a)
		63.6	1.45	232.0	3.3	Wu et al. (2013a)
		26.5	0.23	238.3	3.4	Wu et al. (2013a)
		59.8	0.50	236.3	2.0	Wu et al. (2013b)
		25.4	0.10	237.9	1.6	Wu et al. (2013b)
		26.1	0.10	238.4	2.2	Wu et al. (2013b)
		128.1	0.50	234.5	1.2	Wu et al. (2013b)
		131.1	0.30	233.6	1.3	Wu et al. (2013b)
		33.1	0.27	234.1	3.4	Han et al. (2014)
		42.0	0.31	235.6	3.4	Han et al. (2014)
		10.9	0.09	234.6	3.5	Han et al. (2014)
		38.2	0.32	234.1	3.3	Han et al. (2014)
		59.3	0.52	234.8	3.4	Han et al. (2014)
		41.0	0.34	234.7	3.3	Han et al. (2014)
		56.4	0.45	233.7	3.2	Han et al. (2014)
		63.2	0.56	233.7	3.4	Han et al. (2014)
18	Yuhai	83.1	0.69	353.0	5.0	Wang et al. (2016b)
		22.1	0.13	357.9	4.6	Wang et al. (2016b)
		21.4	0.16	355.6	5.0	Wang et al. (2016b)
		23.0	0.18	355.8	4.9	Wang et al. (2016b)
20	Xiaobaishitou	58.0	0.43	244.2	3.4	Deng et al. (2016)
		44.1	0.33	250.2	3.4	Deng et al. (2016)
		40.3	0.31	251.4	3.6	Deng et al. (2016)
		41.8	0.33	245.9	3.5	Deng et al. (2016)
		55.4	0.45	239.7	3.6	Deng et al. (2016)
		64.7	0.51	241.1	3.5	Deng et al. (2016)
		55.7	0.46	241.6	3.6	Deng et al. (2016)
21	Baishan	114.0	1.30	231.6	3.9	Li et al. (2006a)
		287.3	3.30	228.4	3.9	Li et al. (2006a)
		145.0	1.60	227.0	3.7	Li et al. (2006a)
		23.8	0.30	229.3	4.0	Li et al. (2006a)
		329.9	4.20	230.1	4.0	Li et al. (2006a)
		246.5	3.10	229.7	4.1	Li et al. (2006a)
		167.2		222.0		Zhang et al. (2005)
		194.5		229.0		Zhang et al. (2005)
		188.0		228.6		Zhang et al. (2005)
		73.5		229.4		Zhang et al. (2005)
		238.2		227.9		Zhang et al. (2005)
		249.7		228.1		Zhang et al. (2005)
		107.1		229.9		Zhang et al. (2005)
		236.7		222.3		Zhang et al. (2005)
		303.3	5.70	190.3	4.2	Zhang et al. (2009b)
		250.6	2.10	227.1	3.3	Zhang et al. (2009b)
		222.2	2.20	225.9	3.4	Zhang et al. (2009b)
		200.2	1.70	225.9	3.2	Zhang et al. (2009b)
		176.0	1.60	225.5	3.2	Zhang et al. (2009b)
		276.1	2.30	226.7	3.2	Zhang et al. (2009b)
		139.3	1.10	225.1	3.1	Zhang et al. (2009b)
		245.9	2.50	224.7	3.4	Zhang et al. (2009b)
		84.0	0.76	224.9	3.4	Tu et al. (2014)
		273.6	2.60	224.8	3.3	Tu et al. (2014)
		129.8	1.20	224.4	3.3	Tu et al. (2014)
		187.1	1.60	223.5	3.2	Tu et al. (2014)

(*continued on next page*)

Table 6 (*continued*)

No.	Deposit	Re (ppm)	σ	Age (Ma)	σ	Reference
		192.9	1.80	224.8	3.3	Tu et al. (2014)
		87.1	0.66	227.5	3.1	Tu et al. (2014)
		153.4	1.30	225.0	3.2	Tu et al. (2014)
26	Elegen	326.7	2.55	338.9	3.9	Nie et al. (2005)
		259.4	2.26	340.6	4.1	Nie et al. (2005)
		424.1	3.62	336.9	4.2	Nie et al. (2005)
		402.2	4.25	336.2	4.6	Nie et al. (2005)
		393.0	3.16	338.9	4.0	Nie et al. (2005)
27	Xiaohulishan	24.9	0.23	218.7	3.4	Peng et al. (2010)
		26.7	0.25	220.1	3.4	Peng et al. (2010)
		7.2	0.08	218.3	3.5	Peng et al. (2010)
		15.7	0.11	218.1	2.9	Peng et al. (2010)
		32.9	0.30	219.5	3.2	Peng et al. (2010)
		9.0	0.08	216.3	3.3	Peng et al. (2010)
		9.9	0.09	215.3	3.2	Zhang et al. (2012d)
		7.1	0.07	212.6	3.5	Zhang et al. (2012d)
		11.0	0.08	211.8	3.1	Zhang et al. (2012d)

angle of 60–70°. This ore-bearing interbedding fracture zone is crosscut by a group of NE-trending faults that act as postore structures (Zhang et al., 2005).

More than 16 orebodies have been identified already, and seven of them are high-grade ones.The main orebodies are 2–124 m thick, and 100–2000 m long. They strike ~85° and dip to north with angles of 65–75°. In the dipping direction, they extend over 600 m in depth. These orebodies exhibit stratiform and lenticular shape. The Mo grades range from 0.03 to 0.106 %, with an average of 0.06% (Xiang et al., 2013).

According to mineral association and occurrence, the veinlets were divided into five types composed of quartz + K-feldspar ± pyrite (1), quartz + K-feldspar + molybdenite (2), quartz + molybdenite (3), quartz + polymetallic sulphides (4), and quartz-calcite-fluorite (5). The main ore minerals include molybdenite, chalcopyrite and pyrite, with minor pyrrhotite, magnetite, galena, sphalerite and marcasite. The gangue minerals mainly include quartz, sericite and microcline, flowed by biotite, calcite and chlorite (Xiang et al., 2013).

Main wallrock alteration includes phyllic and potassic alteration, biotitization, chloritization, and carbonatization. Phyllic alteration, occupying the central part of the alteration zones, consists dominantly of sericite, quartz and chlorite, and hosts most of the molybdenite and polymetallic sulfides. Potassic alteration is most conspicuous and characterized by the formation of microcline. Carbonatization is related to a late-stage quartz-calcite veins. According to mineral assemblages and crosscutting relationships of veinlets, four hydrothermal stages can be identified. The first stage is characterized by quartz veins, with magnetite and ilmenite. The second is an assemblage consisting of quartz, pyrite, and a little molybdenite. The third consists of polymetallic sulfides including molybdenite, chalcopyrite and pyrite, with minor galena and sphalerite. The fourth stage is marked by barren calcite-quartz veins (Zhang et al., 2005; Xiang et al., 2013).

5.3. Donggebi porphyry Mo deposit

The Donggebi Mo deposit is located in the area between the Kanggur and Aqishan faults (Fig. 8, Table 1). The Donggebi deposit is strongly covered by the Quaternary deserts, locally outcropped with the Early Carboniferous Gandun Formation. The Gandun Formation consists of terrigenous clastic and carbonate sedimentary rocks, including metamorphic sandstone, conglomeratic sandstone, argillaceous sandstone and pelite, and volcanic tuff and andesite. The structures are dominated by the NE- to ENE-trending and N-trending faults. The ENE-trending anticline and syncline developed in the northwestern sector of the deposit. Diabase and dacitic dykes can be observed at the Donggebi deposit. The

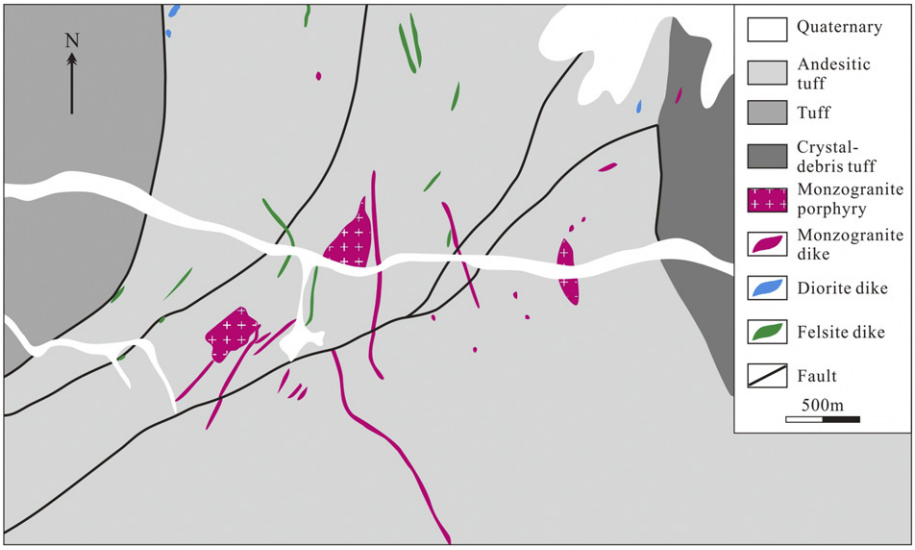

Fig. 6. Geological map of the Suyunhe Mo deposit (modified after Zhong et al., 2015a).

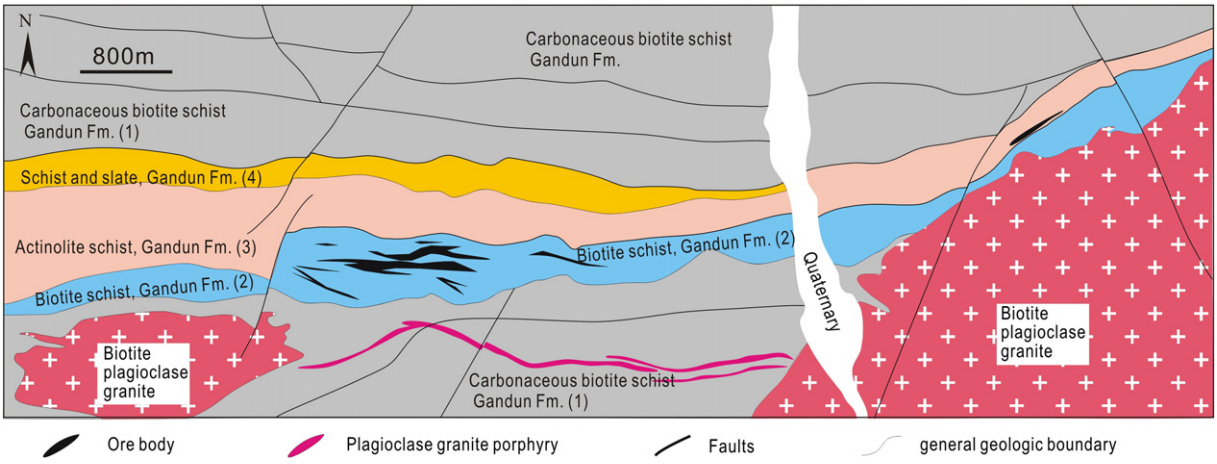

Fig. 7. Geological map of the Baishan Mo deposit (modified after Xiang et al., 2013).

diabase dykes are NE-trending, composed of plagioclase and biotite, with accessory minerals of sphene, epidote and actinolite, as well as pyrite and chalcopyrite. The dacitic porphyry dykes only occur at the northeast corner of the deposit, and contain minor muscovite (Wu et al., 2014).

As revealed by drilling work, the ore-associated Donggebi porphyritic granite stock is buried by 135 m below the surface, intruding the Gandun Formation. Phenocrysts accounts for 30–40% volume of the rock, mainly including plagioclase, K-feldspar and quartz. The matrix is composed of fine-grained K-feldspar, plagioclase, quartz and minor biotite, with accessary zircon, apatite and scheelite (Wu et al., 2014).

The orebodies are located in the outer contact zones, at elevations of 251 to 925 m ASL (above sea level). The largest orebody dips northeast and is about 1534 m long, 2 to 418 m wide, and lenticular in shape. Sulfides include molybdenite and pyrite, followed by chalcopyrite, galena and sphalerite, occurring as disseminations, veinlets and stockworks.

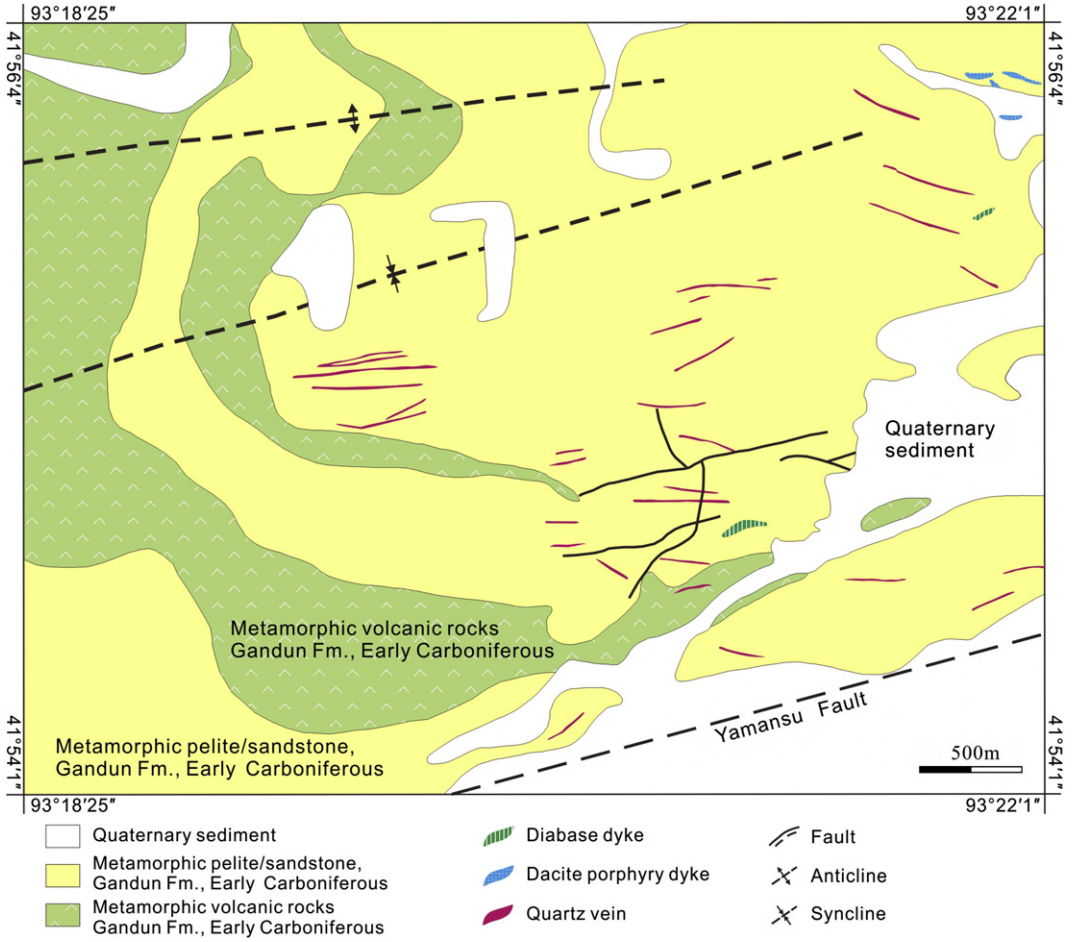

Fig. 8. Geological map of the Donggebi Mo deposit (modified after Wu et al., 2014).

The main gangue minerals are quartz, feldspar, epidote, beryl, biotite, tourmaline, sericite, chlorite, fluorite and calcite (Wu et al., 2014).

According to Wu et al. (2014), the wall-rock alterations at the Donggebi deposit include: (1) potassic alteration, with biotite and K-feldspar as predominant hydrothermal minerals; (2) silicification, in the form of quartz ± sulfide stockworks or veinlets; (3) sericitization, typified by alteration of feldspar and biotite to sericite; (4) propylitization, with epidote, chlorite and calcite as predominant hydrothermal minerals; (5) carbonation, mainly typified by carbonate veinlets; and (6) fluoritization, presented as disseminated purple grains or veinlets. The hydrothermal alteration and mineralization are divided into four stages, mainly according to mineralogical features, associations and crosscutting relationships of veins. Stage 1 is characterized by the assemblage of quartz + K-feldspar ± beryl ± pyrite ± tourmaline veins. Coeval alteration assemblages consist of potassic alteration and silicification. Stage 2 includes two mineral assemblages of quartz + K-feldspar + molybdenite and quartz + molybdenite + tourmaline + fluorite + beryl + pyrite. Silicification, sericitization, tourmalinization and little fluoritization are present in stage 2. The stage 3 veinlets are mainly composed of quartz + polymetallic sulphides ± fluorite. Silicification, sericitization, propylitization and fluoritization are most conspicuous in this stage. Stage 4 is characterized by quartz-calcite and quartz-calcite-fluorite veinlets, with little or no sulphide.

5.4. Tuwu-Yandong porphyry Cu-Mo belt

The Tuwu-Yandong Cu-Mo belt is located in the Dananhu-Tousuquan island arc, about 1–4 km north of the Kanggur Fault (Fig. 9, Table 1). The main lithostratigraphic units in the region are the Carboniferous Qi'eshan Group and the Jurassic Xishanyao Formation. The Xishanyao Formation is mainly composed of sandstone, siltstone, mudstone, and conglomerate, unconformly overlying on the Qi'eshan Group (Wang et al., 2014b). The Qi'eshan Group is eastward striking and dips to the south at angle of 43° to 63°, generally with well-developed schistosity (Shen et al., 2014a). It is typically 600–2000 m thick and can be divided into five units. The lowermost unit is composed of basalt and andesite intercalated with dacite and tuff, which are overlain by

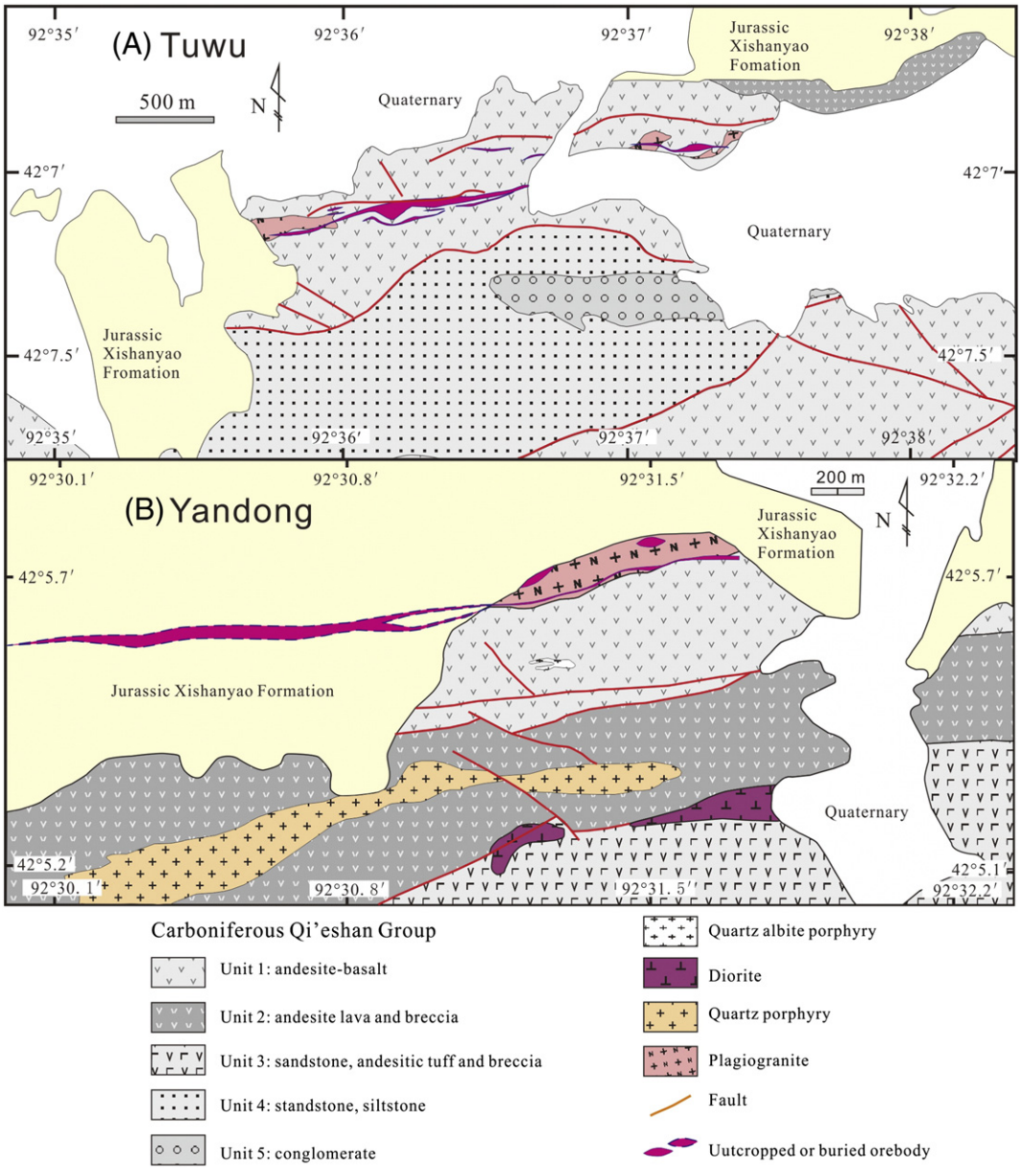

Fig. 9. Geological maps of the Tuwu (A) and Yandong (B) Cu-Mo deposits (modified after Xiao et al., 2015).

andesite intercalated with pebbly sandstones and basalts of unit 2. Unit 3 comprises pebbly sandstone intercalated with tuff, pyroclastic rocks and limestones. Unit 4 comprises lithic sandstone and siltstone, intercalated with tuff. Unit 5 is a polymictic conglomerate assemblge. The basalts in this area are generally porphyritic with phenocrysts of plagioclase with minor augite, biotite and amphibole, and a groundmass of plagioclase with minor magnetite. The andesite is also porphyritic but the phenocrysts and groundmass are typically plagioclase with minor amphibole and quartz. The Qi'eshan Group was generally accepted to have developed in a Carboniferous subduction-realted volcanic arc (Hou et al., 2006; Shen et al., 2014b), but Xia et al. (2004) argued that it was formed in a rift.

The Qi'eshan Group is intruded by the diorites, plagiogranite porphyry, quartz albite porphyry and quartz porphyry. The diorite is composed of plagioclase (>90%) and amphibole (5–10%) with accessory zircon. The ore-bearing plagiogranite porphyry shows massive and porphyritic texture. It contains 35–45% plagioclase, 25–35% quartz and ~5% biotite, with accessory zircon and apatite. The quartz albite porphyry is also massive and porphyritic in texture, and contains 30–40% albite and 30–45% quartz, with accessory zircon and apatite. The quartz porphyry occurs at south of the Yandong deposit (Xiao et al., 2015). It is worthy note that the diorite porphyrite defined in the literature (Shen et al., 2014a,b) has been incorporated into the Qi'eshan Group (Xiao et al., 2015), based on a detailed field and petrographical test.

The Tuwu and Yandong Cu-Mo deposits are mainly controlled by E-, NW- and NE-trending faults. Mineralization presents as dissemination, veinlet and stockworks, with no distinct boundary between the orebodies and the country rocks. The main orebody in the Yandong deposit extends for over 3000 m in length and 10–50 m in width, given 0.50% Cu as cut-off grade. The Tuwu deposit comprises two main orebodies. Orebody I is 1400 m long, 10 to 130 m thick, and dips toward 180° at angles of 65–80°; and orebody II is >1000 m long and 10 to 80 m wide. In the Tuwu deposit, Qi'eshan Group and plagiogranite porphyry host 70% and 30% of the ores, respectively; in the Yandong deposit, however, they host 20% and 80% of the ores, respectively. Ore minerals in both the Tuwu and Yandong deposits are dominated by pyrite, chalcopyrite and molybdenite with minor bornite, chalcocite, magnetite, sphalerite, and galena. Gangue minerals include quartz, sericite, chlorite, epidote, anhydrite, gypsum, muscovite, biotite, apatite, sphene, dolomite, actinolite, barite, albite and calcite (Xiao et al., 2015).

5.5. Suoerkuduke Cu-Mo skarn

The Suoerkuduke Cu–Mo deposit is a medium-size skarn system (Fig. 10 and Table 1). The mining area is characteristic of mid-Devonian pyroclastic rocks and sandstones of the Beitashan Formation intruded by granites and gabbros (Fig. 10). The Beitashan Formation consists of a low-grade metamorphosed succession of limestone, conglomerate, tuffaceous sandstone, pyroclastic sandstone and andesite, associating with minor uncertained andesite porphyries. Altered andesites yield an Rb–Sr isochron age of 288 ± 18 Ma (Zhou et al., 1996). Intrusive rocks in the eastern part of the mine are mostly K-feldspar granites that consist of 45–50% K-feldspar, 5–10% plagioclase, 40–45% quartz and 1–5% biotite. The margins of the granitic bodies are composed of fine-grained granitic porphyry. Between the granites and the volcanic rocks is a narrow contact composed of andalusite + feldspar + quartz hornfels, which is obviously different from the skarn that hosts the ores in the Suoerkuduke deposit, and thus these granites are not considered to be ore-causative (Wan et al., 2014).

According to Wan et al. (2014), the strata in the mine area were deformed by folds with NNW–trending axes. More than 10 orebodies of different size occur in the SW limb of an anticline. The largest o orebody is 1 km long, 1–70 m thick, N–S-trending, dipping to SW at angle of 6–45°. Two largest orebodies provide 80% reserve of the deposit. The orebodies are stratiform or lenticular in shape, and are mostly bordered by pyroxene andesite, andesitic porphyry and tuff of the Beitashan

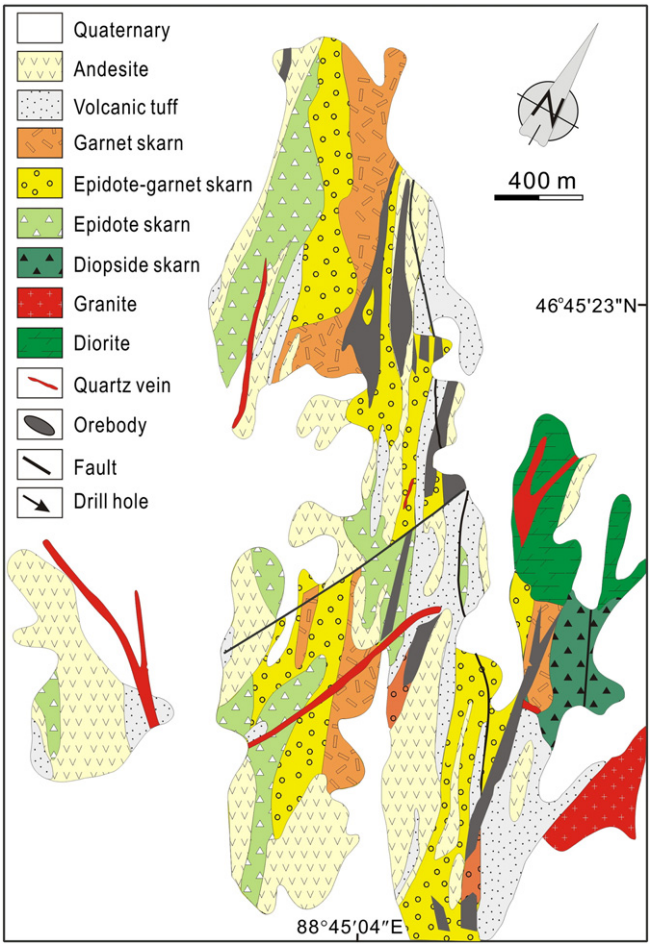

Fig. 10. Geological map of the Suoerkuduke skarn Cu-Mo deposit (modified after Wan et al., 2014).

Formation. The ores are closely associated with calc-silicate skarns mainly comprising garnet, diopside, epidote and actinolite, forming four zones outward from garnet, through epidote–garnet, to epidote, and to diopside skarns. The garnet skarn zone is mainly in the mine center, and enveloped by the epidote–garnet skarn zones. The epidote skarns occur locally and discontinuously along the stratigraphic strikes. The diopside skarn only crops out in the eastern side of the mine. Most of the ores are hosted in epidote skarns, followed by epidote–garnet skarns. The garnets are calcium-rich andradite and grossular (Liu et al., 1992).

The ores are mainly composed of chalcopyrite and pyrite with subordinate molybdenite and pyrrhotite, minor magnetite and native gold. Ore minerals occur in veinlets and dissemination; and at shallow levels, they are oxidized to covellite, limonite, malachite, chrysocolla, azurite and hematite (Wan et al., 2014).

Seven samples of garnet-rich skarns and three samples of epidote-rich skarns yielded a Sm–Nd isochron of 284 ± 4 Ma, and thereby the deposit was interpreted to have formed in Permian (Li and Chen, 2004). However, recent molybdenite Re-Os dationg yields isochron ages of 317.1 ± 7.6 Ma (Liu and Liu, 2013) and 305 ± 7 (Wan et al., 2014), suggesting that the deposit was formed in Late Craboniferous.

5.6. Xiaobaishitou W-Mo skarn

The Xiaobaishitou tungsten(-molybdenum) deposit is situated in the eastern segment of the Central Tianshan Massif, about 18 km northeast of Xingxingxia County (Fig. 11 and Table 1). This deposit has a proven total reserve of 36 Kt of scheelite grading at 0.23 to 3.06 wt.% WO_3, with an average of 0.78 wt.% WO_3 (Deng et al., 2016).

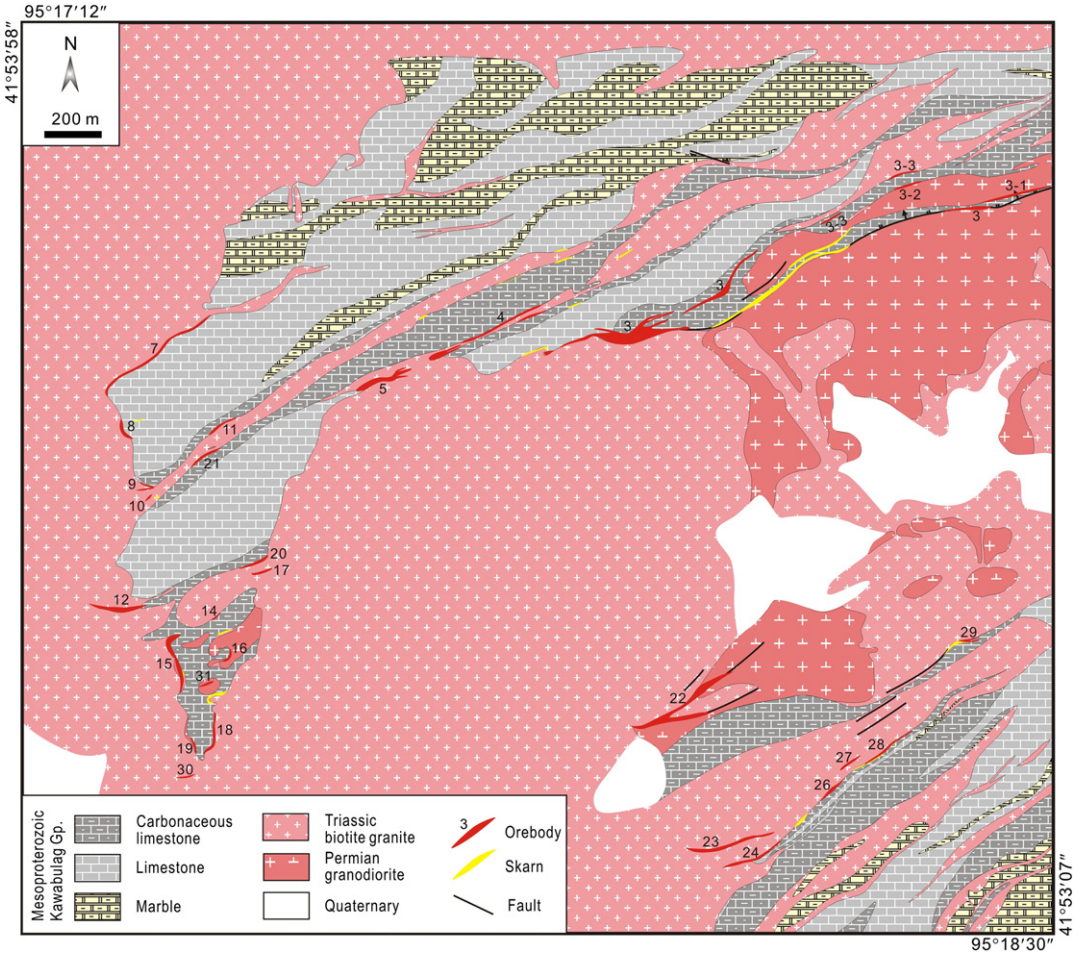

Fig. 11. Geological map of the Xiaobaishiyou skarn W-Mo deposit (modified after Deng et al., 2016).

The lithologies at Xiaobaishitou deposit consist of the Mesoproterozoic Jianshanzi Formation of the Kawabulag Group (Deng et al., 2016). The Kawabulag Group in the Xiaobaishitou district is a suite of metamorphic rocks, mainly composed of marble, crystalline limestone, silicified limestone, wollastonite schist and quartz schist. Permian granodiorite and Triassic biotite granite are widespread in the ore field and its neighboring area. The Permian granodiorite are fine-grained and mainly composed of quartz, feldspar, amphibole and biotite. The rocks were hydrothermally altered, including silicification and sericitization. The Triassic biotite granites are closely related to the W-Mo mineralization, which show hypidiomorphic granular texture and massive structure. The biotite granite is an equigranular batholith, which indicates that it was emplaced in a relatively deep environment than the porphyry ore system. The rocks are grey to grayish and medium-grained. They are composed of quartz (20–30%), K-feldspar (25–35%), plagioclase (20–30%) and biotite (5–8%), with accessory sphene and zircon. Skarn can be found along the contact zones of the biotite granite with limestone, mainly including garnet, diopside, epidote and wollastonite.

Xiaobaishitou is a middle-scale skarn tungsten-molybdenum deposit, associating with extensive garnet, epidote, chlorite, silica, fluorite and carbonate alteration. Five W-Mo prospects with more than 96 economic orebodies have been explored to date. The veins are mainly hosted in the garnet skarns, and discontinuously strike up to several kilometres along the skarn zone. The orebodies are vein, lenticular and crescent in shape (Deng et al., 2016).

The Xiaobaishitou skarn deposit is characterized by a typical calc-silicate mineralogy dominated by prograde garnet, diopside and wollastonite, with minor retrograde epidote, tremolite, actinolite, chlorite, quartz, fluorite and calcite. The main ore minerals are scheelite, molybdenite, bismuthinite, pyrite, sphalerite, galena and chalcopyrite. Based on field investigation and petrographic observation, five stages of hydrothermal process have been recognized, with each stage partially replacing earlier stages (Deng et al., 2016): (1) prograde sakrn stage, forming garnet-clinopyroxene-wollastonite; (2) retrograde skarn stage, forming epidote-tremolite-actinolite-chlorite; (3) oxide stage, forming scheelite-cassiterite-magnetite; (4) sulfide stage, represented by quartz-sulfide veinlets; and (5) calcite-quartz-fluorite.

6. Geochemistry of ore-associated granites

The porphyry-skarn Mo-polymetallic mineralization systems, as well as the quartz vein-type Mo deposits, are commonly considered to be related to the ore-hosting porphyries and their precursor intrusions in space, time and genesis. These ore-hosting intrusions are commonly multiple phases and emplaced during a short time. They are diorite (porphyry), granodiorite (porphyry), plagiogranite porphyry, monzogranite porphyry, porphyritic granite, moyite and biotite granite in lithology. The geochemical data of these intrusions have been summarized in this contribution (available on request from the first or corresponding author). The geochemical varieties of representative granitoids in different regions of NW China and the differences between Cu-Mo and Mo-only or W-Mo and Be-Mo systems are recognized, and will be briefly introduced below.

6.1. Petrography and petrochemistry

The causative intrusions of the Mo-only deposits in NW China exhibit similar petrochemical compositions (Appendix 1), including high

contents of SiO_2 (68.05–77.34%), $K_2O + Na_2O$ (6.09–9.54%) and Al_2O_3 (11.38–15.69%), low and variable contents of TiO_2 (0.07–0.46%), CaO (0.43–3.71%) and MgO (0.06–1.32%), and thus belong to alkaligranite or granite (Fig. 12A). They plot in the metaluminous to peraluminous domains, and show high-K calc-alkaline to shoshonite affinity (Fig. 12B, C), with K_2O/Na_2O values ranging from 0.38 to 2.53 (Appendix 1). All these petrochemical features suggest that the causative intrusions of the Mo-only deposits were sourced from continental crust.

The intrusions associating with Cu-Mo mineralization are mainly diorite, granodiorite, granite and alkaligranite in lithology, as represented by those at the Tuwu-Yandong, Baogutu, Lailisigaoer and Suoerkuduke deposits. They show a wide range of of SiO_2 (53.42–76.30%), Al_2O_3 (11.96–18.07%) and $K_2O + Na_2O$ (3.13–10.30%), with K_2O/Na_2O values of 0.08–7.75, suggesting that they belong to calc-alkaline to shoshonite affinity (Fig. 12A, C). They show metaluminous to peraluminous features (Fig. 12B), with A/CNK and A/NK ranging 0.07–2.71 and 0.07–3.76, respectively. They are also characterized by relatively high contents of TiO_2 (0.08–2.47%) and MgO (0.24–6.59%).

The intrusions associating with Mo-mineralization have higher SiO_2 and K_2O contents and K_2O/Na_2O ratios, but lower Na_2O and MgO contents, compared to those associating with Cu-mineralization. The former class also show younger ages than the latter. This indicates that the magma source became shallower and more felsic, else, the magmas underwent stronger intracontinental differentiation.

6.2. Rare earth and trace elements

The granitic intrusions are generally characterized by enrichments of LILE (Rb, K, U and Th) and LREE, and depletions of HFSE (Nb, Ta, P and Ti) and HREE, with high and variable LREE/HREE (3.41–27.90) and $(La/Yb)_N$ (1.99–52.34) ratios (Fig. 13; Appendix 2). These geochemical features imply the involvement of crustal components (Woodhead et al., 1998), and/or the presence of aqueous fluids in the magma source (Richard, 2011). These causative intrusions have $\sum$REE values of 24.85 to 224.99 ppm, with δEu values of 0.21–1.83 and $(La/Yb)_N$ values of 1.99–52.34, suggesting a variation in origins and sources.

The Hercynian intrusions associtating with porphyry-type Cu-Mo mineralization show no remarkable Eu anomalies, but clear depletions of Nb, Ta and Ti; available data show clear enrichment in Pb and K. These signatures are similar to those of I-type grainitoids or volcanic rocks in subduction-realted arcs, particularly, the adakites (Xiong et al., 2005, 2006), which suggests that the magmas possibly originated from partial melting of the subducted oceanic slab or of a thickened lower crust. The Suoerkuduke skarn-associated intrusion shows more clear enrichments of Pb and K, and depletions of Nb, Ta, P and Ti, and remarkable Eu-depletion, which might result from an involvement of sedimentary rocks into the magma, or alternately, suggests that the magmas originated from a crust-dominated source or intracrustal crystallization differentiation.

The intrusions associating with the Donggebi and Suyunhe Mo-only deposits show flat REE patterns with clear Eu-depletion, strong enrichment of Rb, U, K and Pb, and depletion of Nb, P and Ti, which suggest a crust-dominated source or intracrustal crystallization differentiation. The Sunyunhe intrusion was interpreted to be formed from highly evolved magmas soutrced from subducted ocenic slab or thickened lower crust (Zhong et al., 2015a), considering that it also show Ta depletion. The Baishan granite rocks, however, exibit rightly-inclined REE patterns without Eu-anomolies (Fig. 13), which suggests that the contribution of intracrustal differentiation is neglectable. It show strong enrichment of Rb, U, K and Pb (LILE), but strong depletion of Nb, Ta, Ti and HREE, which indicates that the magmas originated from a thickened

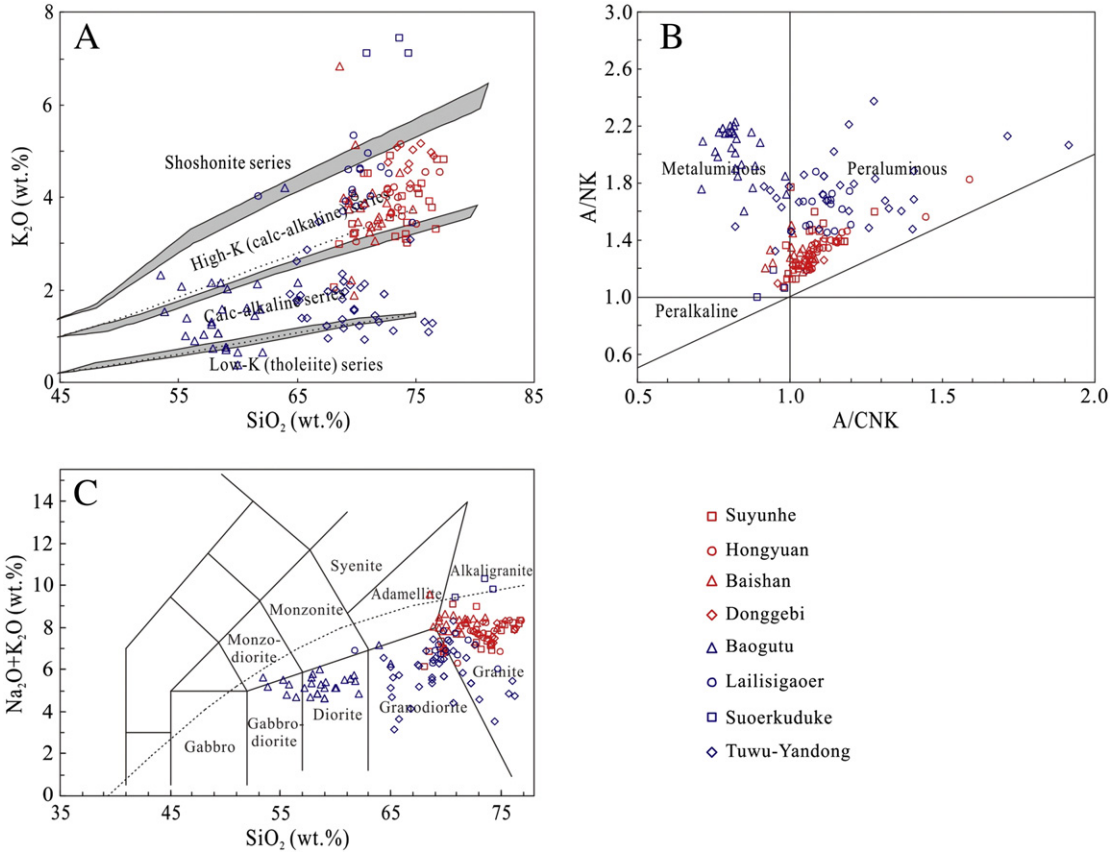

Fig. 12. Petrochemical diagrams of the causative intrusions in NW China

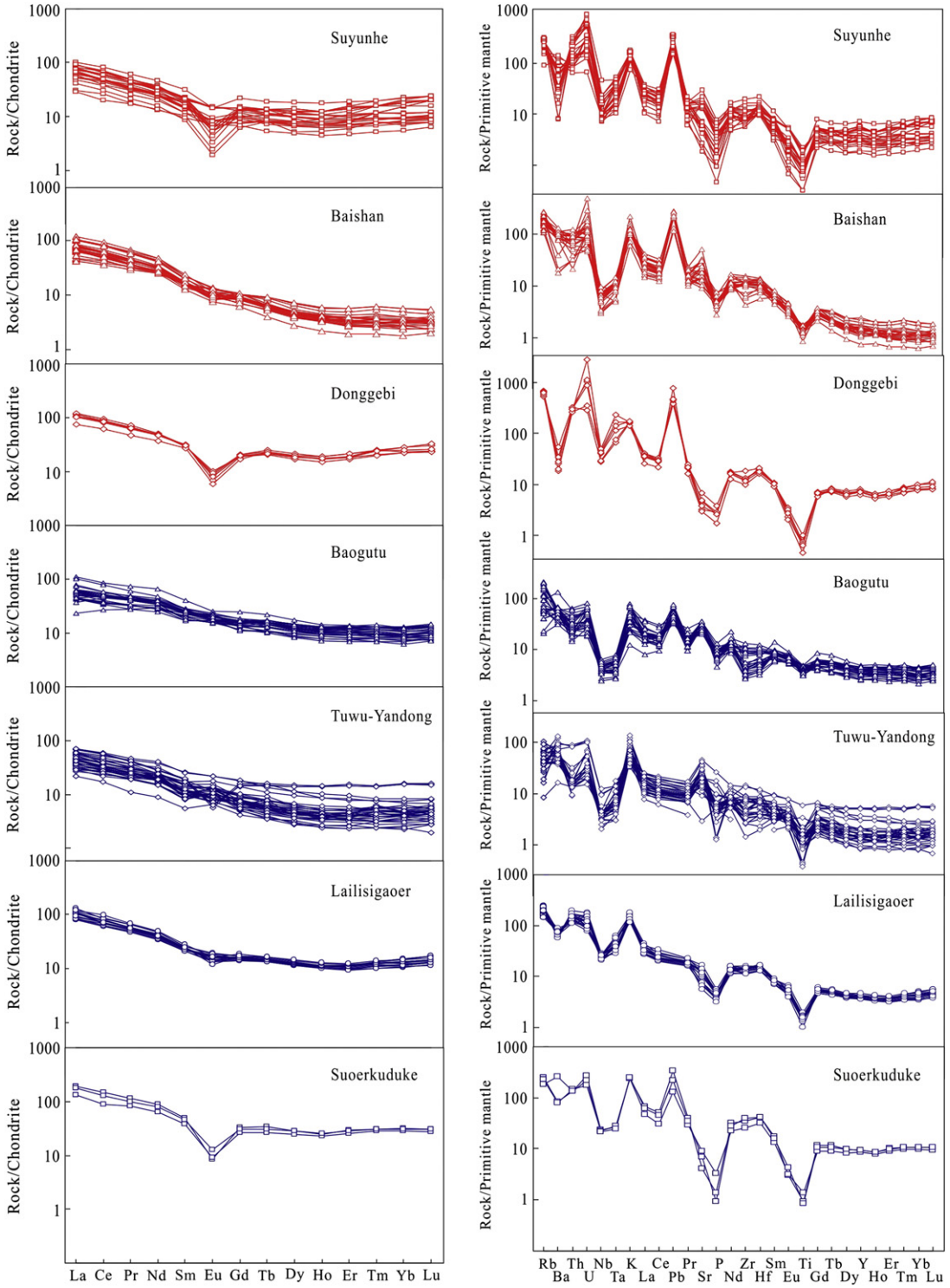

Fig. 13. REE patterns and trace element spider diagrams of the causative intrusions in NW China.

lower crust with depth of >50 km (Zhu et al., 2013b; Xiang et al., 2013). This understanding can be supported by the high Re contents of molybdentite from the deposit (Table 6).

In the Rb-(Y + Nb), Nb- Y, Ta-Yb and Rb/30-Hf-3Ta tectonic discrimination diagrams (Fig. 14), the Hercynian causative intrusions (e.g. Suyunhe, Baogutu, Tuwu-Yandong, Suoerkuduke and Lailisigaoer) mainly plot in the volcanic arc domain, whereas the Indosinian causative intrusions generally plot (e.g. Baishan and Donggebi) in the syn- to post-collision or within-plate granite domains (Fig. 14A, D). Moreover, these intrusions shift from volcanic arc to syn- or post-collision granite domains, which accords well with a tectonic transition from an oceanic subduction regime to post-collisional setting during the period of 320–260 Ma (Fig. 14B, C).

6.3. Isotope signatures

The initial Sr-Nd-Hf isotopic ratios of the ore-associated intrusions are calculated back to the age the rocks formed (Tables 7 and 8). The $^{87}Sr/^{86}Sr$ ratios vary from 0.703657 to 0.768548, with I_{sr} values (initial $^{87}Sr/^{86}Sr$ ratios) ranging 0.6883–0.70941. Some of them are less than

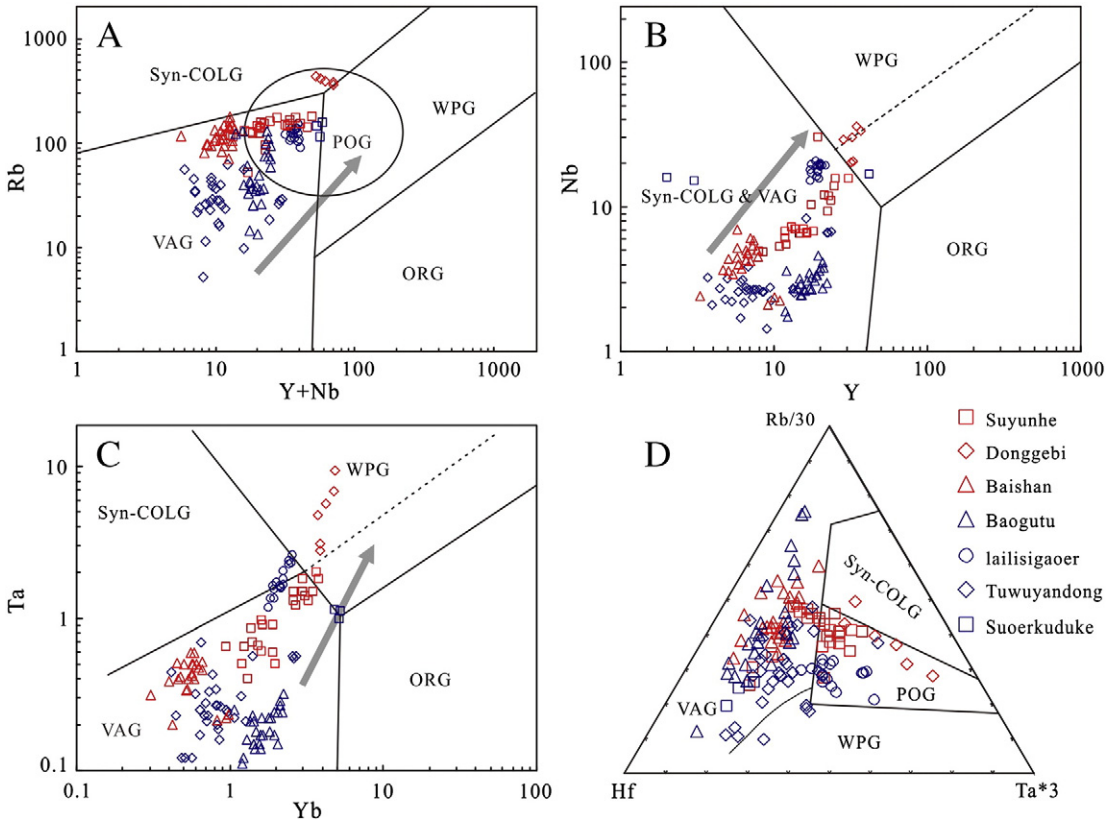

Fig. 14. Tectonic discriminations of the causative intrusions in NW China. (A) Rb vs. (Y + Nb) diagram (Pearce, 1996); (B) Nb vs. Y diagram (Pearce et al., 1984); (C) Ta vs. Yb diagram (Pearce et al., 1984); (D) Rb/30–Hf–Ta * 3 diagram (Harris et al., 1986). VAG, volcanic arc granites; ORG, ocean ridge granites; WPG, within-plate granites; Syn-COLG, syn-collision granites; POG, post-collision granites.

0.700 (e.g. Hongyuan), possibly influenced by hydrothermal alteration, and are geologically unacceptable and not considered in discussion. The $\varepsilon Nd(t)$ values range from −2.33 to 10.86, with $T_{DM2}(Nd)$ of 0.35–1.3 Ga (Fig. 15). Zircon crystals from these intrusions showed the $^{176}Lu/^{177}Hf$ and $^{176}Hf/^{177}Hf$ ratios of 0.000024–0.283222 and 0.282587–0.283201, respectively. The calculated $\varepsilon Hf(t)$ values range from 6.3 to 17.5, with $T_{DM2}(Hf)$ ages from 0.63 to 1.24 Ga (Table 8, Fig. 16). These Sr-Nd-Hf isotope data are identical to a young juvenile crust source originated from the depleted mantle.

The Lailisigaoer deposit is quite different from the other mineral systems (Fig. 15). Its I_{Sr} and $\varepsilon Nd(t)$ values range from 0.70786 to 0.709654, and from −2.94 to −0.61, respectively, with $T_{DM2}(Nd)$ of 1.3–1.26 Ga. These data imply for a relatively old crust source, possibly a Precambrian basement, for the ore-associted intrusions, which is in accordance with the Nd isotope signatures, i.e., $\varepsilon Nd(t) = -11.7$ to −8.5, and $T_{DM2}(Nd) = 2.2–1.2$ Ga (Hu et al., 2000), estimated for the Precambrian rocks of the Ili–Central Tianshan block (e.g. amphibolite). Therefore, the Lailisigaoer granitic rocks can be interpreted to have originated from partial melting of the basement of the Ili–Central Tianshan block, with the involvement of mantle components, induced by magmatism in a continental arc related to the southward subduction of the North Tianshan Oceanic plate beneath the Ili–Central Tianshan block.

Table 7
The Sr-Nd isotopic compositions of the ore-associated intrusions in NW China.
Data sources: Suyunhe (Yang et al., 2015a), Hongyuan (Li, 2013), Lailisigaoer (Xie et al., 2013; Xue et al., 2011), Baogutu (Shen et al., 2009, 2013; Wei and Zhu, 2015), Suoerkuduke (Zhao et al., 2014), Xilekuduke (Long et al., 2009), Donggebi (Wu et al., 2016b), Tuwu–Yandong (Gao et al., 2015; Xiao et al., 2015; Zhang et al., 2006a,b; Xia et al., 2004).

Deposit	No.		$^{87}Rb/^{86}Sr$	$^{87}Sr/^{86}Sr$	Isr	$^{147}Sm/^{144}Nd$	$^{143}Nd/^{144}Nd$	$\varepsilon Nd(t)$	T_{DM2} (Ga)
Suyunhe	3		1.066980–1.204890	0.709220–0.710002	0.704052–0.705313	0.512645–0.512797	0.512645–0.512797	3.64–6.33	0.52–0.70
		Av.	1.1380530	0.709523	0.704520	0.512728	0.512728	5.01	0.61
Hongyuan	4		1.95910–12.785600	0.710436–0.741871	0.688300–0.702600	0.118500–0.130100	0.51277–0.512864	5.52–6.92	
		Av.	5.110725	0.720128	0.698700	0.126800	0.512822	6.19	
Lailisigaoer	15		0.789000–2.849000	0.711790–0.723070	0.707860–0.709410	0.118500–0.126600	0.512425–0.512441	−2.33	1.26–1.30
		Av.	1.576547	0.716603	0.708520	0.117653	0.512331	−1.88	1.29
Baogutu	44		0.013000–2.1361000	0.703710–0.713678	0.703550–0.705520	0.119300–0.163600	0.512675–0.513000	0.70–8.30	0.36–0.77
		Av.	0.234662	0.704879	0.703820	0.135950	0.512873	4.42	0.52
Suoerkuduke	3		2.214000–5.318400	0.714690–0.730350	0.701000–0.703840	0.110000–0.118700	0.512670–0.512710		0.66–0.74
		Av.	3.276333	0.720517	0.702440	0.114567	0.512693		0.71
Xilekuduke	9		0.330600–1.677500	0.705239–0.711408	0.703404–0.703792	0.101300–0.106600	0.512787–0.513034	6.90–10.82	
		Av.	0.792411	0.707364	0.703650	0.111489	0.512844	7.59	
Donggebi	4		6.596727–17.974864	0.728323–0.768548	0.706180–0.708210	0.118205–0.145003	0.512589–0.512602	0.60–1.62	0.88–0.96
		Av.	12.508406	0.749177	0.707190	0.127442	0.512597	1.28	0.90
Tuwu–Yandong	33		0.005000–1.670000	0.703657–0.709420	0.701600–0.70600	0.140000–0.179300	0.512680–0.512972	3.10–9.16	0.35–0.76
		Av.	0.224848	0.704687	0.703650	0.133252	0.512828	6.41	0.58

Table 8
Zircon Lu-Hf isotope data for the ore-associated intrusions in NW China.
Data sources: Asikaerte (Wang et al., 2015a), Baishan (Wang et al., 2015c), Donggebi (Wu et al., 2016b), Tuwu–Yandong (Xiao et al., 2015; Wang et al., 2014b, 2015b).

Deposit	No.		$^{176}Lu/^{177}Hf$	$^{176}Hf/^{177}Hf$	εHf(t)	T_{DM2}/Ga
Asikaerte	29		0.000024–0.00714	0.282624–0.282696	−0.72–1.99	1.13–1.298
		Av.	0.001438	0.282649	0.26	1.24
Baishan	13		0.000377–0.001447	0.282855–0.282943	8.0–11.0	0.556–0.758
		Av.	0.000846	0.282909	9.7	0.64
Donggebi	14		0.000825–0.00166	0.282587–0.282766	−1.58–4.82	0.96–1.36
		Av.	0.001090	0.282674	1.55	1.17
Tuwu–Yandong	76		0.000781–0.283222	0.282743–0.283201	1.8–22.6	0.25–0.94
		Av.	0.057787	0.282891	11.3	0.63

7. Tectonic setting

7.1. Palaeozoic Mo mineralization

In NW China, the Palaeozoic Mo mineralization was dominated by the porphyry Cu-Mo systems, except for three Mo-only deposits (Suyunhe, Hongyuan and Kumutage). As constrained by the molybdenite Re–Os ages, all these Cu-Mo deposits were formed in Late Palaeozoic, from Early Devonian to Permian (Fig. 2). The Suyunhe and Hongyuan porphyry Mo deposits were formed in the beginning Permian in the Western Junggar, which show characteristics of the Endako-type porphyry Mo deposits. The Kumutage skarn-type Mo deposit was formed at ~319 Ma. This shows that the Mo-only deposits began to appear in Late Carboniferous, and thus the Palaeozoic mineralization can be divided into two different periods, i.e., Devonian-Early Carboniferous (420–320 Ma) and Late Carboniferous-Permian (320–260 Ma).

In the period of Devonian–Early Carboniferous, the NW China was characterized by Cu-Mo deposits and related magmatism, and was thus accepted to be a subduction-related arc-basin system (Avdeyev, 1984; Chen, 2000; Xiao et al., 2008a, 2009a). The Cu-Mo deposits formed in this period can be related to magmatic arc setting.

In the period of Late Carboniferous-Permian (320–260 Ma), the NW China accommodated the formation of both the porphyry Cu-Mo and Mo-only deposits. In this period, the tectonic setting of NW China has not been well constrained and thus hotly debated between the views of subduction-related arc-basin system (Xiao et al., 2008a; Chen et al., 2012c) and syn- to post-collisional orogeny (Chen, 1997; Han et al., 2006a, 2010; Shen et al., 2017). Considering the diachroneity and non-isochronism of the oceanic closure at different areas, we envisage a coexisting scenario of both oceanic plate subduction and inter-continental collision, alike the present-day Mediterranean ocean. For example, in the Western Junggar, the oceanic plate subduction along the Dalabute and Karamay sutures was believed to continue in Permian (Xiao et al., 2008a, 2009a), which caused the formation of the I-type granite rocks and their associated Endako-type Sunyunhe and Hongyuan porphyry Mo deposits, as well the Baogutu Cu-Mo deposit. On ther contrary, Shen et al. (2017) argued that the Suyunhe was formed in a post-collisional tectonic setting.

In the Beishan Orogen, the development of arc-basin system ended in Permian (Xiao et al., 2010), followed by Late Permian-Triassic continental collision orogeny that resulted in a widespread development of S-type granitic rocks and Mo deposits (Mu et al., 1992; Zhang et al., 2012c,d; Zheng et al., 2012b, 2013; Li et al., 2012a). Cerntainly, the Liushashan porphyry Mo deposit was formed in a continental collision orogeny. Therefore, the period of Late Carboniferous-Permian was the time the tectonic setting transformed from subduction-related arc-basin systems to continental collision regime in the NW China.

7.2. Triassic Mo mineralization

In the Triassic period, or Indosinian Orogeny, many kinds of metallic deposits were formed in NW China, associated with intensive granitic magmatism, which suggests the Traissic is an important metallogenic epoch (Chen et al., 2014). The Mo-only or Mo-dominated deposits mainly occurred in the NW China, as exemplified by the giant Donggebi (231.9 ± 6. 5 Ma; Wu et al., 2013b) and Baishan (224.8 ± 4.5 Ma; Zhang et al., 2005) porphyry Mo deposits and and the Xiaobaishitou skarn W-Mo deposit (240.8 ± 2.0 Ma; Deng et al., 2016) in the Eastern Tianshan.

The tectonic setting of Indosinian Mo mineralization in NW China has been debated between various models including: (1) an intracontinental extension (Li et al., 2005; Zhang et al., 2008a; Xiao et al., 2009a; Zhou et al., 2010) or rifting (Qin et al., 2003); (2) a

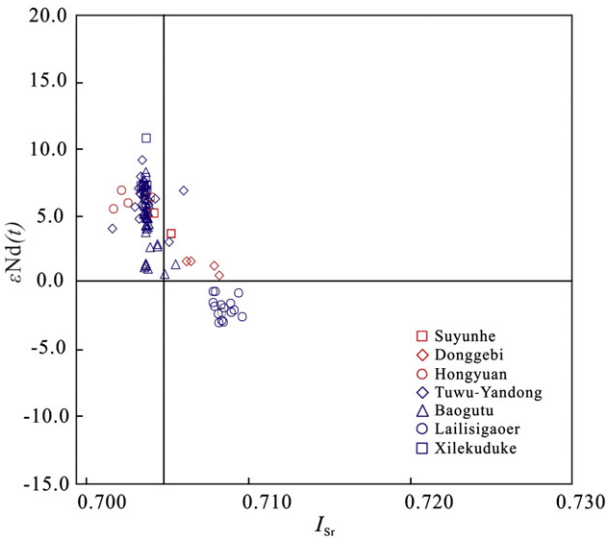

Fig. 15. Plot of εNd(t) vs. I_{Sr} for the causative intrusions in NW China.

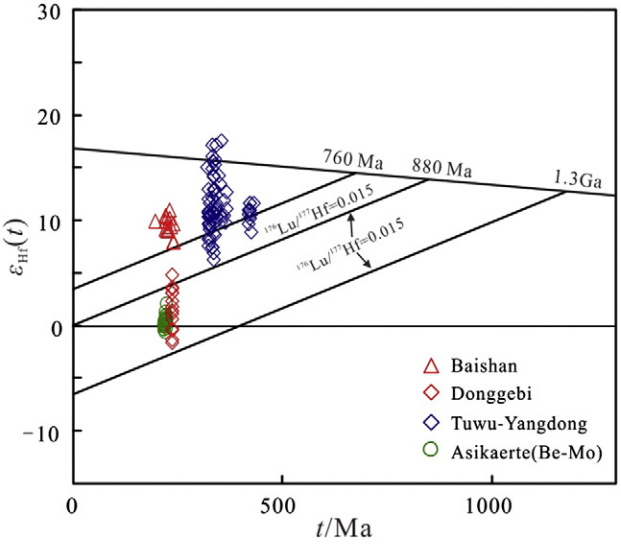

Fig. 16. Plot of zircon εHf(t) versus U-Pb ages for causative intrusions in NW China.

compression after the post-collisional stage resulted from the far-field impact of the Paleo-Tethys closure (Zhu et al., 2009; Zhang et al., 2009a), or a geodynamic conversion from the Paleo-Asian subduction-collision system to the Paleo-Tethys (Zhang et al., 2006e); (3) a tectonic transition from syn-collisional compression to post-collisional extension (Chen et al., 2007a, 2012a, 2014; Wu et al., 2014; Zhang et al., 2014b); and (4) transition from subduction-related marginal accretion to post-subduction continental collision (Xiao et al., 2009a), i.e., the continuous southward accretion along the wide southern active margin of Siberia (including Altai, Junggar, and Tianshan areas) terminated by the amalgamation with Tarim during the end-Permian to mid-Triassic. Despite of the divergence in understandings, all these models admit that the Paleo-Asia Ocean was completely closed no later than mid-Triassic, and thus the Triassic must be under a syn- or/to post-collisional setting, or even an intracontinental tectonic setting. The Triassic deposits in NW China must have been formed in a tectonic setting from syn-collisional crust shortening and thickening to post-collisional or intracontinental crust extension and thinning, which is similar to the Yanshanian Mo deposits in eastern Qinling Orogen (Chen et al., 2000c) and Dabie Shan (Chen et al., 2017a), or the Indosinian to Early Yanshanian Mo deposits in the southern Great Hinggan Range (Zhang and Li, 2014; Chen et al., 2017b). This understanding of the tectonic setting and mineralization evolution can be powerfully supported by the fact that no Cu-Mo deposit has been reported later than 260 Ma (Fig. 2).

8. Conclusions

(1) The location of the Mo deposits of porphyry, skarn and quartz vein types and their combinations in NW China were mainly controlled by the EW-, NW–NNW-trending faults and their subsidiary fractures. The subsidiary structures also -control the occurrence orebodiesthat usually occur in the causative porphyries and contact zones.

(2) Hydrothermal alteration mainly includes the formation of quartz, K-feldspar, sericite, chlorite, epidote, carbonate, flourite and skarn minerals. The alteration in most porphyry-skarn Mo deposits is zoned outward or temporally evolved from high-temperature assemblage of K-feldspathization, silicification, biotitization and albitization, through moderate-temperature phyllic alteration, to low-temperature propylitic and argillic alteration.

(3) The Mo deposits in NW China were mainly formed by the magmatic fluids with high temperatures and high salinities, as indicated by daughter mineral-bearing fluid inclusions. Fluid boiling is the most conductive mechanism for metal precipitation, can be divided into two groups, one is the Cu-Mo systems, and the other includes Mo-only, Mo-dominated and W-Mo or Be-Mo deposits. The Mo-only and Mo-dominated deposits usually contain CO_2-bearing inclusions, except for the Suyunhe deposit. The Cu-Mo systems generally show higher oxygen fugacity than the Mo-only or Mo-dominated systems.

(4) The Re contents in molybdenites from porphyry or porphyry-skarn Cu-Mo systems are >50 ppm, mainly >100 ppm, suggesting a source significantly contributed by the mantle; whereas the Re contents in molybdenites from the Mo-only or W-Mo deposits are around 100 ppm, mainly <100 ppm, indicating a genetic relation to the crust-sourced granitic magmatism.

(5) All the Mo deposits in NW China were formed in the period of Devonian to Triassic. During the Devonian-Early Carboniferous (420–320 Ma), the NW China only accommodated the development of the porphyry Cu-Mo deposits, no Mo-only or Mo-dominated deposit was formed, which was generally related to island or continental arcs. By contrast, in the Triassic or 260–200 Ma, no porphyry Cu-Mo deposit was formed in NW China, but the Mo-only, Mo-dominated and W-Mo and Be-Mo deposits associated with crust-sourced granitic rocks were formed there, which was commonly related to a syn- to post-collisional tectonic setting. The Late Carboniferous-Permian (320–260 Ma), connected the two abovementioned constrasting tectonic regimes in time, must be the period accommodated the coexistence and/or the transition from subduction-related arc-basin system to continental collision orogeny, when both the porphyry-type Mo-only and Cu-Mo deposits were formed.

Conflict of interest

We declare that we have no conflict of interest to the work we submitted.

Acknowledgements

This is a contribution from the Working Group on Mineral Deposits in Collisional Orogens (IAGOD), and has been financially granted by the 973-Project (No. 2014CB440800, 2014CB448000), National Nature Science Foundation of China (Nos. U1139301, 41572070, 41572077, 41572065), Major Basic Research Project (grant No. 201330121) of Xinjiang Uygur Autonomous Region, and China Geological Survey (1212011140056, 12120114081701). The authors would like to thank Drs. Nuo Li, Pin Wang, Yongfei Yang and ChengMing Wang for their help. Comments and suggestions from two reviewers greatly improved the quality of the paper.

Appendix 1. Major elements of ore-bearing porphyries in NW China (wt.%).

Sample no.	Rock type	SiO_2	Al_2O_3	FeO^{Total}	MgO	CaO	Na_2O	K_2O	MnO	TiO_2	P_2O_5	LOI	Total
Suyunhe													
Syh1-1	Monzonitic granite porphyry	77.34	11.57	1.60	0.13	0.65	3.07	4.83	0.02	0.07	0.02	1.19	99.96
Syh1-2	Monzonitic granite porphyry	73.22	13.10	3.98	0.71	2.02	3.76	3.16	0.06	0.24	0.08	1.24	99.89
Syh1-3	Monzonitic granite porphyry	73.84	12.96	2.55	0.56	1.01	3.62	4.03	0.05	0.23	0.07	1.69	99.92
Syh1-4	Monzonitic granite porphyry	70.97	14.63	4.83	0.69	2.04	3.10	4.53	0.10	0.32	0.11	1.04	#####
Syh1-5	Monzonitic granite porphyry	76.80	12.25	1.14	0.13	0.59	3.47	4.83	0.02	0.07	0.01	0.67	99.62
Syh2-1	Monzonitic granite	72.78	13.91	2.22	0.32	1.10	4.05	4.91	0.04	0.14	0.03	1.35	99.90
Syh2-2	Monzonitic granite	75.17	12.52	2.84	0.42	0.85	4.07	4.07	0.06	0.18	0.04	0.90	99.92
Syh2-3	Monzonitic granite	76.64	12.33	2.07	0.27	0.62	4.79	3.32	0.04	0.14	0.02	0.62	#####
Syh2-4	Monzonitic granite porphyry	76.09	13.45	2.00	0.22	1.00	4.26	3.91	0.03	0.12	0.02	0.36	#####
Syh2-5	Monzonitic granite porphyry	75.41	12.94	2.07	0.29	1.03	3.79	4.31	0.05	0.14	0.03	0.37	99.70
Syh3-1	Monzonitic granite porphyry	69.80	14.73	4.28	0.96	1.97	3.78	3.22	0.06	0.37	0.11	1.99	99.95
Syh3-2	Monzonitic granite porphyry	69.60	14.84	4.61	1.02	2.06	3.88	3.42	0.06	0.38	0.12	1.42	99.91
Syh3-3	Monzonitic granite	68.05	15.69	5.72	1.32	3.71	4.03	2.06	0.06	0.46	0.16	0.94	99.98
Syh3-4	Monzonitic granite porphyry	75.12	12.75	2.40	0.36	1.10	3.64	4.18	0.05	0.17	0.04	0.28	99.14

(continued on next page)

(*continued*)

Sample no.	Rock type	SiO_2	Al_2O_3	FeO^{Total}	MgO	CaO	Na_2O	K_2O	MnO	TiO_2	P_2O_5	LOI	Total
Syh3-5	Monzonitic granite porphyry	70.61	15.18	2.95	0.47	1.39	4.53	4.51	0.06	0.19	0.05	0.38	99.20
Syh3-6	Monzonitic granite porphyry	76.30	13.20	2.34	0.34	1.13	4.08	3.77	0.05	0.16	0.04	0.28	#####
S-12	Monzonitic granite porphyry	74.22	14.08	1.25	0.52	1.74	3.87	3.01	0.04	0.25	0.08	1.07	#####
S-15	Monzonitic granite porphyry	74.22	13.76	1.29	0.59	1.12	3.75	3.44	0.05	0.22	0.07	0.94	99.59
S-16	Monzonitic granite porphyry	72.80	13.91	1.85	0.64	1.38	3.73	3.55	0.06	0.23	0.08	1.32	99.75
S-17	Monzonitic granite porphyry	73.79	13.81	1.40	0.63	1.03	3.60	3.73	0.05	0.22	0.08	1.03	99.52
S-19	Monzonitic granite porphyry	69.75	15.31	2.48	1.12	1.30	3.72	3.21	0.03	0.42	0.14	1.77	99.52
S-20	Monzonitic granite porphyry	68.48	15.19	1.93	1.18	2.53	3.81	2.99	0.04	0.41	0.14	3.32	#####

Appendix 2. Trace elements of ore-bearing porphyries in the NW China (ppm).

Sample	La	Ce	Pr	Nd	Sm	Eu	Gd	Tb	Dy	Ho	Er	Tm	Yb
Suynhe													
Syh1-1	9.7	18.7	2	7.4	1.3	0.11	1.27	0.3	1.9	0.4	1.4	0.3	2.6
Syh1-2	14.2	23.6	2.9	10.3	1.8	0.48	1.52	0.3	1.3	0.3	1	0.2	1.2
Syh1-3	11.5	22.7	2.4	9.3	1.8	0.37	1.64	0.3	1.9	0.4	1.3	0.3	1.9
Syh1-4	24	50.3	5.7	21.4	4.8	0.83	4.48	0.7	4.6	1	3.1	0.5	3.7
Syh1-5	7.2	15.9	1.7	6.1	1.6	0.14	1.57	0.3	2	0.5	1.8	0.3	2.6
Syh2-1	16.6	29.5	3.7	12.9	2.6	0.31	2.07	0.4	2.5	0.5	1.8	0.4	2.7
Syh2-2	18.7	36.3	4.2	15	3	0.35	2.93	0.5	3.1	0.7	2.3	0.4	3.3
Syh2-3	12.7	28.8	3.1	11.5	2.7	0.19	2.53	0.4	3	0.6	2.1	0.4	3
Syh2-4	12.3	26.7	3	11.4	2.9	0.25	2.73	0.5	3.5	0.7	2.6	0.5	3.8
Syh2-5	14.3	30.6	3.4	12.8	3	0.31	2.77	0.5	3.2	0.7	2.5	0.4	3
Syh3-1	18.3	33.8	3.9	15.4	3.3	0.82	2.96	0.5	2.8	0.6	1.7	0.3	2
Syh3-2	18.8	35.7	4.2	16.3	3.5	0.85	2.99	0.5	2.9	0.6	1.6	0.3	1.9
Syh3-3	22.2	39.2	4.5	17.7	3.1	0.88	2.62	0.5	2.3	0.4	1.2	0.2	1.3
Syh3-4	17.3	36.9	4.1	14.6	3.2	0.31	2.64	0.5	3.1	0.7	2.3	0.4	3.1
Syh3-5	19.5	41.4	4.6	16	3.5	0.39	3.15	0.5	3.5	0.7	2.4	0.4	3.5
Syh3-6	21.4	43.8	4.7	16.3	3.3	0.36	2.82	0.4	3	0.7	2.3	0.4	3
S-12	6.7	12.2	1.62	6.31	1.44	0.42	1.38	0.2	1.23	0.25	0.78	0.13	0.94
S-15	15.2	28.2	3.24	11.6	2.2	0.48	2	0.29	1.73	0.37	1.15	0.19	1.41
S-16	22.3	40.2	4.2	14.3	2.55	0.55	2.37	0.34	2.08	0.45	1.37	0.23	1.65
S-17	15.4	30.3	3.16	11.2	2.11	0.49	1.89	0.27	1.65	0.35	1.05	0.17	1.24
S-19	18.4	37.6	4.2	16.2	3.22	0.82	2.96	0.43	2.52	0.51	1.5	0.24	1.6
S-20	18	35.8	4.15	15.9	3.21	0.82	2.94	0.42	2.45	0.49	1.44	0.23	1.52
S-21	15.5	29.6	3.34	12	2.28	0.48	2.08	0.3	1.75	0.37	1.13	0.19	1.37
S-22	15.9	30.5	3.37	12.2	2.36	0.47	2.21	0.32	1.98	0.42	1.31	0.22	1.62
Donggebi													
ZK1232-1	27.5	54.9	6.38	23	4.55	0.6	3.92	0.83	4.77	0.97	3.03	0.53	3.86
KZK0003-1	28.3	58.6	6.77	24.2	4.73	0.51	4.23	0.92	5.42	1.08	3.59	0.65	4.8
ZK0206-57	25.8	52.9	6.1	22.9	4.58	0.55	4.24	0.88	4.88	1.01	3.18	0.63	3.91
ZK0408-24	24	49.9	5.86	21.7	4.8	0.39	3.94	0.77	4.31	0.86	2.79	0.51	3.76
ZK0408-22	17.9	38.2	4.48	17.1	4.1	0.35	3.49	0.86	4.95	1.06	3.49	0.62	4.89
ZK0408-23	24.8	51.6	6.02	22.3	4.68	0.46	4.15	0.81	4.71	0.98	3.09	0.61	4.25
Baishan													
BS-3102-2	17.5	34.4	4.04	15.6	2.72	0.53	2.15	0.3	1.39	0.25	0.7	0.11	0.66
BS-3102-16	19	36.1	4.1	15.4	2.45	0.49	1.95	0.24	1.01	0.19	0.55	0.09	0.56
BS-3102-18	15.8	29.8	3.5	13.4	2.36	0.48	1.83	0.25	1.2	0.22	0.64	0.11	0.66
BS-3102-39	11.2	24.5	3.2	12.9	2.42	0.64	2.09	0.34	1.6	0.29	0.81	0.14	0.82
BS-3102-40	11.5	25.9	3.17	12.5	2.4	0.76	2.1	0.34	1.74	0.32	0.93	0.16	0.95
BS-3102-42	10.3	22	2.83	11.7	2.41	0.75	2.14	0.35	1.81	0.34	0.96	0.16	0.97
ZK31-2-02	16	33.8	3.9	13.8	2.44	0.52	1.8	0.24	1.29	0.23	0.63	0.09	0.56
ZK31-2-06	18.6	37.1	4.16	14.6	2.52	0.51	1.7	0.24	1.23	0.22	0.63	0.09	0.57
ZK31-2-07	17.9	37.2	4.23	15	2.53	0.62	1.83	0.24	1.17	0.23	0.59	0.08	0.58
ZK31-2-13	16.7	33	3.65	12.8	2.12	0.58	1.42	0.2	0.99	0.2	0.54	0.09	0.6

References

Avdeyev, A.V., 1984. Ophiolite zones and the geologic history of Kazakhstan from the mobilist standpoint. Int. Geol. Rev. 26, 995–1005.

BGMRX (Bureau of Geology and Mineral Resources of Xinjiang Uygur Autonomous Region), 1993U. Regional Geology of Xinjiang Uygur Autonomous Region, People's Republic of China. Geological Publishing House, Beijing, pp. 6–206 (in Chinese).

Cao, M.J., Qin, K.Z., Li, G.M., Evans, N.J., He, H.Y., Jin, L.Y., 2015. A mixture of mantle and crustal derived He–Ar–C–S ore-forming fluids at the Baogutu reduced porphyry Cu deposit, western Junggar. J. Asian Earth Sci. 98, 188–197.

Carten, R.B., White, W.H., Stein, H.J., 1993. High-grade granite-related molybdenum systems: classification and origin. In: Kirkham, R.V., Sinclair, W.D., Thope, R.I., Duke, J.M. (Eds.), Mineral Deposit Modeling. Geological Association of Canada Special Paper 40, pp. 521–554.

Chen, Y.J., 1997. Mineralization during collisional orogenesis and its control of the distribution of gold deposits in Junggar Mountains, Xinjiang. China. Acta Geol. Sin. 71, 69–79.

Chen, Y.J., 2000. Progress in the study of Central Asia-type orogenesis-metallogenesis in Northwest China. Geol. J. China Univ. 6, 17–22 (in Chinese).

Chen, Y.J., 2010. On epizonogenism and genetic classification of hydrothermal deposits. Earth Sci. Front. 17, 27–34 (in Chinese with English abstract).

Chen, Y.J., 2013. The development of continental collisionmetallogeny and its application. Acta Petrol. Sin. 29, 1–17 (in Chinese with English abstract).
Chen, B., Arakawa, Y., 2005. Elemental and Nd–Sr isotopic geochemistry of granitoids from the West Junggar fold belt (NW China), with implications for Phanerozoic continental growth. Geochim. Cosmochim. Acta 69, 1307–1320.
Chen, B.W., Chen, T.Y., 2007. Trans-Asian tectonic belt: its principal characteristics and metallogeny. Acta Petrol. Sin. 23, 865–876 (in Chinese with English abstract).
Chen, B., Jahn, B.M., 2004. Genesis of post-collisional granitoids and basement nature of the Junggar Terrane, NW China: Nd–Sr isotope and trace element evidence. J. Asian Earth Sci. 23, 691–703.
Chen, Y.J., Li, N., 2009. Nature of ore-fluids of intercontinental inclusion-related hypothermal deposits and its difference from those in island arcs. Acta Petrol. Sin. 25, 2477–2508 (in Chinese with English abstract).
Chen, Y.J., Wang, Y., 2011. Fluid inclusion study of the Tangjiaping Mo deposit, Dabie Shan, Henan Province: implications for the nature of porphyry systems of post-collisional tectonic settings. Int. Geol. Rev. 53, 635–655.
Chen, Y.J., Fu, S.G., Wu, D.H., Wu, X.D., Jing, J., 1995. The coupling of the gold mineralization with the collisional orogenesis and the distribution of gold deposits, northern Xinjiang. Gold Geol. 3, 8–16 (in Chinese).
Chen, H.Y., Bao, J.X., Zhang, Z.J., Liu, Y.L., Ni, P., Ling, H.F., 2000a. Isotope indication to source of ore materials and fluids of the Wangfeng gold deposit in Tianshan: a case study of metallogenesis during collisional orogenesis. Sci. China Ser. D 43 (supplement), 156–166.
Chen, Y.B., Hu, A.Q., Zhang, G.X., Zhang, Q.F., 2000b. Precambrian basement age and characteristics of Southwestern Tianshan: zircon U–Pb geochronology and Nd–Sr isotopic compositions. Acta Petrol. Sin. 16, 91–98 (in Chinese with English abstract).
Chen, Y.J., Li, C., Zhang, J., Li, Z., Wang, H.H., 2000c. Sr and O isotopic characteristics of porphyries in the Qinling molybdenum deposit belt and their implication to genetic mechanism and type. Sci. China Ser. D 43 (Suppl.), 82–94.
Chen, H.Y., Chen, Y.J., Liu, Y.L., 2001. Metallogenesis of the Ertix gold belt, Xinjiang and its relationship to Central Asia-type orogenesis. Sci. China Ser. D 44, 245–255.
Chen, F.W., Li, H.Q., Chen, Y.C., Wang, D.H., Wang, J.L., Liu, D.Q., Tang, Y.L., Zhou, R.H., 2005. Zircon SHRIMP U-Pb dating and its geological signif icance of mineralization in Tuwu–Yandong porphyry copper mine, east Tianshan mountain. Acta Geol. Sin. 79, 256–261 (in Chinese with English abstract).
Chen, H.Y., Chen, Y.J., Ni, P., Zhang, Z.J., 2007a. Chemical composition of fluid inclusions of the Sawayardun gold deposit, Xinjiang and its implications for metallogeny and exploration. Acta Petrol. Sin. 23, 2189–2197 (in Chinese with English abstract).
Chen, Y.J., Chen, H.Y., Zaw, K., Pirajno, F., Zhang, Z.J., 2007b. Geodynamic settings and tectonic model of skarn gold deposits in China: an overview. Ore Geol. Rev. 31, 139–169.
Chen, Y.J., Ni, P., Fan, H.R., Pirajno, F., Lai, Y., Su, W.C., Zhang, H., 2007c. Diagnostic fluid inclusions of different types hydrothermal gold deposits. Acta Petrol. Sin. 23, 2085–2108 (in Chinese with English abstract).
Chen, Y.J., Zhai, M.G., Jiang, S.Y., 2009. Significant achievements and open issues in study of orogenesis andmetallogenesis surrounding the North China continent. Acta Petrol. Sin. 25, 2695–2726 (in Chinese with English abstract).
Chen, H.Y., Chen, Y.J., Baker, M.J., 2012a. Evolution of ore-forming fluids in the Sawayaerdun gold deposit in the Southwestern Chinese Tianshan metallogenic belt. J. Asian Earth Sci. 49, 131–144.
Chen, Y.J., Pirajno, F., Wu, G., Qi, J.P., Xiong, X.L., Zhang, L., 2012b. Epithermal deposits in north Xinjiang. Int. J. Earth Sci. 101, 889–917.
Chen, Y.J., Santosh, M., Somreville, I.D., Chen, H.Y., 2014. Indosinian tectonics and mineral systems in China: an introduction. Geol. J. 49, 331–337.
Chen, Y.J., Wang, P., Li, N., Yang, Y.F., Pirajno, F., 2017a. The collision-type porphyry Mo deposits in Dabie Shan, China. Ore Geol. Rev. 81, 405–430.
Chen, Y.J., Zhang, C., Wang, P., Pirajno, F., Li, N., 2017b. The Mo deposits of Northeast China: a powerful indicator of tectonic settings and associated evolutionary trends. Ore Geol. Rev. 81, 602–640.
Chiaradia, M., Konopelko, D., Seltmann, R., Cliff, R.A., 2006. Lead isotope variations across terrane boundaries of the Tien Shan and Chinese Altay. Mineral. Deposita 41, 411–428.
Deng, X.H., Yao, J.M., Li, J., Liu, G.F., 2011. Fluid inclusion and Re–Os isotopic constraints on the timing and origin of the Shimengou Mo deposit, Xixia County, Henan Province. Acta Petrol. Sin. 27, 1439–1452 (in Chinese with English abstract).
Deng, X.H., Chen, Y.J., Santosh, M., Yao, J.M., 2013a. Genesis of the 1.76 Ga Zhaiwa Mo–Cu and its linkwith the Xiong'er volcanics in the North China Craton: implications for accretionary growth along the margin of the Columbia supercontinent. Precambrian Res. 227, 337–348.
Deng, X.H., Chen, Y.J., Santosh, M., Zhao, G.C., Yao, J.M., 2013b. Metallogeny during continental outgrowth in the Columbia supercontinent: isotopic characterization of the Zhaiwa Mo–Cu system in the North China Craton. Ore Geol. Rev. 51, 43–56.
Deng, X.H., Chen, Y.J., Santosh, M., Yao, J.M., 2013c. Re–Os geochronology, fluid inclusions and genesis of the 0.85 Ga Tumen molybdenite-fluorite deposit in Eastern Qinling, China: implications for pre-Mesozoic Mo-enrichment and tectonic setting. Geol. J. 48, 484–497.
Deng, X.H., Chen, Y.J., Santosh, M., Wang, J.B., Li, C., Yue, S.W., Zheng, Z., Chen, H.J., Tang, H.S., Dong, L.H., Qu, X., 2016. U–Pb zircon, Re–Os molybdenite geochronology and Rb–Sr geochemistry from the XiaobaishitouW(–Mo) deposit: Implications for Triassic tectonic setting in eastern Tianshan, NW China. Ore Geol. Rev. http://dx.doi.org/10.1016/j.oregeorev.2016.05.013.
Dong, Y.P., Zhang, G.W., Neubauer, F., Liu, X.M., Hauzenberger, C., Zhou, D.W., Li, W., 2011. Syn- and post-collisional granitoids in the Central Tianshan orogen: geochemistry, geochronology and implications for tectonic evolution. Gondwana Res. 20, 568–581.
Duan, S.G., Zhang, Z.H., Jiang, Z.S., Zhao, J., Zhang, Y.P., Li, F.M., Tian, J.Q., 2014. Geology, geochemistry and geochronology of the Dunde iron–zinc ore deposit in western Tianshan, China. Ore Geol. Rev. 57, 441–461.
Gao, J., Li, M.S., Xiao, X.C., Tang, Y.Q., He, G.Q., 1998. Paleozoic tectonic evolution of the Tianshan Orogen, northwestern China. Tectonophysics 287, 213–231.
Gao, J., Long, L.L., Klemd, R., Qian, Q., Liu, D.Y., Xiong, X.M., Su, W., Liu, W., Wang, Y.T., Yang, F.Q., 2009a. Tectonic evolution of the South Tianshan orogen and adjacent regions, NW China: geochemical and age constraints of granitoid rocks. Int. J. Earth Sci. 98, 1221–1238.
Gao, J., Qian, Q., Long, L.L., Zhang, X., Li, J.L., Su, W., 2009b. Accretionary orogenic process of Western Tianshan, China. Geol. Bull. China 28, 1804–1816 (in Chinese with English abstract).
Gao, J.F., Zhou, M.F., Qi, L., Chen, W., Huang, X.W., 2015. Chalcophile elemental compositions and origin of the Tuwu porphyry Cu deposit, NW China. Ore Geol. Rev. 66, 403–421.
Geng, H.Y., Sun, M., Yuan, C., Zhao, G.C., Xiao, W.J., 2011. Geochemical and geochronological study of early Carboniferous volcanic rocks from the West Junggar: petrogenesis and tectonic implications. J. Asian Earth Sci. 42, 854–866.
Geng, X.X., Yang, F.Q., Zhang, Z.X., Liu, F., Cai, F.M., Gao, W.J., 2013. Ore-forming fluid of Yulekenhalasu Cu—Mo deposit on the northern margin of Junggar Basin, Xinjiang. Geol. Rev. 52, 235–247 (in Chinese with English abstract).
Goldfarb, R.J., Mao, J.W., Hart, C., Wang, D., Anderson, E., Wang, Z., 2003. Tectonic and metallogenic evolution of the Altay Shan, Northern Xinjiang Uygur Autonomous Rgeion, northwestern China. In: Mao, J.W., Godlfarb, R.J., Seltmann, R., Wang, D.H., Xiao, W.J., Hart, C. (Eds.), Tectonic Evolution and Metallogeny of the Chinese Altay and Tianshan. International Association on the Genesis of Ore Deposits, Centre for Russian and Central Asian Mineral Studies, Natural History Museum, London, pp. 17–30.
Goldfarb, R.J., Taylor, R.D., Collins, G.S., Goryachev, N.A., Orlandini, O.F., 2014. Phanerozoic continental growth and gold metallogeny of Asia. Gondwana Res. 25, 48–102.
Gong, Q.S., Liu, M.Q., Li, H.L., Liang, M.H., Dai, W.J., 2003. The type and basic characteristics of Beishan orogenic belt, Gansu. Northwest. Geol. 35, 28–34 (in Chinese with English abstract).
Gu, L.X., Zhang, Z.Z., Wu, C.Z., Wang, Y.X., Tang, J.H., Wang, C.S., Xi, A.H., Zheng, Y.C., 2006. Some problems on the vertical growth of the continental crust in the eastern Tianshan, NW China. Acta Petrol. Sin. 22, 1103–1120 (in Chinese with English Abstract).
Guo, Q.Q., Pan, C.Z., Xiao, W.J., Qu, J.F., Ao, S.J., Zhang, J.E., Song, D.F., Tian, Z.H., Wan, B., Han, C.M., 2010. Geological and geochemical characteristic of the Yandong porphyry copper deposits in Hami, Xinjiang. Xinjiang Geol. 28, 419–426 (in Chinese with English Abstract).
Guo, Q.Q., Xiao, W., Windley, B.F., Mao, Q., Han, C., Qu, J., Ao, S., Li, J., Song, D., Yong, Y., 2012. Provenance and tectonic settings of Permian turbidites from the Beishan Mountains, NW China: implications for the Late Paleozoic accretionary tectonics of the southern Altaids. J. Asian Earth Sci. 49, 54–68.
Han, B.F., Ji, J.Q., Song, B., Chen, L.H., Zhang, L., 2006a. Late Paleozoic vertical growth of continent al crust around the Junggar Basin, Xinjiang, China (Part I): timing of postcollisional plutonism. Acta Petrol. Sin. 22, 1077–1086 (in Chinese with English abstract).
Han, C.M., Xiao, W.J., Zhao, G.C., Mao, J.W., Yang, J.M., Wang, Z.L., Yan, Z., Mao, Q.G., 2006b. Geological characteristics and genesis of the Tuwu porphyry copper deposit, Hami, Xinjiang, Central Asia. Ore Geol. Rev. 29, 77–94.
Han, B.F., Guo, Z.J., Zhang, Z.C., Zhang, L., Chen, F.J., Song, B., 2010. Age, geochemistry, and tectonic implications of a late Paleozoic stitching pluton in the North Tianshan suture zone, western China. Geol. Soc. Am. Bull. 122, 627–640.
Han, C.M., Xiao, W.J., Zhao, G.C., Sun, M., Qu, W.J., Du, A.D., 2014. Re–Os geochronology on molybdenites from the Donggebi Mo deposit in the Eastern Tianshan of the Central Asia Orogenic Belt and its geological significance. Resour. Geol. 64, 136–148.
Harris, N.B.W., Pearce, J.A., Tindle, A.G., 1986. Geochemical characteristics of collision-zone magmatism. In: Coward, M.P., Ries, A.C. (Eds.), Collision Tectonics. Geological Society, London, Special Publication vol. 19, pp. 67–81.
He, Z.Z., Dong, Q.W., 2012. Study on the geological characteristics and prospecting of the Huanangou W–Mo deposit in Guazhou City, Gansu. Gansu Sci. Technol. 28, 32–35 (in Chinese with English abstract).
He, S.P., Ren, B.S., Yao, W.G., Fu, L.P., 2002. The division of tectonic units of Beishan area, Gansu–Inner Mongolia. Northwest. Geol. 35, 29–40 (in Chinesewith English abstract).
Hoefs, J., 2009. Stable Isotope Geochemistry. sixth ed. Springer, Berlin, pp. 1–285.
Hou, G.S., Tang, H.F., Liu, S.Q., Wang, Y.B., 2005. Geochronological and geochemical study on the wallrock of Tuwu-Yandong porphyry copper deposits, eastern Tianshan mountains. Acta Petrol. Sin. 21, 1729–1736 (in Chinese with English abstract).
Hou, G.S., Tang, H.F., Liu, C.Q., 2006. Geochemical characteristics of the Late Paleozoic Volcanics in Jueluotage tectonic belt, eastern Tianshan and its implications. Acta Petrol. Sin. 22, 1167–1177.
Hsu, K.J., Guitang, P., Sengor, A.M.C., Ueli, B., Chen, H., Chen, C., Harris, N., Hsu, P., Li, J., Luo, J., Lee, T., Li, Z.X., Lu, C., Powell, C., Wang, Q., Winterer, E.L., 1995. Tectonic evolution of the Tibetan Plateau: a working hypothesis based on the archipelago model of orogenesis. Int. Geol. Rev. 37, 473–508.
Hu, A.Q., Jahn, B.M., Zhang, G.X., Chen, Y.B., Zhang, Q.F., 2000. Crustal evolution and Phanerozoic crustal growth in northern Xinjiang: Nd isotopic vidence. Part I. Isotopic characterization of basement rocks. Tectonophysics 328, 15–51.
Huang, Z.Y., Long, X.P., Kröner, A., Yuan, C., Wang, Q., Sun, M., Zhao, G.C., Wang, Y.J., 2013. Geochemistry, zircon U–Pb ages and Lu–Hf isotopes of early Paleozoic plutons in the northwestern Chinese Tianshan: petrogenesis and geological implications. Lithos 182–183, 48–66.
Jahn, B.M., Wu, F.Y., Chen, B., 2000. Massive granitoid generation in central Asia: Nd isotope evidence and implication for continental growth in the Phanerozoic. Episodes 23, 82–92.
Jia, Z.Y., 2011. Study on the magmatic processes and Cu-Mo mineralization in the Lailigaoer-Kengdenggaoer region, western Tianshan, Xinjiang, China, (Master Thesis). China University of Geosciences, Beijing, pp. 1–81.

Jia, Z.Y., Xue, C.J., Qu, W.J., Zhao, Q., Zhang, Q., 2011. Geology, S, Pb, O and H isotopic compositions and Re–Os chronology of Kendenggaoer Cu–Mo deposit in Xinjiang. Mineral Deposits 30, 74–86 (in Chinese with English abstract).
Jiang, Z.S., Zhang, Z.H., Wang, Z.H., Duan, S.G., Li, F.M., Tian, J.Q., 2014. Geology, geochemistry, and geochronology of the Zhibo iron deposit in theWestern Tianshan, NW China: constraints on metallogenesis and tectonic setting. Ore Geol. Rev. 57, 406–424.
Klemm, L.M., Pettke, T., Heinrich, C.A., 2008. Fluid and source magma evolution of the Questa porphyry Mo deposit, New Mexico, USA. Mineral. Deposita 43, 533–552.
Lawley, C.J.W., Richard, J.P., Anderson, R.G., Creaser, R.A., Heaman, L.M., 2010. Geochronology and geochemistry of the MAX porphyry Mo deposit and its relationship to Pb–Zn–Ag mineralization, Kootenay Arc, Southern British Columbia, Canada. Econ. Geol. 105, 1113–1142.
Li, Y., 2012. Geological and Geochemical Characteristics and Genesis of Dabate Cu-Mo deposit, Western Tianshan, Xinjiang (Phd thesis) China University of Geosciences, Beijing, pp. 1–59.
Li, W.D., 2013. The Geological Characteristics and Genesis of the Hongyuan porphyry Mo (Cu) Deposit From West Junggar (Phd thesis) China University of Geosciences, Beijing, pp. 1–113 (in Chinese).
Li, H.Q., Chen, F.W., 2004. Isotopic Geochronology of Regional Mineralization in Xinjiang, NW China. Geology Publishing House, Beijing (391 pp. (in Chinese)).
Li, J.Y., Xiao, X.C., 1999. Brief reviews on some issues of framework and tectonic evolution of Xijiang crust, Northwest China. Sci. Geol. Sin. 34, 405–419 (in Chinese with English abstract).
Li, J.Y., Xu, X., 2004. Major problems on geological structures and metallogenesis of northern Xinjiang, Northwest China. Xinjiang Geol. 22, 119–124 (in Chinese with English abstract).
Li, H.Q., Chen, F.W., Lu, Y.F., Yang, H.M., Guo, J., Mei, Y.P., 2004. Zircon SHRIMP U-Pb Age and Strontium Isotopes of Mineralized Granitoids in the Sanchakou Copper Polymetallic Depoist, East Tianshan Mountains. Acta Geosci. Sin. 25, 191–195 (in Chinese with English abstract).
Li, H.Q., Chen, F.W., Lu, Y.F., Yang, H.M., Guo, J., Mei, Y.P., 2005. New chronological evidence for Indosinian diagenetic mineralization in Eastern Xinjiang, NW China. Acta Geol. Sin. 79, 264–275 (in Chinese with English abstract).
Li, H.Q., Chen, F.W., Li, J.Y., Qu, W.J., Wang, D.H., Wu, H., Deng, G., Mei, Y.P., 2006a. Age of mineralization and host rocks in the Baishan rhenium-molybdenum district, East Tianshan, Xinjiang, China: Revisited. Geol. Bull. China 25, 916–922 (in Chinese with English abstract).
Li, H.Q., Wang, D.H., Wan, Y., Qu, W.J., Zhang, B., Lu, Y.F., Mei, Y.P., Zou, S.L., 2006b. Isotopic geochronology study and its significance of the Lailisigaoer Mo deposit, Xinjiang. Acta Petrol. Sin. 22, 437–2443 (in Chinese with English abstract).
Li, J.Y., He, G.Q., Xu, X., Li, H.Q., Sun, G.H., Yang, T.N., Gao, L.M., Zhu, Z.X., 2006c. Crustal tectonic framework of northern Xinjiang and adjacent regions and its formation. Acta Geol. Sin. 80, 148–168 (in Chinese with English abstract).
Li, J.L., Su, W., Zhang, X., Liu, X., 2009a. Zircon Cameca U–Pb dating and its significance for granulite-facies gneisses from the western Awulale Mountains, West Tianshan, China. Geol. Bull. China 28, 1852–1862 (in Chinese with English abstract).
Li, S., Wang, T., Tong, Y., Hong, D.W., Ouyang, Z.X., 2009b. Identification of the Early Devonian Shuangfengshan A-type granites in Liuyuan area of Beishan and its implications to tectonic evolution. Acta Petrol. Mineral. 28, 407–422 (in Chinese with English abstract).
Li, S., Wang, T., Wilde, S.A., Tong, Y., Hong, D., Guo, Q., 2012a. Geochronology, petrogenesis and tectonic implications of Triassic granitoids from Beishan, NW China. Lithos 134–135, 123–145.
Li, N., Ulrich, T., Chen, Y.J., Thomsen, T.B., Pease, V., Pirajno, F., 2012b. Fluid evolution of the Yuchiling porphyry Mo deposit, East Qinling, China. Ore Geol. Rev. 48, 442–459.
Li, D.P., Du, Y.S., Pang, Z.S., Tu, Q.J., Zhang, Y.P., Ge, S.S., Shen, L.J., Wang, K.H., 2013a. Zircon U–Pb chronology and geochemistry of Carboniferous volcanic rocks in Awulale area, western Tianshan Mountains. Acta Geosci. Sin. 34, 176–192 (in Chinese with English abstract).
Li, S., Wilde, S.A., Wang, T., 2013b. Early Permian post-collisional high-K granitoids from Liuyuan area in southern Beishan orogen, NW China: petrogenesis and tectonic implications. Lithos 179, 99–119.
Li, N., Chen, Y.J., Pirajno, F., Ni, Z.Y., 2013c. Timing of the Yuchiling giant porphyry Mo system, and implications for ore genesis. Mineral. Deposita 48, 505–524.
Li, G.M., Cao, M.J., Qin, K.Z., Evans, N.J., Mcinnes, B.I.A., Liu, Y.S., 2014. Thermal-tectonic history of the Baogutu porphyry Cu deposit, west Junggar as constrained from Zircon U–Pb, biotite Ar/Ar and Zircon/Apatite (U–Th)/He dating. J. Asian Earth Sci. 79, 741–758.
Li, C., Xiao, W.J., Han, C.M., Zhou, K.F., Zhang, J.E., Zhang, Z.X., 2015. Late Devonian–early Permian accretionary orogenesis along the North Tianshan in the southern Central Asian Orogenic Belt. Int. Geol. Rev. 57, 1023–1050.
Linnen, R.L., Williams-Jones, A.E., 1990. Evolution of aqueous-carbonic fluids during contact metamorphism, wall-rock alteration, and molybdenite deposition at Trout Lake, British Columbia. Econ. Geol. 85, 1840–1856.
Liu, X.J., Liu, W., 2013. Re–Os dating of the Suoerkuduke Cu (Mo) deposit, Fuyun County, Xinjiang, and its geodynamic implications. J. Earth Sci. 24, 188–202.
Liu, T.G., Mei, H.J., Yu, X.Y., Qiu, Y.Z., Wang, Y.X., Yang, T.D., 1992. Discussion on the ore genesis of the Suoerkuduke Cu–Mo deposit based on its geochemical characteristics. Xinjiang Geol. 10, 176–183.
Liu, D.Q., Chen, Y.C., Wang, D.H., Tang, Y.L., Zhou, R.H., Wang, J.L., Li, H.Q., Chen, F.W., 2003. A discussion on problems related to mineralization of Tuwu–Yandong Cu–Mo orefield in Hami, Xinjiang. Mineral Deposits 22, 335–344 (in Chinese with English abstract).
Liu, X.C., Chen, B.L., Jahn, B.M., Wu, G.G., Liu, Y.S., 2011. Early Paleozoic (ca. 465 Ma) eclogites from Beishan (NW China) and their bearing on the early evolution of the southern Central Asia Orogenic Belt. J. Asian Earth Sci. 42, 715–731.
Liu, W.Z., Zhang, H., Tang, H.F., Tang, Y., Lv, Z.H., 2015. Molybdenite Re–Os dating of the Asikaerte Be–Mo deposit in Xinjiang, China and its genetic implications. Geochimica 44, 145–154 (in Chinese with English abstract).
Long, L.L., Wang, J.B., Wang, Y.W., Wang, L.J., Wang, S.L., Pu, K., 2009. Geochronology and geochemistry of the ore-bearing porphyry in Xilekuduke Cu–Mo deposit, Fuyun area, Xinjiang, China. Geol. Bull. China 28, 1840–1851 (in Chinese with English abstract).
Long, L.L., Wang, Y.W., Du, A.D., Wang, J.B., Wang, L.J., Wang, S.L., Pu, K.X., Qu, W.J., 2011. Molybdenite Re–Os age of Xilekuduke Cu–Mo deposit in Xinjiang and its geological significance. Mineral Deposits 30, 635–644 (in Chinese with English abstract).
Long, X.P., Yuan, C., Sun, M., Safonova, I., Xiao, W.J., Wang, Y.Y., 2012. Geochemistry and U–Pb detrital zircon dating of Paleozoic graywackes in East Junggar, NW China: insights into subduction–accretion processes in the southern Central Asian Orogenic Belt. Gondwana Res. 21, 637–653.
Long, L.L., Wang, J.B., Wang, Y.W., Wang, L.J., Liao, Z., Zhao, L.T., Sun, Z.Y., Gao, L.M., 2015. Sulfur-isotope characteristics and discussion on the source of ore-forming material of the Xilekuduke Cu-Mo deposit, Xinjiang Province. Acta Petrol. Sin. 31, 545–554.
Ma, R.S., Wang, C.Y., Ye, S.F., 1993. Tectonic Framework and Crust Evolution of Eastern Tianshan. Nanjing University Press, Nanjing, p. 225 (in Chinese with English abstract).
Ma, R.S., Shu, L.S., Sun, J.Q., 1997. Tectonic Framework and Crust Evolution of Eastern Tianshan Mountains. Geo1ogical Publishing House, Beijing, p. 202 (in Chinese).
Mao, J.W., Zhang, Z.C., Zhang, Z.H., Du, A.D., 1999. Re–Os isotopic dating ofmolybdenites in the Xiaoliugou W (Mo) deposit in the northern Qilian mountains and its geological significance. Geochim. Cosmochim. Acta 63, 1815–1818.
Mao, J.W., Goldfarb, R.T., Wang, Y.T., Hart, C.J., Wang, Z.L., Yang, J.M., 2005. Late Paleozoic base and precious metal deposits, East Tianshan, Xinjiang, China, characteristics and geodynamic setting. Episodes 28, 23–36.
Mao, Q.G., Xiao, W.J., Windley, B.F., Han, C.M., Qu, J.F., Ao, S.J., Zhang, J.E., Guo, Q.Q., 2012a. The Liuyuan complex in the Beishan, NW China: a Carboniferous–Permian ophiolitic fore-arc sliver in the southern Altaids. Geol. Mag. 149, 483–506.
Mao, Q.G., Xiao, W.J., Fang, T.H., Wang, J.B., Han, C.M., Sun, M., Yuan, C., 2012b. Late Ordovician to early Devonian adakites and Nb-enriched basalts in the Liuyuan area, Beishan, NWChina: implications for early Paleozoic slab-melting and crustal growth in the southern Altaids. Gondwana Res. 22, 534–553.
Mi, M., Chen, Y.J., Yang, Y.F., Wang, P., Li, F.L., Wan, S.Q., Xu, Y.L., 2015. Geochronology and geochemistry of the giant Qian'echong Mo deposit, Dabie Shan, eastern China: implications for ore genesis and tectonic setting. Gondwana Res. 27, 1217–1235.
Mu, Z.G., Liu, C.Y., Huang, B.L., Hou, G.T., Zuo, G.C., Liu, C.Y., Feng, Y.Z., 1992. Isotopic ages and tectonomagmatic events of the Beishan area, Gansu Province. J. Peking Univ. (Nat. Sci.) 28, 486–497 (in Chinese with English abstract).
Ni, P., Wang, G.G., Yu, W., Chen, H., Jiang, L.L., Wang, B.H., Zhang, H.D., Xu, Y.F., 2015. Evidence of fluid inclusions for two stages of fluid boiling in the formation of the giant Shapinggou porphyry Mo deposit, Dabie orogen, Central China. Ore Geol. Rev. 65, 1078–1094.
Nie, F.J., Jiang, S.H., Zhao, S.M., Bai, D.M., Liu, Y., Zhao, Y.M., Wang, X.L., Su, X.X., 2002. Gelological features and metallogenic type of the Liushashan gold (molybdenum) deposit in Ejin Qi (prefecture), western Inner Mongolia. Geol. Geochem. 30 (1), 1–7 (in Chinese with English abstract).
Nie, F.J., Qu, W.J., Liu, Y., Du, A.D., Jiang, S.H., 2005. Re–Os isotopic age dating of molybdenite separates from Elegen porphyry Mo (Cu)mineralized area, northwestern Alxa, western Inner Mongolia. Mineral Deposits 24, 638–646 (in Chinese with English abstract).
Niu, H., Sato, H., Zhang, H., Ito, J.I., Yu, X., Nagao, T., Terada, K., Zhang, Q., 2006. Juxtaposition of adakite, boninite, high-TiO_2 and low-TiO_2 basalts in the Devonian southern Altay, Xinjiang, NW China. J. Asian Earth Sci. 28, 439–456.
Ohmoto, H., Rye, R.O., 1979. Isotopes of sulfur and carbon. In: Barns, H.L. (Ed.), Geochemistry of Hydrothermal Ore Deposits. Wiley Interscience, New York, pp. 509–567.
Pearce, J.A., 1996. Sources and settings of granitic rocks. Episodes 19, 120–125.
Pearce, J.A., Harris, N.B.W., Tindle, A.G., 1984. Trace element discrimination diagrams for the tectonic interpretation of granitic rocks. J. Petrol. 25, 956–983.
Peng, Z.A., Li, H.H., Qu, W.J., Zhang, S.Q., Ding, H.J., Chen, X.R., Zhang, B., Zhang, Y.Z., Xu, M., Cai, M.H., 2010. Molybdenite Re–Os age of Xiaohulishan molybdenum deposit in Beishan area, Inner Mongolia. Mineral Deposits 29, 510–516 (in Chinese with English abstract).
Pirajno, F., 2009. Hydrothermal Processes and Mineral Systems. Springer, Berlin (1250 pp.).
Pirajno, F., 2013. The Geology and Tectonic Settings of China's Mineral Deposits. Springer, Berlin (679 pp.).
Pirajno, F., Zhou, T.F., 2015. Intracontinental porphyry and porphyry–skarn mineralsystems in Eastern China: scrutiny of a special case “made-in-China”. Econ. Geol. 110, 603–629.
Pirajno, F., Mao, J.W., Zhang, Z.C., Zhang, Z.H., Chai, F.M., 2008. The association of mafic-ultramafic intrusions and A-type magmatism in the Tianshan and Altay orogens, NW China. Implications for geodynamic evolution and potential for the discovery of new ore deposits. J. Asian Earth Sci. 32, 165–183.
Pirajno, F., Ernst, R.E., Borisenko, A.S., Fedoseev, G., Naumov, E.A., 2009. Intraplate magmatism in Central Asia and China and associated metallogeny. Ore Geol. Rev. 35, 114–136.
Pirajno, F., Seltmann, R., Yang, Y.Q., 2011. A reviewofmineral systems and associated tectonic settings of northern Xinjiang, NW China. Geosci. Front. 2, 157–185.
Qin, K.Z., Sun, S., Li, J.L., Fang, T.H., Wang, S.L., Liu, W., 2002. Paleozoic epithermal Au and porphyry Cu deposits in North Xinjiang, China: epochs, features, tectonic linkage and exploration significance. Resour. Geol. 52, 291–300.
Qin, K.Z., Zhang, L.C., Xiao, W.J., Xu, X.W., Yan, Z., Mao, J.W., 2003. Overview of major Au, Cu, Ni and Fe deposits and metallogenic evolution of the Eastern Tianshan Mountains, Northwestern China. In: Mao, J.W., Goldfarb, R.J., Seltmann, R., Wang, D.W., Xiao, W.J.,

Hart, C. (Eds.), Tectonic Evolution and Metallogeny of the Chinese Altay and Tianshan, London, pp. 227–249.
Qin, K.Z., Zhang, L.C., Ding, K.S., Xu, Y.X., Tang, D.M., Xu, X.W., Ma, T.L., Li, G.M., 2009. Mineralization type, petrogenesis of ore-bearing intrusions and mineralogical characteristics of Sanchakou copper deposit in eastern Tianshan. Acta Petrol. Sin. 25, 845–861 (in Chinese with English abstract).
Qin, K.Z., Su, B.X., Sakyi, P.A., Tang, D.M., Li, X.H., Sun, H., Xiao, Q.H., Liu, P.P., 2011. SIMS zircon U–Pb geochronology and Sr–Nd isotopes of Ni–Cu-bearing mafic-ultramafic intrusions in eastern Tianshan and Beishan in correlation with flood basalts in Tarim Basin (NW China): constraints on a ca. 280 Ma mantle plume. Am. J. Sci. 311, 237–260.
Qu, X., 2011. Mineralization Regularities and Prediction of Targets of Porphyry Copper Deposit in East Junggar, Xinjiang, China (Ph.D. thesis) China University of Geosciences, Beijing, pp. 1–186 (in Chinese with English abstract).
Qu, X., Xu, X.W., Liang, G.L., Qu, W.J., Du, S.J., Jiang, N., Wu, H.P., Zhang, Y., Xiao, H., Dong, L.H., 2009. Geological and geochemical characteristics of the Mengxi Cu–Mo deposit and ite constraint to tectonic setting of the Qiongheba magmatic arc in eastern Junggar, Xinjiang. Acta Petrol. Sin. 25, 765–776 (in Chinese with English abstract).
Qu, J.F., Xiao, W.J., Windley, B.F., Han, C.M., Mao, Q.G., Ao, S.J., Zhang, J.E., 2011. Ordovician eclogites from the Chinese Beishan: implications for the tectonic evolution of the southern Altaids. J. Metamorph. Geol. 29, 803–820 (in Chinese with English abstract).
Richard, J.P., 2011. Magmatic to hydrothermal metal fluxes in convergent and collided margins. Ore Geol. Rev. 40, 1–26.
Rui, Z.Y., Goldfarb, R.J., Qiu, Y.M., Zhou, T.H., Chen, R.Y., Pirajno, F., Yun, G., 2002a. Paleozoic-early Mesozoic gold deposits of the Xinjiang Autonomous Region, northwestern China. Mineral. Deposita 37, 393–418.
Rui, Z.Y., Wang, L.S., Wang, Y.T., 2002b. Discussion on metallogenic epoch of Tuwu and Yandong Porphyry copper deposits in Eastern Tianshan Mountains, Xinjiang. Mineral Deposits 21, 16–22 (in Chinese with English abstract).
Seedorff, E., Einaudi, M., 2004a. Henderson porphyry molybdenum system, Colorado: I. Sequence and abundance of hydrothermal mineral assemblages, flow paths of evolving fluids, and evolutionary style. Econ. Geol. 99, 3–37.
Seedorff, E., Einaudi, M., 2004b. Henderson porphyry molybdenum system, Colorado: II. Decoupling of introduction and deposition of metals during geochemical evolution of hydrothermal fluids. Econ. Geol. 99, 39–72.
Selby, D., Nesbitt, B.E., Muehlenbachs, K., Prochaska, W., 2000. Hydrothermal alteration and fluid chemistry of the Endako porphyry molybdenite deposit, British Columbia. Econ. Geol. 95, 183–202.
Sengor, A.M.C., Natalîn, B.A., 1996. Paleotectonics of Asia: frangments of synthesis. In: Yin, A., Harrison, T.M. (Eds.), The Tectonic Evolution of Asia. Cambridge University Press, Cambridge, pp. 480–640.
Shen, P., Shen, Y.C., Liu, T.B., Meng, L., Dai, H.W., Yang, Y.H., 2009. Geochemical signature of porphyries in the Baogutu porphyry copper belt, western Junggar, NW China. Gondwana Res. 16, 227–242.
Shen, P., Shen, Y.C., Pan, H.D., Wang, J.B., Zhang, R., Zhang, Y.X., 2010. Baogutu Porphyry Cu–Mo–Au deposit, West Junggar, Northwest China: petrology, alteration, and mineralization. Econ. Geol. 105, 947–970.
Shen, P., Shen, Y.C., Pan, H.D., Li, X.H., Dong, L.H., Wang, J.B., Zhu, H.P., Dai, H.W., Guan, W.N., 2012. Geochronology and isotope geochemistry of the Baogutu porphyry copper deposit in the West Junggar region, Xinjiang, China. J. Asian Earth Sci. 49, 99–115.
Shen, P., Xiao, W.J., Pan, H.D., Dong, L.H., Li, C.F., 2013. Petrogenesis and tectonic settings of the Late Carboniferous Jiamantieliek and Baogutu ore-bearing porphyry intrusions in the southern West Junggar, NW China. J. Asian Earth Sci. 75, 159–173.
Shen, P., Pan, H.D., Dong, L.H., 2014a. Yandong porphyry Cu deposit, Xinjiang, China-geology, geochemistry and SIMS U–Pb zircon geochronology of host porphyries and associated alteration and mineralization. J. Asian Earth Sci. 80, 197–217.
Shen, P., Pan, H.D., Zhou, T.F., Wang, J.B., 2014b. Petrography, geochemistry and geochronology of the host porphyries and associated alteration at the Tuwu Cu deposit, NW China: a case for increased depositional efficiency by reaction with mafic hostrock. Mineral. Deposita 49, 709–731.
Shen, P., Pan, H.D., Shen, Y.C., Yana, Y.H., Zhong, S.H., 2015. Main deposit styles and associated tectonics of the West Junggar region, NW China. Geosci. Front. 6, 175–190.
Shen, P., Pan, H.D., Cao, C., Zhong, S.H., Li, C.B., 2017. The formation of the Suyunhe large porphyry Mo deposit in the West Junggar terrain, NW China: Zircon U–Pb age, geochemistry and Sr–Nd–Hf isotopic results. Ore Geol. Rev. 81, 808–828.
Shi, Y.X., Li, N., Yang, Y., 2009. Ore geology and fluid inclusion geochemistry of the Sandaozhuang Mo–W deposit in Luanchuan County, Henan Province. Acta Petrol. Sin. 25, 2575–2587 (in Chinese with English abstract).
Shu, L.S., Wang, Y.J., 2003. Late Devonian–Early Carboniferous radiolarian fossils from siliceous rocks of the Kelameili ophiolite, Xinjiang. Geol. Rev. 49, 408–413.
Shu, L.S., Lu, H.F., Yin, D.H., Ma, R.S., Jacques, C., Sebastie, L.C., 2001. Late Paleozoic continental accretionary tectonics in northern Xinjiang. Xinjiang Geol. 19, 59–63 (in Chinese with English abstract).
Sillitoe, R.H., 2010. Porphyry copper systems. Econ. Geol. 105, 3–41.
Song, H.X., Liu, Y.L., Qu, W.J., Song, B., Zhang, R., Cheng, Y., 2007. Geological characters of Baogutu porphyry copper deposit in Xinjiang, NW China. Acta Petrol. Sin. 23, 1981–1988 (in Chinese with English abstract).
Stein, H.J., Markey, R.J., Morgan, J.W., 2001. The remarkable Re–Os chronometer inmolybdenite: how and why it works. Terra Nova 13, 479–486.
Tang, H.S., Chen, Y.J., Liu, Y.L., Huang, B.L., 2006. Isotope dating of the Be'erkuduke tin deposit in the eastern Junggar area. J. Mineral. Petrol. 26, 71–73 (in Chinese with English abstract).
Tang, G.J., Chen, H.H., Wang, Q., Zhao, Z.H., Derek, A.W., Jiang, Z.Q., Jia, X.H., 2008. Geochronological age and tectonic background of the Dabate A-type granite pluton in the west Tianshan. Acta Petrol. Sin. 24, 947–958 (in Chinese with English abstract).
Tang, G.J., Wang, Q., Zhao, Z.H., Derek, A.W., Chen, H.H., Jia, X.H., Jiang, Z.Q., 2009. Geochronology and geochemistry of the ore-bearing porphyries in the Baogutu Area (Western Junggar): petrogenesis and their implications for tectonics and Cu–Au mineralization. Earth Sci. 34, 56–74 (in Chinese with English abstract).
Tang, G.J., Wang, Q., Wyman, D.A., Sun, M., Li, Z.X., Zhao, Z.H., Sun, W.D., Jia, X.H., Jiang, Z.Q., 2010a. Geochronology and geochemistry of Late Paleozoic magmatic rocks in the Lamasu-Dabate area, northwestern Tianshan (west China): evidence for a tectonic transition from arc to post-collisional setting. Lithos 119, 393–411.
Tang, G.J., Wang, Q., Wyman, D.A., Li, Z.X., Zhao, Z.H., Jia, X.H., Jiang, Z.Q., 2010b. Ridge subduction and crustal growth in the Central Asian Orogenic Belt: evidence from Late Carboniferous adakites and high-Mg diorites in the western Junggar region, northern Xinjiang (west China). Chem. Geol. 277, 281–300.
Tang, G.J., Chung, S.L., Wang, Q., Wyman, D.A., Dan, W., Chen, H.Y., Zhao, Z.H., 2014. Petrogenesis of a Late Carboniferous mafic dike-granitoid association in the western Tianshan: response to the geodynamics of oceanic subduction. Lithos 202–203, 85–99.
Taylor, H.P., 1974. The application of oxygen and hydrogen isotope studies to problems of hydrothermal alteration and ore deposition. Econ. Geol. 69, 843–883.
Tu, G.Z., Ding, K., 1986. The Qinling–Central Asia Sb–Hg belt—the third Sb–Hg belt of global significance. Geochemical Collections. Science Press, Beijing, pp. 8–13 (in Chinese with English abstract).
Tu, Q.J., Dong, L.H., Wang, K.Z., 2012. Molybdenite Re–Os dating and its geological implication for the east Gebi molybdenum deposit of the eastern Tianshan Mountain in Xinjiang. Xinjiang Geol. 30, 272–276.
Tu, Q.J., Wang, Y.S., Dong, L.H., 2014. Re–Os dating of molybdenite from the Baishan molybdenum deposit in the Eastern Tianshan Area of Xinjiang and its geological significance. Xinjiang Geol. 32, 322–327 (in Chinese with English Abstract).
Wallace, S.R., 1995. SEG presidential address: the climax-type molybdenite deposits: what they are, where they are, and why they are. Econ. Geol. 90, 1359–1380.
Wan, B., Xiao, W.J., Zhang, L.C., Windley, B.F., Han, C.M., Quinn, C.D., 2011. Contrasting styles of mineralization in the Chinese Altai and East Junggar, NW China: implications for the accretionary history of the southern Altaids. J. Geol. Soc. 168, 1311–1321.
Wan, B., Xiao, W.J., Han, C.M., Windley, B.F., Zhang, L.C., Qu, W.J., Du, A.D., 2014. Re–Os molybdenite age of the Cu–Mo skarn ore deposit at Suoerkuduke in East Junggar, NW China and its geological significance. Ore Geol. Rev. 56, 541–548.
Wang, S.J., Wang, J.L., 2010. The geochemical characteristics and chronology of the K-feldspar granite in Baluntai area, Xinjiang. J. Northwest Univ. 40, 105–110 (in Chinese with English abstract).
Wang, Z.H., Sun, S., Li, J.L., Hou, Q.L., Qin, K.Z., Xiao, W.J., Hao, J., 2003. Paleozoic tectonic evolution of the northern Xinjiang, China: geochemical and geochronological constraints from the ophiolites. Tectonics 22, 1014.
Wang, J.B., Wang, Y.W., Wang, L.J., 2004. The Junggar immature continental crust province and its mineralization. Acta Geol. Sin. 78, 337–344 (in Chinese with English abstract).
Wang, Z.L., Mao, J.W., Zhang, Z.H., Zuo, G.C., Wang, L.S., 2006. Geology, time–space distribution and metallogenic geodynamic evolution of porphyry copper (molybdenum) deposits in the Tianshan Mountains. Acta Geol. Sin. 80, 943–955 (in Chinese with English abstract).
Wang, L.J., Wang, J.B., Wang, Y.W., Long, L.L., Wang, S.L., Pu, K.X., 2009. Geology and ore-forming fluids of Xilekuduke porphyry Cu–Mo deposit in northern Junggar. Acta Petrol. Sin. 25, 944–954 (in Chinese with English abstract).
Wang, J., Nie, F.J., Liu, Y., 2010a. Geological and geochemical characteristics and geological implications of the Mengxi porphyry copper-molybdenum deposit in East Junggar region. Geol. China 37, 1151–1161.
Wang, Y.W., Wang, J.B., Wang, S.L., Long, L.L., Wang, L.J., Pu, K.X., Wang, S.D., Tang, P.Z., 2010b. Geological characteristics and genesis of the Xilekuduke Cu–Mo deposit, Xinjiang. Xinjiang Geol. 28, 370–376.
Wang, D.Q., Liu, C.J., Zhang, H.D., Zheng, L.H., Wang, R.M., 2013. Study of tectonic environment and U–Pb dating of zircons from the Mengxi plagioclase granite porphyry. J. Mineral. Petrol. 33, 63–69 (in Chinese with English abstract).
Wang, P., Chen, Y.J., Fu, B., Yang, Y.F., Mi, M., Li, Z.L., 2014a. Fluid inclusion and H–O–C isotope geochemistry of the Yaochong porphyry Mo deposit in Dabie Shan, China: a case study of porphyry systems in continental collision orogens. Int. J. Earth Sci. 103, 777–797.
Wang, Y.H., Xue, C.J., Wang, J.P., Peng, R.M., Yang, J.T., Zhang, F.F., Zhao, Z.N., Zhao, Y.J., 2014b. Petrogenesis of magmatism in the Yandong region of Eastern Tianshan, Xinjiang: geochemical, geochronological, and Hf isotope constraints. Int. Geol. Rev. 57, 1–22.
Wang, C.L., Qin, K.Z., Tang, D.M., Zhou, Q.F., Shen, M.D., Guo, Z.L., Guo, X.J., 2015a. Geochronology and Hf isotope of zircon for the Arskartor Be–Nb–Mo deposit in Altay and its geological implications. Acta Petrol. Sin. 31, 2337–2352 (in Chinese with English abstract).
Wang, Y.H., Xue, C.J., Liu, J.J., Wang, J.P., Yang, J.T., Zhang, F.F., Zhao, Z.N., Zhao, Y.J., Liu, B., 2015b. Early Carboniferous adakitic rocks in the area of the Tuwu deposit, eastern Tianshan, NW China: slab melting and implications for porphyry copper mineralization. J. Asian Earth Sci. 103, 332–349.
Wang, Y.H., Zhang, F.F., Liu, J.J., Xue, C.J., Wang, J.P., Liu, B., Lu, W.W., 2015c. Petrogenesis of granites in Baishan molybdenum deposit, eastern Tianshan, Xinjiang: zircon U–Pb geochronology, geochemistry, and Hf isotope constraints. Acta Petrol. Sin. 31, 1962–1976 (in Chinese with English abstract).
Wang, P., Chen, Y.J., Wang, C.M., Wang, S.X., 2017a. Genesis and tectonic setting of the giant Diyanqinamu porphyry Mo deposit in Great Hingan Range, NE China: constraints from U–Pb and Re–Os geochronology and Hf isotopic geochemistry. Ore Geol. Rev. 81, 760–779.
Wang, Y.H., Zhang, F.F., Liu, J.J., 2016b. The genesis of the ores and intrusions at the Yuhai Cu–Mo deposit in eastern Tianshan, NW China: constraints from geology, geochronology, geochemistry, and Hf isotope systematics. Ore Geol. Rev. 77, 312–331.

Wei, S.N., Zhu, Y.F., 2015. Petrology, geochronology and geochemistry of intermediate-acidic intrusions in Baogutu area, West Junggar, Xinjiang. Acta Petrol. Sin. 31, 143–160.
Windley, B.F., Alexeiev, D., Xiao, W.J., Kroner, A., Badarch, G., 2007. Tectonic models for accretion of the Central Asian Orogenic Belt. J. Geol. Soc. Lond. 64, 31–47.
Woodhead, J.D., Eggins, S.M., Johnson, R.W., 1998. Magma genesis in the New Britain island arc: further insights into melting and mass transfer processes. J. Petrol. 39, 1641–1668.
Wu, C.Z., Zhang, Z.Z., Zaw, K., Della-Pasque, F., Tang, J.H., Zheng, Y.C., Wang, C.S., San, J.Z., 2006a. Geochronology, geochemistry and tectonic significances of the Hongyuntan granitoids in the Qoltag area, Eastern Tianshan. Acta Petrol. Sin. 22, 1121–1134 (in Chinese with English Abstract).
Wu, H., Li, H.Q., Chen, F.W., Lu, Y.F., Deng, G., Mei, Y.P., Ji, H.G., 2006b. Zircon SHRIMP U–Pb dating of plaglogranite porphyry in the Chihu molybdenum-copper district, Hami, East Tianshan. Geol. Bull. China 25, 549–552 (in Chinese with English Abstract).
Wu, Y.H., Xiong, X.L., Zhao, T.P., Zhu, Z.M., Li, L., 2013a. Zircon U–Pb age of the ore-bearing granite and molybdenite Re–Os isotopic age of the Donggebi Mo deposit, Xinjiang and their geological significance. Geotecton. Metallog. 37, 743–753 (in Chinese with English abstract).
Wu, Y.S., Xiang, N., Tang, H.S., Zhou, K.F., Yang, Y.F., 2013b. Molybdenite Re–Os isotope age of the Donggebi Mo deposit and the Indosinian metallogenic event in Eastern Tianshan. Acta Petrol. Sin. 29, 121–130 (in Chinese with English abstract).
Wu, Y.S., Wang, P., Yang, Y.F., Xiang, N., Li, N., Zhou, K.F., 2014. Ore geology and fluid inclusion study of the Donggebi giant porphyry Mo deposit, Eastern Tianshan, NW China. Geol. J. 49, 559–573.
Wu, G., Li, X.Z., Xu, L.Q., Wang, G.R., Liu, J., Zhang, T., Quan, Z.X., Wu, H., Li, T.G., Zeng, Q.T., Chen, Y.C., 2016a. Geochronology, geochemistry, and Sr–Nd–Hf–Pb isotopes of the Caosiyao porphyry Mo deposit in Inner Mongolia, China, and their geological significance. Ore Geol. Rev. (this special issue).
Wu, Y.S., Zhou, K.F., Li, N., Chen, Y.J., 2017b. Zircon U–Pb dating and Sr–Nd–Pb–Hf isotopes of the ore-causative porphyry at the giant Donggebi Mo deposit, Eastern Tianshan, NW China. Ore Geol. Rev. 81, 794–807.
Xia, L.Q., Xu, X.Y., Xia, Z.C., Li, X.M., Ma, Z.P., Wang, L.S., 2004. Petrogenesis of Carboniferous rift-related volcanic rocks in the Tianshan, northwestern China. Geol. Soc. Am. Bull. 116, 419–433.
Xiang, P., Zhang, L.C., Xu, X.W., Liu, G.R., Liu, Z.J., Jin, X.D., Li, W.J., 2012. Geological characteristics and genesis of Yuleken-Halasu superimposed and tectonically reworked porphyry copper-gold (molybdenum) deposit in Qinghe, Xinjiang. Acta Petrol. Sin. 28, 2369–2380 (in Chinese with English abstract).
Xiang, N., Yang, Y.F., Wu, Y.S., Zhou, K.F., 2013. Fluid inclusion study of the Baishan porphyry Mo deposit in the Eastern Tianshan ore field, Xinjiang Province. Acta Petrol. Sin. 29, 146–158 (in Chinese with English abstract).
Xiao, W.J., Kusky, T., 2009. Geodynamic processes and metallogenesis of the Central Asia and related orogenic belts. Gondwana Res. 16, 167–169.
Xiao, W.J., Han, C.M., Yuan, C., Sun, M., Lin, S.F., Chen, H.L., Li, Z.L., Li, J.L., Sun, S., 2008a. Middle Cambrian to Permian subduction-related accretionary orogenesis of Northern Xinjiang, NW China: implications for the tectonic evolution of central Asia. J. Asian Earth Sci. 32, 102–117.
Xiao, W.J., Shu, L.S., Gao, J., Xiong, X.L., Wang, J.B., Guo, Z.J., Li, J.Y., Sun, M., 2008b. Continental dynamics of the central Asian orogenic belt and its metallogeny. Xinjiang Geol. 26, 4–7 (in Chinese with English abstract).
Xiao, W.J., Windley, B.F., Huang, B.C., Han, C.M., Yuan, C., Chen, H.L., Sun, M., Sun, S., Li, J.L., 2009a. End-Permian to mid-Triassic termination of the accretionary processes of the southern Altaids: implications for the geodynamic evolution, Phanerozoic continental growth and metallogeny of Central Asia. Int. J. Earth Sci. 98, 1189–1217.
Xiao, W.J., Windley, B.F., Yuan, C., Sun, M., Han, C.M., Lin, S.F., Chen, H.L., Yan, Q.R., Liu, D.Y., Qin, K.Z., Li, J.L., Sun, S., 2009b. Paleozoic multiple subduction–accretion processes of the southern Altaids. Am. J. Sci. 309, 221–270.
Xiao, W.J., Mao, Q.G., Windley, B.F., Han, C.M., Qu, J.F., Zhang, J.E., Ao, S.J., Guo, Q.Q., Cleven, N.R., Lin, S.F., Shan, Y.H., Li, J.L., 2010. Paleozoic multiple accretionary and collisional processes of the Beishan orogenic collage. Am. J. Sci. 310, 1553–1594.
Xiao, Y., Zhang, H., Shi, J.A., Su, B., Sakyi, P.A., Lu, X., Hu, Y., Zhang, Z., 2011. Late Paleozoic magmatic record of East Junggar, NW China and its significance: implication from zircon U–Pb dating and Hf isotope. Gondwana Res. 20, 532–542.
Xiao, B., Chen, H.Y., Hollings, P., Han, J.S., Wang, Y.F., Yang, J.T., Cai, K.D., 2015. Magmatic evolution of the Tuwu-Yandong Porphyry Cu Belt, NW China: constraints from geochronology, geochemistry and Sr–Nd–Hf isotopes. Gondwana Res. http://dx.doi.org/10.1016/j.gr.2015.09.003.
Xie, H.J., Wu, G., Zhu, M.T., Zhong, W., Liu, J., Mi, M., 2013. Geochronology, geochemistry and petrogenesis of the Lailisigaoer intrusion in northwestern Tien Shan, NW China. Chin. J. Geol. 48, 827–846 (in Chinese with English abstract).
Xiong, X.L., Cai, Z.Y., Niu, H.C., Chen, Y.B., Wang, Q., Zhao, Z.H., Wu, J.H., 2005. The late Paleozoic adakites in eastern Tianshan area and their metallogenetic significance. Acta Petrol. Sin. 21, 967–976 (in Chinese with English abstract).
Xiong, X.L., Adam, J., Green, T.H., 2006. Trace element characteristics of partial melts of metabasalt and the formation conditions of adakitic melts. Sci. China Earth Sci. 49, 915–925.
Xue, C.J., Zhao, Z.F., Wu, G.G., Dong, L.H., Feng, J., Zhang, Z.C., Zhou, G., Chi, G.X., Gao, J.G., 2010. The multiperiodic superimposed porphyry copper mineralization in Central Asian Tectonic Region: a case study of geology, geochemistry and chronology of Halasu copper deposit, Southeastern Altai, China. Earth Sci. Front. 17, 53–82 (in Chinese with English abstract).
Xue, C.J., Chen, B., Jia, Z.Y., Zhang, B., Wang, Y., 2011. Geology, geochemistry and chronology of Lailisigao'er-3571 porphyry Cu-Mo orefield, western Tianshan, Xinjiang. Earth Sci. Front. 18, 149–165 (in Chinese with English abstract).
Yan, H.Y., Shen, P., Pan, H.D., Wang, J.N., Zhong, S.H., Liu, X.G., 2014. Research on the fluid inclusion and Re–Os dating of Hongyuan (Cu) Mo deposit and Tuketuke Mo–Cu deposit, West Junggar, Xinjiang. Chin. J. Geol. 49, 287–304.
Yan, Y.H., Wang, J.N., Shen, P., Pan, H.D., Zhong, S.H., Li, J., 2015. Geological characteristics and mineralization fluid of Hongyuan Mo deposit in the West Junggar, Xinjiang. Acta Petrol. Sin. 31, 491–504.
Yang, F.Q., Mao, J.W., Bierlein, F.P., Pirajno, F., Xia, H., Zhao, C., Ye, H., Liu, F., 2009a. A review of the geological characteristics and geodynamic mechanisms of Late Paleozoic epithermal gold deposits in North Xinjiang, China. Ore Geol. Rev. 35, 217–234.
Yang, Y.F., Li, N., Ni, Z.Y., 2009b. Fluid inclusion study of the Jinduicheng porphyry Mo deposit, Hua county, Shaanxi province. Acta Petrol. Sin. 25, 2983–2993 (in Chinese with English abstract).
Yang, S.S., Wang, S.G., Shen, C.L., Zhang, M., Zhang, H.X., Zheng, B.J., Jia, L.L., Zhang, Y., Zhou, L.J., 2012a. Rock-forming and ore-forming ages of Xiaohulishan molybdenum-polymetallic deposit in Inner Mongolia and its geological significance. Geoscience 26, 261–268 (in Chinese with English abstract).
Yang, W.B., Niu, H.C., Shan, Q., Luo, Y., Sun, W.D., Li, C.Y., Li, N.B., Yu, X.Y., 2012b. Late Paleozoic calc-alkaline to shoshonitic magmatism and its geodynamic implications, Yuximolegai area, western Tianshan, Xinjiang. Gondwana Res. 22, 325–340.
Yang, Y.F., Li, N., Chen, Y.J., 2012c. Fluid inclusion study of the Nannihu giant porphyry Mo-W deposit, Henan Province, China: implications for the nature of porphyry ore-fluid systems formed in continental collision regime. Ore Geol. Rev. 46, 83–94.
Yang, F.Q., Liu, G.R., Qin, J.H., Zhang, Z.X., Liu, Z.J., Zhang, L.W., Wei, G.Z., Liu, F., Geng, X.X., 2012d. Fluid inclusion and stable isotope study of Yulekenhalasu copper-(molybdenum) deposit in northern margin of Junggar, Xinjiang. Mineral Deposits 31, 965–982 (in Chinese with English abstract).
Yang, Y., Chen, Y.J., Zhang, J., Zhang, C., 2013a. Ore geology, fluid inclusions and four-stage hydrothermal mineralization of the Shangfanggou giant Mo–Fe deposit in Eastern Qinling, central China. Ore Geol. Rev. 55, 146–161.
Yang, Y.F., Chen, Y.J., Li, N., Mi, M., Xu, Y.L., Li, F.L., Wan, S.Q., 2013b. Fluid inclusion and isotope geochemistry of the Qian'echong giant porphyry Mo deposit, Dabie Shan, China: a case of NaCl-poor, CO_2-rich fluid systems. J. Geochem. Explor. 124, 1–13.
Yang, Y.Q., Zhao, J.H., Meng, G.X., Yan, J.Y., Lv, B., Wang, S.G., Jia, L.L., Han, J.G., 2013c. Rock-forming and ore-forming ages as well as formation environments of porphyry molybdenum deposits in Beishan Area, Inner Mongolia. Acta Geosci. Sin. 34, 401–412.
Yang, M., Wang, J.L., Wang, J.Q., Liu, C., 2015a. Late Carboniferous intra-oceanic subduction and mineralization in western Junggar: evidence from the petrology, geochemistry and zircon U–Pb geochronology of I# ore-bearing granite body in Suyunhe molybdenite orefield, Xinjiang. Acta Petrol. Sin. 31, 523–533 (in Chinese with English abstract).
Yang, Y.F., Chen, Y.J., Pirajno, F., Li, N., 2015b. Evolution of ore fluids in the Donggou giant porphyry Mo system, East Qinling, China, a new type of porphyry Mo deposit: evidence from fluid inclusion and H–O isotope systematics. Ore Geol. Rev. 65, 148–164.
Yang, S., Ma, Y.Z., Yi, A.Q., 2016a. Geological characteristics and genesis of Kekesai Copper–Molybdenum deposit in Sailimu Lake area, Xinjiang. Xinjiang Geol. 34, 124–128 (in Chinese with English abstract).
Yang, Y.F., Wang, P., Chen, Y.J., Li, Y., 2017b. Geochronology and geochemistry of the Tianmugou Mo deposit, Dabie Shan, Eastern China: implications for ore genesis and tectonic setting. Ore Geol. Rev. 81, 484–503.
Zhai, W., Sun, X.M., Sun, W.D., Su, L.W., He, X.P., Wu, Y.L., 2009. Geology, geochemistry, and genesis of Axi: a Paleozoic low-sulfidation type epithermal gold deposit in Xinjiang, China. Ore Geol. Rev. 36, 265–281.
Zhang, D.Y., 2011. Petrogenesis of Late Phanerozoic Ore-forming Porphyries in the Western Tianshan, Xinjiang, NW China: Implications for Metallogenetic Geology Background (Ph.D. thesis) China University of Geosciences, Beijing, pp. 1–133 (in Chinese with English abstract).
Zhang, C., Li, N., 2014. Geology, geochemistry and tectonic setting of the Indosinian Mo deposits in southern Geart Hinggan Range, NE China. Geol. J. 49, 537–558.
Zhang, C., Li, N., 2017. Geochronology and zircon Hf isotope geochemistry of the granites at the giant ChalukouMo deposit, NE China: implication for tectonic setting. Ore Geol. Rev. 81, 780–793.
Zhang, Z.J., Chen, Y.J., Chen, H.Y., Bao, J.X., Liu, Y.L., 2003. The petrochemical characteristics of the Hercynian granitoids in Tianshan and its geodynamic implications. J. Mineral. Petrol. 23, 15–24 (in Chinese with English abstract).
Zhang, L.C., Xiao, W.J., Qin, K.Z., Qu, W.J., Du, A.D., 2005. Re–Os isotopic dating of molybdenite and pyrite in the Baishan Mo–Re deposit, eastern Tianshan, NW China, and its geological significance. Mineral. Deposita 39, 960–969.
Zhang, L.C., Wan, B., Li, W.Q., Tang, H.F., 2006a. Geochemistry and tectonic setting of copper-bearing porphyries on the southern margin of Tuba basin, Xinjiang. Acta Petrol. Sin. 22, 225–235.
Zhang, L.C., Xiao, W.J., Qin, K.Z., Zhang, Q., 2006b. The adakite connection of the Tuwu–Yandong copper porphyry belt, eastern Tianshan, NW China: trace element and Sr–Nd–Pb isotope geochemistry. Mineral. Deposita 41, 188–200.
Zhang, Z.C., Yan, S.H., Chen, B.L., Zhou, G., He, Y.K., Chai, F.M., He, L.X., Wan, Y.S., 2006c. SHRIMP zircon U–Pb dating for subduction-related granitic rocks in the northern part of east Junggar, Xinjiang. Chin. Sci. Bull. 51, 952–962.
Zhang, Z.H., Mao, J.W., Wang, Z.L., Du, A.D., Zuo, G.C., 2006d. Geology and metallogenetic epoch of the Dabate porphyry copper deposit in West Tianshan Mountains, Xinjiang. Geol. Rev. 52, 683–689 (in Chinese with English abstract).
Zhang, Z.Z., Gu, L.X., Wu, C.Z., Zhai, J.P., Li, W.Q., Tang, J.H., 2006e. Weiya quartz syenite in early Indosinian from eastern Tianshan Mountains: petrogenesis and tectonic implications. Acta Petrol. Sin. 22, 1135–1149 (in Chinese with English abstract).
Zhang, L.F., Ai, Y.L., Li, X.P., Rubatto, D., Song, B., Williams, S., Song, S.G., Ellis, D., Liou, J.G., 2007. Triassic collision of western Tianshan orogenic belt, China: evidence from SHRIMP U–Pb dating of zircon from HP/UHP eclogitic rocks. Lithos 96, 266–280.

Zhang, L.C., Qin, K.Z., Xiao, W.J., 2008a. Multiple mineralization events in the eastern Tianshan district, NW China: isotopic geochronology and geological significance. J. Asian Earth Sci. 32, 236–246.
Zhang, H., Shen, X., Ma, L., Niu, H., Yu, X.Y., 2008b. Geochronology of the Fuyun adakite, north Xinjiang and its constraint to the initiation of the Paleo-Asian Ocean subduction. Acta Petrol. Sin. 24, 1054–1058 (in Chinese with English abstract).
Zhang, Z.H., Mao, J.W., Du, A.D., Pirajno, F., Wang, Z.L., Chai, F.M., Zhang, Z.C., Yang, J.M., 2008c. Re–Os dating of two Cu–Ni sulfide deposits in northern Xinjiang, NW China and its geological significance. J. Asian Earth Sci. 32, 204–217.
Zhang, Z.H., Wang, Z.L., Zuo, G.C., Liu, M., Wang, L.S., Wang, J.W., 2008d. Ages and tectonic settings of the volcanic rocks in Dabate ore district in West Tianshan Mountains and their constraints on the porphyry-type mineralization. Acta Geol. Sin. 82, 1494–1503.
Zhang, Y.P., Wang, R., Wang, D.G., 2008e. Kekesai granite diorite-porphyry body zircon SHRIMP U–Pb dating and the prosprcting significance in Bole city, Xinjiang. Xinjiang Geol. 26, 340–342 (in Chinese with English abstract).
Zhang, D.Y., Zhang, Z.C., Ai, Y., Su, H.M., 2009a. Geochronology, geochemistry of the ores-bearing porphyries in the Lailisigao'er region, western Tianshan: implications for their tectonic setting and mineralization. Acta Petrol. Sin. 25, 1319–1331 (in Chinese with English abstract).
Zhang, D.Y., Zhou, T.F., Yuan, F., Fan, Y., 2009b. The H, O isotopic characteristics and mineralization age of the Baishan molybdenum deposit in Eastern Tianshan. Geochim. Cosmochim. Acta 73, 1503.
Zhang, Z., Zhou, G., Kusky, T.M., Yan, S., Chen, B., Zhao, L., 2009c. Late Paleozoic volcanic record of the Eastern Junggar terrane, Xinjiang, Northwestern China: major and trace element characteristics, Sr–Nd isotopic systematics and implications for tectonic evolution. Gondwana Res. 16, 201–215.
Zhang, Z.H., Wang, Z.L., Chen, W.S., Zuo, G.C., Liu, M., 2009d. Mineralization and fluid geochemistry of Dabate prophyry copper deposit, western Tianshan in Xinjiang. Acta Petrol. Sin. 25, 1310–1318 (in Chinese with English abstract).
Zhang, C.Q., Lou, D.B., Xiao, K.Y., Dong, Q.J., Ding, J.H., Wang, P., Zhang, Z.H., Qu, W.J., 2010a. Geological characteristics and molybdenite Re–Os isotopic dating of Kumutage Mo deposit, in Hami area, Xinjiang, China. Geol. Bull. China 29, 1586–1593 (in Chinese with English abstract).
Zhang, D.Y., Zhang, Z.C., Xue, C.J., Zhao, Z.D., Liu, J.L., 2010b. Geochronology and geochemistry of the ore-forming porphyries in the Lailisigao'er–Lamasu Region of the Western Tianshan Mountains, Xinjiang, NW China: implications for petrogenesis, metallogenesis, and tectonic setting. J. Geol. 118, 543–563.
Zhang, Y., Liang, G.L., Qu, X., Du, S.J., Wu, Q., Zhang, Z.F., Dong, L.H., Xu, X.W., 2010c. Evidence of U–Pb age and Hf isotope of zircons for Early Paleozoic magmatism in the Qiongheba arc, East Junggar. Acta Petrol. Sin. 26, 2389–2398.
Zhang, Z.X., Yang, F.Q., Yan, S.H., Zhang, R., Chai, F.M., Liu, F.L., Geng, X.X., 2010d. Sources of ore-forming fluids and materials of the Baogutu porphyry copper deposit in Xinjiang: constrains from sulfur–hydrogen–oxygen isotopes geochemistry. Acta Petrol. Sin. 26, 707–716 (in Chinese with English abstract).
Zhang, J.E., Xiao, W.J., Han, C.M., Mao, Q.G., Ao, S.J., Guo, Q.Q., Ma, C., 2011. A Devonian to Carboniferous intra-oceanic subduction system in Western Junggar, NW China. Lithos 125, 592–606.
Zhang, W., Pease, V., Wu, T., Zheng, R., Feng, J., He, Y., Luo, H., Xu, C., 2012a. Discovery of an adakite-like pluton near Dongqiyishan (Beishan, NW China): its age and tectonic significance. Lithos 142–143, 148–160.
Zhang, W., Wu, T.R., Zheng, R.G., Feng, J.C., Luo, H.L., He, Y.K., Xu, C., 2012b. Post-collisional Southeastern Beishan granites: geochemistry, geochronology, Sr–Nd–Hf isotopes and their implications for tectonic evolution. J. Asian Earth Sci. 58, 51–63.
Zhang, X., Tian, J.Q., Guo, J., Klemd, R., Dong, L.H., Fan, J.J., Jiang, T., Hu, C.J., Qian, Q., 2012c. Geochronology and geochemistry of granitoid rocks from Zhibo syngenic volcanogenic iron ore deposit in the Western Tianshan Mountains (NW-China): constraints on the age of mineralization and tectonic setting. Gondwana Res. 22, 585–596.
Zhang, Z.C., He, Z.Z., Dong, Q.W., 2012d. Study on the geological characteristics and prospecting of the Hongshanjing Mo deposit in Subei City, Gansu. Gansu Sci. Technol. 28, 27–30 (in Chinese with English abstract).
Zhang, Y.L., Xu, R.K., Shan, L., Jia, Q.Z., Song, Z.B., Chen, X.Y., Zhang, X.F., Chen, B., Li, Y.Z., Quan, S.C., 2012e. Rock-forming and ore-forming ages of the Xiaohulishan molybdenum deposit in Beishan area, Inner Mongolia. Geol. Bull. China 31, 469–475.
Zhang, Z.H., Hong, W., Jiang, Z.S., Duan, S.G., Li, F.M., Shi, F.P., 2014a. Geological characteristics and metallogenesis of iron deposits in western Tianshan, China. Ore Geol. Rev. 57, 425–440.
Zhang, Z.J., Chen, H.Y., Hu, M.Y., Zhang, J., Li, D.F., 2014b. Isotopic geochemistry of the Jinwozi gold deposit in the Eastern Tianshan orogen, Northwest China: implications for the ore genesis. Geol. J. 49, 574–583.
Zhang, D.Y., Zhou, T.F., Yuan, F., Xiao, W.J., White, N.C., Deng, Y.F., Lu, W.W., Deng, G., 2015a. Petrogenesis and mineralization potential of a granite porphyry intrusion beneath the Baishan Mo deposit, Eastern Tianshan, NW China. J. J. Asian Earth Sci. 113, 254–265.
Zhang, Y.Y., Yuan, C., Sun, M., Long, X.P., Xia, X.P., Wang, X.Y., Huang, Z.Y., 2015b. Permian doleritic dikes in the Beishan Orogenic Belt, NW China: asthenosphere–lithosphere interaction in response to slab break-off. Lithos 233, 174–192.
Zhang, Z.W., Zang, Y.S., Wang, Y.L., Chen, S.B., 2016. Zircon SHRIMP U-Pb Age of the Yuhai porphyry copper deposit in eastern Tianshan Mountains of Xinjiang and its tectonic implications. Acta Geoscientica Sin. 37, 59–68 (in Chinese with English abstract).
Zhao, Z.F., Xue, C.J., Zhang, L.B., Wen, C.S., Zhou, G., Liu, G.R., 2009. U–Pb dating of zircons from acid intrusions in Yulekenhalasu copper deposit of Qinghe, Xinjiang, and its geological significance. Mineral Deposits 28, 425–433 (In Chinese with English abstract).
Zhao, L.T., Wang, J.B., Wang, Y.W., Ding, R.F., Long, L.L., Zou, T., Shi, Y., Gao, Y.H., 2014. Petrology, geochemistry and petrogenesis of the ore-bearing trachydacite porphyry from the Suoerkuduke Cu–Mo deposit, Xinjiang, NW China. Geochimica 43, 88–99 (In Chinese with English abstract).
Zhao, L.T., Wang, J.B., Wang, Y.W., Wang, L.J., Ding, R.F., Long, L.L., Li, D.D., 2015. Zircon SHRIMP geochronology of Suoerkuduke Cu–Mo deposit in Xinjiang, and its geological significance. Acta Petrol. Sin. 31, 435–448 (In Chinese with English abstract).
Zheng, H.L., Hui, Z., Yong, T., Shen, J.G., 2012a. Petrogenesis and magmatic–hydrothermal evolution time limitation of Kelumute No. 112 pegmatite in Altay, Northwestern China: evidence from zircon U–Pb and Hf isotopes. Lithos 154, 374–391.
Zheng, R., Wu, T., Zhang, W., Xu, C., Meng, Q., 2012b. Early Devonian tectono-magmatic events in the Middle Beishan, Gansu Province: evidence from chronology and geochemistry of Gongpoquan granite. J. Peking Univ. (Nat. Sci.) 43, 603–616.
Zheng, R., Wu, T., Zhang, W., Xu, C., Meng, Q., 2013. Late Paleozoic subduction system in the southern Central Asian Orogenic Belt: evidences from geochronology and geochemistry of the Xiaohuangshan ophiolite in the Beishan orogenic belt. J. Asian Earth Sci. 62, 463–475.
Zhong, S.H., Shen, P., Pan, H.D., Zheng, G.P., Yan, Y.H., Li, J., 2015a. The ore-forming fluid and geochronology of the Suyunhe Mo deposit, West Junggar, Xinjiang. Acta Petrol. Sin. 31, 449–464 (In Chinese with English abstract).
Zhong, S.H., Shen, P., Pan, H.D., Zheng, G.P., Yan, Y.H., Li, J., 2015b. Geochemistry and geochronology of ore-bearing granites in Suyunhe Mo deposit, West Junggar, Xinjiang. Mineral Deposits 34, 39–62 (In Chinese with English abstract).
Zhong, J., Chen, Y.J., Pirajno, F., 2017. Geology, geochemistry and tectonic settings of the molybdenum deposits in South China: a review. Ore Geol. Rev. 81, 829–855.
Zhou, S., Cai, H., Xie, C., 1996. Geochronology of Suoerkuduke copper (molybdenum) deposit, Northern Xinjiang. Geol. Miner. Resour. South China 12, 52–56.
Zhou, M.F., Robinson, P.T., Malpas, J., Aitchison, J., Sun, M., Bai, W.J., Hu, X.F., Yang, J.S., 2001. Melt/mantle interaction and melt evolution in the Sartohay high-Al chromite deposits of the Dalabute ophiolite (NW China). Int. J. Earth Sci. 19, 517–534.
Zhou, T.F., Yuan, F., Fan, Y., Zhang, D.Y., Cooke, D., Zhao, G.C., 2008. Granites in the Saur region of the west Junggar, Xinjiang Province, China: geochronological and geochemical characteristics and their geodynamic significance. Lithos 106, 191–206.
Zhou, T.F., Yuan, F., Zhang, D.Y., Fan, Y., Liu, S., Peng, M.X., Zhang, J.D., 2010. Geochronology, tectonic setting and mineralization of granitoids in Jueluotage area, eastern Tianshan, Xinjiang. Acta Petrol. Sin. 26, 478–502 (in Chinese with English abstract).
Zhu, Y.F., Xu, X., 2006. The discovery of early Ordovian ophiolite mélange in Taerbahatai Mts., Xinjiang, NW China. Acta Petrol. Sin. 22, 2833–2842 (in Chinese with English abstract).
Zhu, Y.F., Guo, X., Song, B., Zhang, L.F., Gu, L.B., 2009. Petrology, Sr–Nd–Hf isotopic geochemistry and zircon chronology of the Late Palaeozoic volcanic rocks in the southwestern Tianshan Mountains, Xinjiang, NW China. J. Geol. Soc. 166, 1085–1099.
Zhu, M.T., Wu, G., Xie, H.J., Wan, Y., Zhong, W., Mi, M., Liu, J., 2010. Re–Os isotopic geochronology and fluid inclusion study of the Lailisigao'er porphyry Cu–Mo deposit in western Tianshan, Xinjiang, NW China. Acta Petrol. Sin. 26, 3667–3682 (in Chinese with English abstract).
Zhu, M.T., Wu, G., Xie, H.J., Liu, J., Zhang, L.C., 2011. Geochronology and geochemistry of the Kekesai intrusion in western Tianshan, NW China and its geological implications. Acta Petrol. Sin. 27, 3041–3054 (in Chinese with English abstract).
Zhu, M.T., Wu, G., Xie, H.J., Liu, J., Mi, M., 2012. Geochronology and fluid inclusion studies of the Lailisigaoer and Lamasu porphyry–skarn Cu–Mo deposits in Northwestern Tianshan, China. J. Asian Earth Sci. 49, 116–130.
Zhu, J., Lv, X.B., Chen, C., Cao, X.F., Hu, Q.C., 2013a. Geological characteristics, metallogenic time and tectonic setting of the Triassic molybdenum deposits in the east part of the east Tianshan and the Beishan area, NW China. Xinjiang Geol. 31, 21–28 (in Chinese with English abstract).
Zhu, Z.M., Xiong, X.L., Chu, F.Y., Wu, Y.H., 2013b. Geochemistry and petrogenesis of core samples from Baishan molybdenum deposit, East Tianshan Mountains, Xinjiang. Acta Petrol. Sin. 29, 167–177 (in Chinese with English abstract).
Zhu, J., Lv, X.B., Peng, S.G., Gong, Y.J., 2014. Ore genesis and hydrothermal evolution of the Huaheitan molybdenum deposit, NW China: evidence from fluid inclusions and sulfur isotope analyses. Geochimica 43, 245–254 (in Chinese with English abstract).
Zuo, G.C., Zhang, S.L., Wang, X., Jin, S.Q., He, G.Q., Zhang, Y., Li, H.C., Bai, W.C., 1990. Plate Tectonics and Metallogenic Regularities in Beishan Region. Peking University Publishing House (48 pp. (in Chinese with English abstract)).
Zuo, G.C., Zhang, S., He, G., Zhang, Y., 1991. Plate tectonic characteristics during the early Paleozoic in Beishan near the Sino-Mongolian border region, China. Tectonophysics 188, 385–392.